

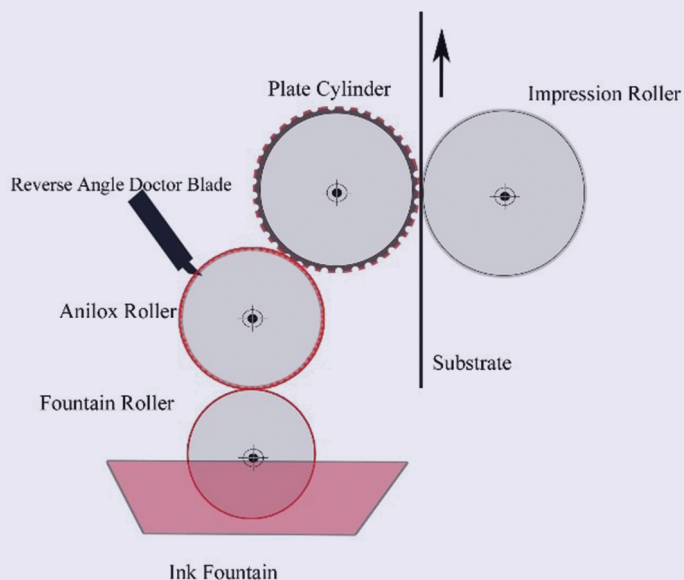


University of Novi Sad
Faculty of Technical Sciences
DEPARTMENT OF GRAPHIC
ENGINEERING AND DESIGN

Volume **16**
Number **4**
December **2025**

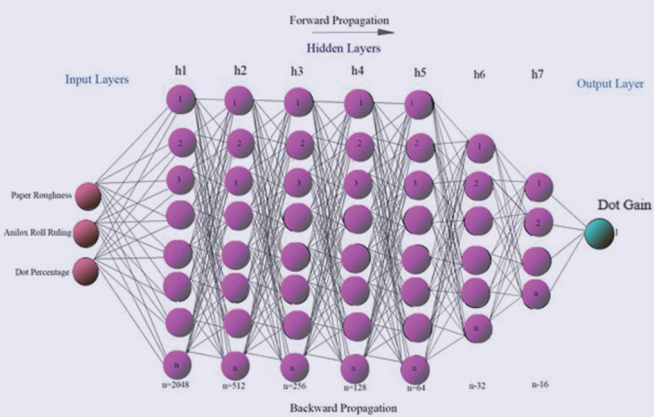
JGED

JOURNAL OF GRAPHIC
ENGINEERING AND DESIGN



Production of pH indicators from starch and anthocyanins for use in smart packaging
Sanja Mahović Poljaček, Eva Đakulović, Tamara Tomašegović, Sonja Jamnicki Hanzer, Maja Strižić Jakovljević, Urška Kavčič, Gregor Lavrič, Igor Karlovits

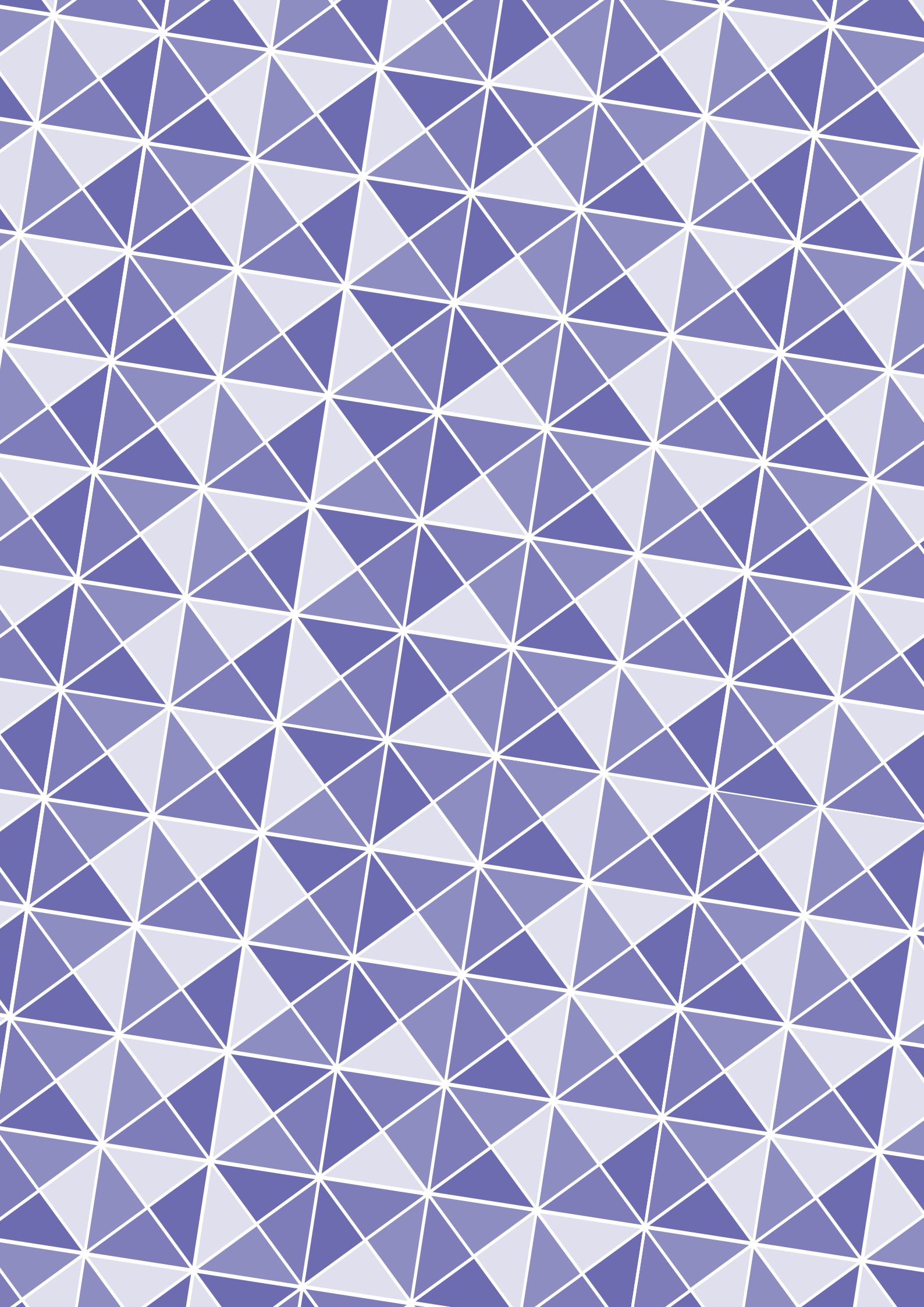
Geometric synthesis and kinematic analysis of a combined double-wedging mechanism of the pressure plate drive in the die-cutting press
Vitalii Vlakh, Ivan Rehei, Oleh Knysh



A framework of project-based learning (PBL) pedagogy for graphic design education
Kanupriya Taneja

Prediction of dot gain in flexographic color printing using machine learning
Soumen Basak, Saritha P.C, Alenrex Maity, Kanai Chandra Paul

Sustainable active packaging for the EU green transition: HEC/vitamin C antioxidant films enhancing food safety and reducing waste
Emine Arman Kandirmaz, Arif Ozcan



JGED

JOURNAL OF GRAPHIC
ENGINEERING AND DESIGN

4/2025

Volume 16, Number 4, December 2025.

Published by

UNIVERSITY OF NOVI SAD, SERBIA
Faculty of Technical Sciences
Department of Graphic Engineering and Design

PUBLISHED BY



University of Novi Sad
Faculty of Technical Sciences
DEPARTMENT OF GRAPHIC
ENGINEERING AND DESIGN

Address:

Faculty of Technical Sciences,
Department of Graphic
Engineering and Design,

Trg Dositeja Obradovića 6
21000 Novi Sad, Serbia

Telephone numbers:

+381 21 485 26 20
+381 21 485 26 26
+381 21 485 26 21

Fax number:

+381 21 485 25 45

Email:

jged@uns.ac.rs

Web address:

www.grid.uns.ac.rs/jged

Frequency: 4 issues per year

Printing: Faculty of Technical Sciences,
Department of Graphic Engineering and Design

Circulation: 200

Electronic version of journal available on
www.grid.uns.ac.rs/jged

E-ISSN 2217-9860

The journal is abstracted/indexed
in the Scopus and Directory of Open Access Journals



CIP - Katalogizacija u publikaciji
Biblioteka Matice srpske, Novi Sad
655

JGED : Journal of Graphic Engineering and Design /
editor Dragoljub Novaković. - Vol. 1, No. 1 (nov. 2010) -
Sciences, Department of Graphic Engineering and
Design,
2010-. 30 cm
Četiri puta godišnje
ISSN 2217-379X
COBISS.SR-ID 257662727



© 2025 Authors. Published by the University of Novi Sad, Faculty of
Technical Sciences, Department of Graphic Engineering and Design.
All articles are an open access articles distributed under the terms and
conditions of the Creative Commons Attribution license 4.0 Serbia
(<https://creativecommons.org/licenses/by/4.0/deed.en>).

EDITOR

Nemanja Kašiković, University of Novi Sad, Novi Sad, Serbia

EDITORIAL BOARD

Rafael Huertas

University of Granada, Granada, Spain

Joanna Ewa Izdebska

Warsaw University of Technology, Warsaw, Poland

Igor Majnarić

University of Zagreb, Zagreb, Croatia

Peter Nussbaum

Norwegian University of Science and Technology, Gjøvik, Norway

Raša Urbas

University of Ljubljana, Ljubljana, Slovenia

Miljana Prica

University of Novi Sad, Novi Sad, Serbia

Iskren Spiridonov

University of Chemical Technology and Metallurgy,
Sofia, Bulgaria

Mladen Stančić

University of Banja Luka, Banja Luka, Bosnia and Herzegovina

Tomáš Syrový

University of Pardubice, Pardubice, Czech Republic

Gojko Vladić

University of Novi Sad, Novi Sad, Serbia

Thomas Sabu

Mahatma Gandhi University, Kottayam, India

Behudin Mešić

Karlstad University, Karlstad, Sweden

Vladan Končar

ENSAIT, Roubaix, France

Arif Özcan

Marmara University, Istanbul, Turkey

Tim C. Claypole

Swansea University, Swansea, United Kingdom

Alexandra Pekarovicova

Western Michigan University, Kalamazoo, USA

Michal Čeppan

Slovak University of Technology in Bratislava, Slovakia

Panagiotis Kyratsis

University of Western Macedonia, Kozani, Greece

Art Director

Uroš Nedeljković

Layout design

Bojan Banjanin
Tamara Ilić

Journal cover design

Nada Miketić

JOURNAL OF GRAPHIC ENGINEERING AND DESIGN

Volume 16, Number 4, December 2025.

Contents

- 5 **Production of pH indicators from starch and anthocyanins for use in smart packaging**
Sanja Mahović Poljaček, Eva Đakulović, Tamara Tomašegović, Sonja Jamnicki Hanzer, Maja Strižić Jakovljević, Urška Kavčič, Gregor Lavrič, Igor Karlovits
- 13 **Geometric synthesis and kinematic analysis of a combined double-wedging mechanism of the pressure plate drive in the die-cutting press**
Vitalii Vlakh, Ivan Rehej, Oleh Knysh
- 25 **A framework of project-based learning (PBL) pedagogy for graphic design education**
Kanupriya Taneja
- 37 **Prediction of dot gain in flexographic color printing using machine learning**
Soumen Basak, Saritha P.C, Alenrex Maity, Kanai Chandra Paul
- 51 **Sustainable active packaging for the EU green transition: HEC/vitamin C antioxidant films enhancing food safety and reducing waste**
Emine Arman Kandirmaz, Arif Ozcan

Production of pH indicators from starch and anthocyanins for use in smart packaging

ABSTRACT

In this research, natural pigments, anthocyanins, were used to produce bio-based films that can be used in smart packaging, as they serve as pH indicators to monitor the freshness of the packaged products. The aim of the research is to analyse the colorimetric and optical differences in the produced films before and after they are exposed to the environment with different pH values. In order to evaluate the possibility of using the produced films in printing processes, the adhesion of the produced pH indicators to packaging material was determined. This research has shown that it is possible to produce pH indicators from anthocyanins extracted from plant residues as well as from different types of starch. The influence of the anthocyanins immobilised in the starches on the colorimetric properties of the produced films and the adhesion of the films to the packaging material was evaluated. The research results showed that it is possible to produce a pH-responsive indicator based on the ingredients used. Different types of starch showed no significant difference in the visual appearance of the films, but a difference was found when different anthocyanins were used. It was proposed to use potato starch with anthocyanins from red cabbage and maize starch with anthocyanins from red onions to produce pH indicators. These polymer composites showed clear color shifts that are easy to recognise visually.

KEY WORDS

smart packaging, pH-indicators, anthocyanins, biodegradable composite films

Sanja Mahović Poljaček¹ 

Eva Đakulović¹

Tamara Tomašegović¹ 

Sonja Jamnicki Hanzer¹ 

Maja Strižić Jakovljević¹ 

Urška Kavčič² 

Gregor Lavrič² 

Igor Karlovits^{3,4} 

¹ University of Zagreb, Faculty of Graphic Arts, Zagreb, Croatia

² Pulp and Paper Institute, Ljubljana, Slovenia

³ Danfoss Trata d.o.o., Šentvid, Slovenia

⁴ National Institute of Chemistry, Ljubljana, Slovenia

Corresponding author:

Sanja Mahović Poljaček

e-mail:

sanja.mahovic.poljacek@grf.unizg.hr

First received: 25.11.2024.

Revised: 10.3.2025.

Accepted: 27.3.2025.

Introduction

Over the last two decades, the concept of packaging has been evolved and the basic functions of traditional food packaging have been updated. A new and innovative approach to packaging has been introduced by adding new and enhanced functions to traditional packaging. Beyond the basic functions of protecting and storing goods, functions have been introduced that can monitor, sense, and communicate important information about the condition of the product throughout its life cycle. For food packaging, a number of additional advanced systems have been introduced to improve food quality, increase product safety, extend the shelf life of the

packaged product and provide more information about the packaged product through communication with the consumer (Gregor-Sveteč, 2018; Schaefer & Cheung, 2018; Thirupathi Vasuki, Kadirvel & Pejavara Narayana, 2023). Whether for food, pharmaceuticals or consumer goods, smart packaging systems provide real-time data on factors such as freshness, temperature and integrity, helping to ensure product quality and safety. Basically, smart packaging comprises two types of advanced systems: active packaging that interacts with the contents to extend shelf life or increase safety, and intelligent packaging that provides information about the condition of the product, such as time-temperature and freshness indicators, sensors and even RFID tags

that enable traceability through supply chains. By bridging the gap between the product and the consumer, smart packaging not only improves the user experience, but also plays a crucial role in reducing waste, complying with regulations and promoting sustainability (Brockgreitens & Abbas, 2016; Halonen et al., 2020).

In this research pH indicators that can be used in smart packaging applications, were produced and analysed. This type of indicator is mainly used in food packaging, as food spoilage is often associated with changes in the natural pH of fresh food, so that the freshness or spoilage of perishable food can be detected by monitoring pH changes in the packaging. By incorporating a pH indicator into the packaging, the fluctuating pH of the packaged food can be detected by a visual colorimetric response. pH indicators are usually made from natural, renewable ingredients that are biodegradable and environmentally friendly (Luo et al., 2021; Păușescu et al., 2022; Yong & Liu, 2020). They usually consist of biopolymers such as chitosan, gelatin, starch, agar and cellulose and their derivatives, which ensure the stability and flexibility of the film (Benalaya et al., 2024; Contessa et al., 2023, Liu et al., 2022).

The pH-sensing elements used are mainly the natural pigments found in fruits and vegetables (anthocyanins, red radish extracts, curcumin and beetroot extract), which can change colour in response to pH fluctuations (Chayavanich et al., 2023; Mahović Poljaček et al., 2024a). In addition, various types of plasticizers are added to ensure the flexibility and processability of the functional films, as well as crosslinking agents and additives such as various antioxidants and antimicrobial agents (Mahović Poljaček et al., 2024b).

Currently, most studies focus on the application of freshness indicators in food packaging, and the applications of smart packaging with freshness indicators in the food sector are limited. Before widespread commercial use can be achieved, several limitations associated with freshness indicators that rely on a broad color spectrum need to be addressed. A more accurate correlation between color response, product type, target metabolites and organoleptic quality and safety is needed. For this reason, further studies that provide a reliable indication of actual spoilage should be conducted to ensure the use of indicators without the risk of false negative results. In this research, potato and maize starch were used to produce biodegradable composite films. Anthocyanins extracted from the peels of red onions and red cabbage leaves were used as a pH-sensing element. The colorimetric and optical properties of the produced films were measured before and after exposure to environments with different pH values. To evaluate the possibility of using the produced films in the printing process, the adhesion of the pH indicators to the packaging material was determined.

Materials and methods

Materials and film preparation

The polymer composite for the preparation of a film-forming solution consisted of potato starch (extra pure, CAS: 9005-25-8) (Carl Roth, Germany), maize starch (extra pure, CAS: 9005-25-8) (Carl Roth, Germany), distilled water, glycerol (purity 99.5%, CAS: 56-81-5, Gram-Mol d.o.o., Croatia) and glacial acetic acid (1% v/v, CAS: 64-19-7, VWR BDH Prolabo, USA) in different concentrations. Red cabbage (*Brassica oleracea L.*) and red onions (*Allium cepa L.*) used for the extraction of anthocyanins were obtained from the local market. Commercially available pH buffers (Gram-Mol d.o.o., Croatia) (pH2-pH4 [$C_6H_8O_7$ (1-hydrate), NaOH, HCl, H_2O], pH5-pH7 [$C_6H_8O_7$ (1-hydrate), NaOH, H_2O], pH8 [H_3BO_3 , NaOH, HCl, H_2O], pH9-pH10 [H_3BO_3 , NaOH, $CaCl_2$, H_2O]) were used for the detection of color changes.

Anthocyanins were extracted from the outer leaves of red cabbage and the peels of red onions using the modified method described in the previously published study (Tan et al., 2022). The samples were milled and mechanically mixed in a 96% (v/v) ethanol solution (Pharmachem, Slovenia). Extraction was performed by mixing 200 g of sliced samples in 300 ml of ethanol. The resulting mixture was placed in a water bath at 60 °C for 90 minutes. The samples were then cooled and filtered using Whatman® Quantitative Filter Paper, ashless, grade 40 (Cytiva, USA). The anthocyanin extracts were stored in the refrigerator before use.

The film-forming solutions containing potato and maize starch were prepared by mixing starch with other components in different concentrations. The first set of samples was based on potato starch (PS) and the second on maize starch (MS). Each starch sample was dissolved in distilled water to obtain 2% (w/v) film-forming solutions and heated on a temperature-controlled hotplate (Tehtnica, Rotamix 550 MMH, Domel, Slovenia) under stirring (DLS Digital Overhead Stirrer, Velp Scientifica Srl, Italy). The pH-sensing elements, anthocyanins, extracted from red cabbage leaves (RCA) and peels of red onions (ROA) were added to each film-forming solution. Acetic acid and glycerol was slowly added to the film forming solution by gradually increasing the temperature to ensure solubilization and complete gelatinization of the ingredients. The PS film-forming solution was heated to 60 °C and the MS solution to 80 °C, as they are different types of starch and different processes occur during the production of the film samples (Pounds et al., 2021). The preparation of each starch-based film took about 30 minutes, after which the film-forming solution was poured into a Petri dish. The films were dried and stored in a ventilated climate chamber at 25 °C and 50% relative humidity (RH) for seven days.

A total of six starch-based films were produced: two samples based on PS and MS starch without anthocyanins and four samples based on PS and MS starch with anthocyanins (RCA and ROA). The samples produced and their ingredients are summarized in Table 1. The amount of ingredients refers to the total amount of film-forming solutions required for the production of starch-based films.

Table 1

The composition of film-forming solutions

Produced films	Acetic acid (%)	Glycerol (%)	ROA (%)	RCA (%)	Designation of samples
PS starch	15	3	/	/	PS
	15	3	/	14	PS_RCA
	15	3	12	/	PS_ROA
MS starch	20	5	/	/	MS
	20	5	/	14	MS_RCA
	20	5	12	/	MS_ROA

Methods

The CIE $L^*a^*b^*$ color values were measured on dry film samples before and after they were immersed in different buffer solutions. The lightness value (L^*) of a color describes its relative lightness, the a^* chromatic coordinate defines the position of the measured color between green and red and the coordinate b^* defines the position of the color between yellow and blue in the CIE color space (Fairchild, 2013). The Techkon Spectro-Dens spectro-densitometer (TECHKON GmbH, Germany) was used for the measurements. The measurement conditions were set to illuminant D50/2°, M1 filter according to ISO 13655:2017 (International Organization for Standardization, 2017). Calibration was carried out on the integrated absolute white standard and the relative CIE $L^*a^*b^*$ values (with paper as white point) were calculated. After immersing the anthocyanin-containing samples in different pH buffers for twenty minutes, the colorimetric parameters were also measured.

Images of the films immersed in different buffer solutions were taken to observe the visual change in the starch-based films produced.

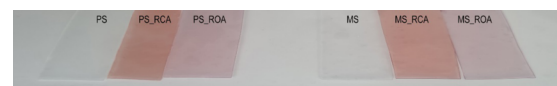
The surface properties of the dry films were investigated by calculating the surface free energy (SFE) of the samples. The SFE of the solid surface is usually measured indirectly using the results of contact angle measurements (θ) with sample liquids of known surface tension. In this study, demineralized water, glycerol and diiodomethane were used. The total surface tension, dispersive surface tension and polar surface tension,

expressed in mJ/m^2 , were 72.8, 21.8 and 51.0 for water, 64.0, 34.0 and 30.0 for glycerol and 50.8, 50.8 and 0 for diiodomethane, respectively. The contact angles were calculated according to Young's equation and the SFE according to the Owens-Wendt-Rabel and Kaelble method (Israelachvili, 2011; Owens & Wendt, 1969; Żenkiewicz, 2007). The measurements were carried out using a DataPhysics OCA 30 goniometer (DataPhysics Instruments GmbH, Germany). To determine the adhesion properties of the produced starch-based films and the polypropylene substrate, which is most commonly used for food packaging, the adhesion parameters were calculated, i.e., the spreading coefficient (S_{12}), work of adhesion (W_{12}) and the interfacial tension (γ_{12}) (Israelachvili, 2011).

Results and discussion

Optical properties of produced films

Figure 1 shows the samples of the starch-based films produced. The images were taken after the drying process, which took about seven days in a ventilated climate chamber. The films were separated from the Petri dishes for image capturing, cut into strips and applied to a transparent substrate. The transparent films (on the left side of the film sets, labeled MS and PS) are films that were produced without the addition of anthocyanins. In the middle are film samples that were produced by adding anthocyanins from red cabbage and have a pale pink color (MS_RCA and PS_RCA). The samples on the right were produced by adding anthocyanins from red onion peels and have a pale purple color (MS_ROA and PS_ROA).



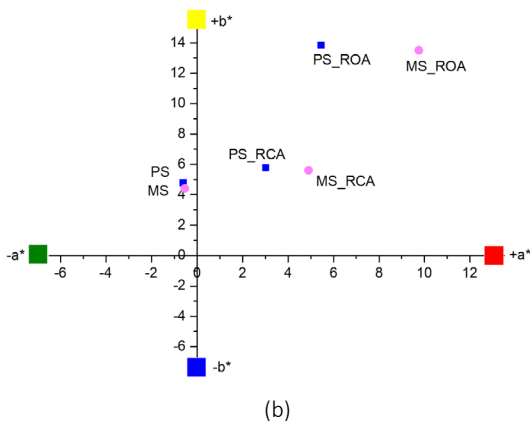
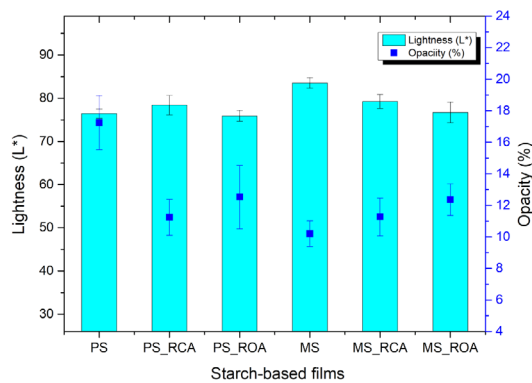
» **Figure 1:** Potato (PS) and maize (MS) starch-based films without and with anthocyanins

Figure 2 shows the optical properties of the dry films produced. The results of absolute lightness (L^*) and opacity are shown in Figure 2a. When looking at the lightness results, it can be seen that the values for all samples are relatively uniform and are between 75 and 80 lightness units. The lightness values are slightly higher for the film samples made from maize starch.

When looking at the opacity values, it can be seen that the film made from potato starch has the highest opacity (approx. 17.25 %) and the film made from maize starch has the lowest value (approx. 10.2 %). The addition of anthocyanins reduces the opacity values in the films made from potato starch and slightly increases them in the samples made from maize starch. The different types of anthocyanins show no significant difference in the optical properties of the films.

Since the starch-based films produced are relatively translucent, the color change of the samples varied depending on the composition and could sometimes be observed and visually compared better when placed on a white substrate.

For this reason, the samples were measured while placed on a white paper that served as a substrate. The relative CIE a^*/b^* color values (with paper as the white point) measured on the PS and MS film samples are shown in Figure 2b. It can be seen that the PS and MS films without the addition of anthocyanins have similar CIE a^*/b^* color coordinates with no significant differences. The addition of anthocyanins to the films shifted the color. Samples containing anthocyanins from red cabbage have lower CIE a^*/b^* color values (MS_RCA and PS_RCA) compared to samples prepared by adding anthocyanins from the peels of red onions to the films (MS_ROA and PS_ROA).



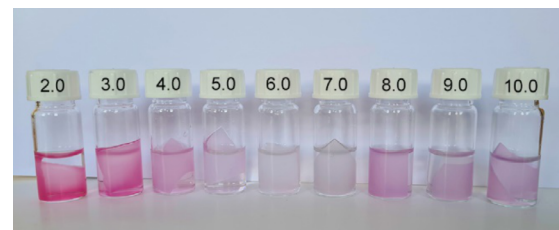
» **Figure 2:** (a) CIE lightness (L^*) values and the opacity and (b) CIE a^*/b^* color coordinates of the starch-based films

It can be said that these results were expected and that the addition of anthocyanins has a significant effect on the color shifts of the starch-based films produced. Since the intention of this research is to produce an indicator that shows a visually detectable color shift by varying the pH value, these results show the potential of the anthocyanins used for the production of a pH indicator.

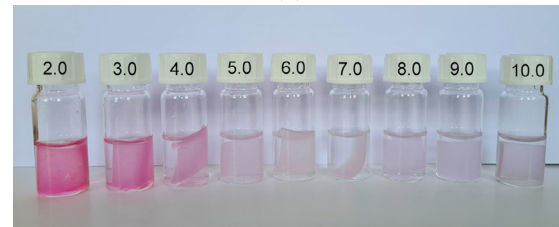
Visual analysis of produced films in varied-pH environment

To observe the color changes in the films when exposed to an environment with different pH values, the anthocyanin-containing samples were immersed in buffer solutions with a pH value of 2 to 10. The images of the samples immersed in buffer solutions for 20 minutes are shown in Figure 3.

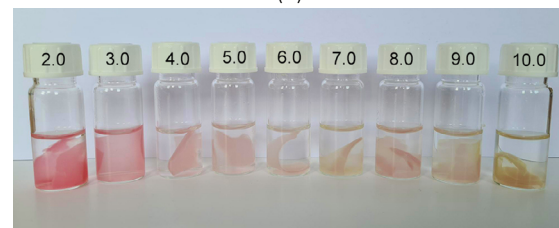
Figures 3a and 3b show PS and MS films containing anthocyanins from red cabbage and Figures 3c and 3d show films containing anthocyanins from red onion peels. It can be seen that the samples show considerable color differences at different pH values, which is primarily due to the fact that the anthocyanins are extracted from different plants. The color of the starch-based films with red cabbage anthocyanins changed from pink (pH2) to colorless (pH7) and light pink at pH10. The color of the starch-based films with anthocyanins from the peel of red onions changed from reddish-pink (pH2) to light red (pH7) and pinkish-yellowish at pH10.



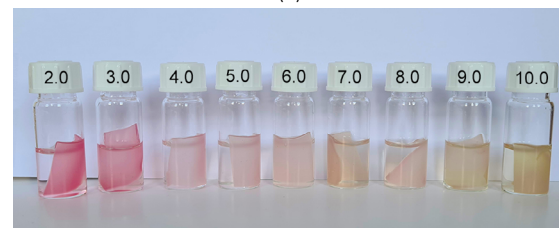
(a)



(b)



(c)



(d)

» **Figure 3:** Images of the films immersed in different buffer solutions: (a) PS_RCA, (b) MS_RCA, (c) PS_ROA and (d) MS_ROA

These visual color changes observed on starch-based films proved that the films produced can provide information on whether the pH of the food or the pH of the environment is varying. Different fresh meat must have a pH in the range of 5.5 to 6.2 (Sujiwo, Kim & Jang, 2018). The initial spoilage of meat or fish occurs at a pH of around 6, and then the pH continues to drop in small intervals to around 4 or 5. When the pH drops to around 2, yeasts and other microorganisms can continue to grow on the food and make it unusable and spoiled (Pounds et al., 2021). On the other hand, increased pH is associated with the production of nitrogenous basic compounds, mainly amino groups, which also cause the microbial spoilage of packaged foods (Triki et al., 2018).

Colorimetric properties of produced films in varied-pH environment

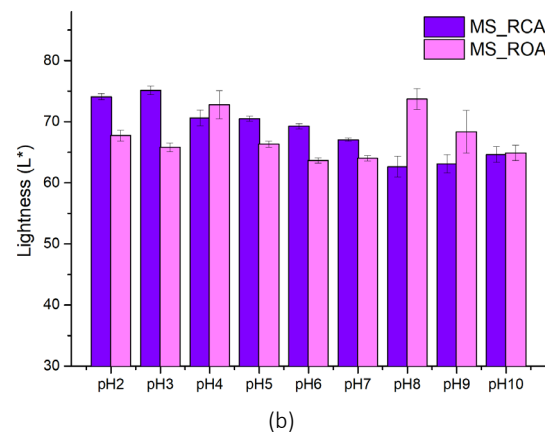
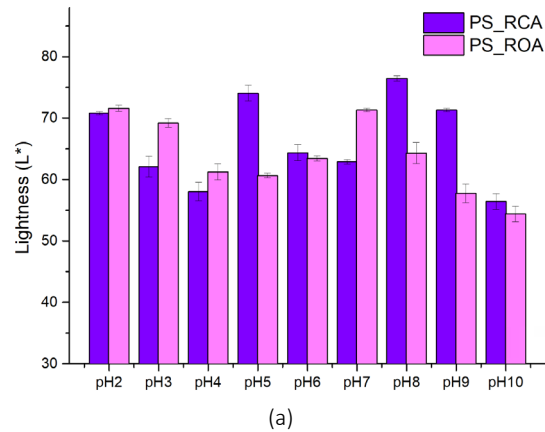
After immersion, the films were dried and additional measurements of the colorimetric properties were carried out. The results of the lightness are shown in Figure 4. Figure 4a shows the PS-starch-based films with RCA and ROA anthocyanins and Figure 4b shows the MS-starch-based films with RCA and ROA anthocyanins. It can be seen that the lightness values for the films produced with the same starch type are similar and that the addition of different anthocyanins has no significant effect on the lightness. There are some exceptions with PS-based films where it appears that the RCA causes the higher lightness values, but these results may be the consequence of the irregular measurement conditions due to the uneven surfaces and thickness of the films. Overall, the lightness results show that higher values are obtained for MS films than for PS films, which may be due to the higher initial value of MS films (compared to PS films) produced without anthocyanins, as shown in Figure 2a.

Figures 5 and 6 show the changes in the CIE color coordinates a^* and b^* of the dried PS- and MS-based films after immersion in different buffer solutions from pH2 to pH10; a polynomial trendline was added to the plots. The results are presented according to the type of anthocyanins used in the film production. Figure 5 shows the relative CIE a^*/b^* values of the PS_RCA and MS_RCA films and Figure 6 shows the relative CIE a^*/b^* values of the PS_ROA and MS_ROA films. The circled ellipses show the ranges of the chromatic CIE a^*/b^* coordinates for films immersed in pH5 and pH6 solutions corresponding to the pH values of fresh meat and seafood (depending on type of product). Deviations from these pH values may indicate possible spoilage of the packaged food due to irregular storage, improper handling, expiration date and other causes.

The results shown in Figure 5 show that the changes in the CIE a^* and b^* values of PS_RCA and MS_RCA films (films with red cabbage anthocyanins) lie in the range

between the red and blue color coordinates. It can be said that PS films show a slightly wider range of color shifts than MS films after immersion in different buffer solutions and that the PS_RCA films show a more pronounced shift to the reddish hue ($+a^*$ values).

These results may indicate that the color changes that can occur due to the variation in pH are visually more pronounced in the PS-based films compared to MS films.

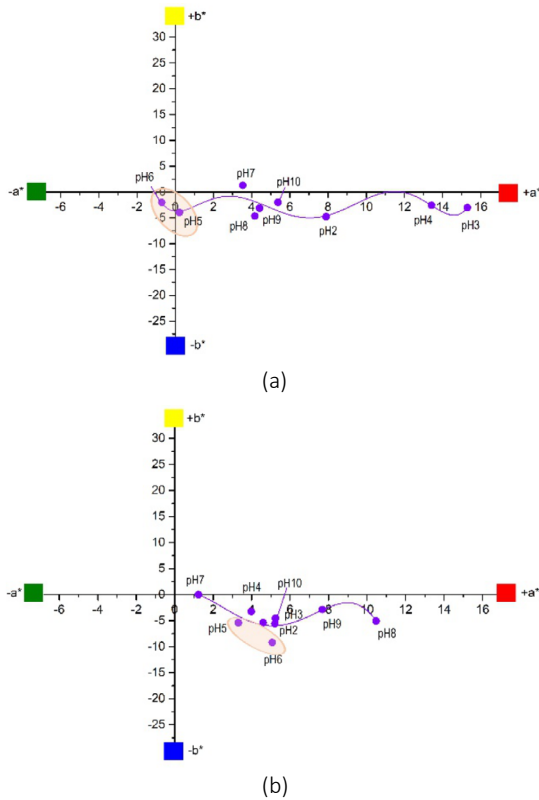


» **Figure 4:** Relative CIE L^* values of the films immersed in different buffer solutions: (a) PS_RCA and PS_ROA, (b) MS_RCA and MS_ROA

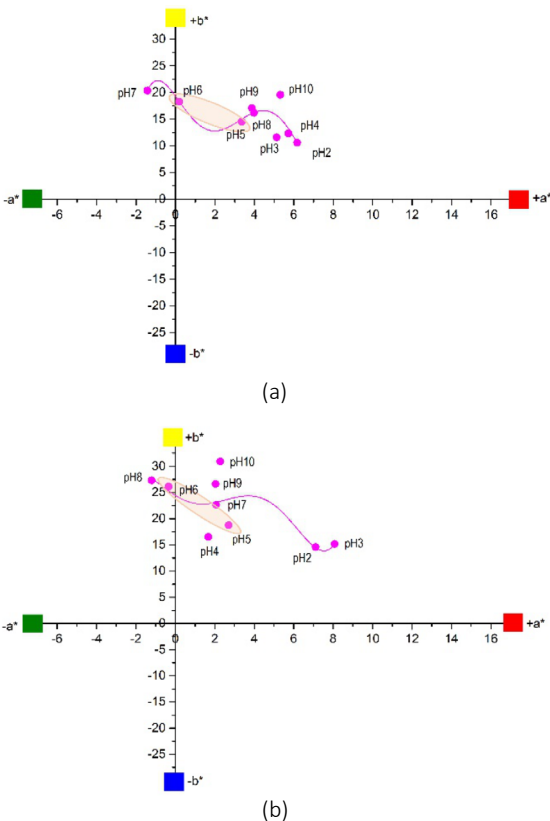
The results of the PS and MS films with anthocyanins from the peels of red onions are shown in Figure 6 and show the color shifts in the areas between the yellow and red coordinates. Compared to the MS_ROA films, the PS_ROA films show a slightly stronger color shift towards the yellowish ($+b^*$ values) and reddish hue ($+a^*$ values).

From the results shown in Figures 5 and 6, it can be concluded that the produced films show visible color shifts when exposed to a different pH environment.

It can be suggested that to prepare a pH indicator from PS and MS starch, PS starch with red cabbage anthocyanins and MS starch with red onion anthocyanins should be used. These polymeric composites show expressed color shifts that are easy to detect visually.



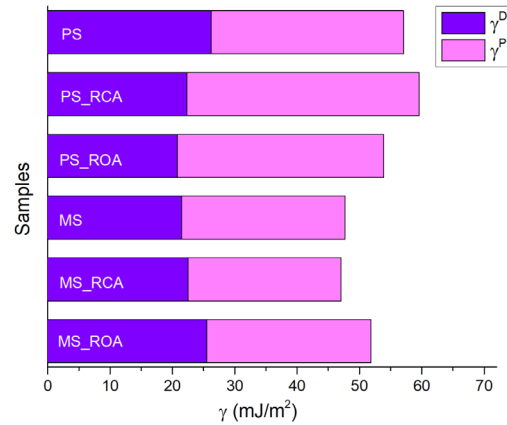
» **Figure 5:** Relative CIE a^*/b^* values of the films immersed in different buffer solutions: (a) PS_RCA and (b) MS_RCA



» **Figure 6:** Relative CIE a^*/b^* values of the films immersed in different buffer solutions: (a) PS_ROA and (b) MS_ROA

Surface and adhesion properties of the films

Figure 7 presents the results of the calculated surface free energy (γ) and its dispersive (γ^D) and polar (γ^P) components for PS- and MS-based films. The evaluation of the SFE results of the starch-based films is particularly important for packaging as it can predict the interactions with the specific substrate that comes into contact with the pH-sensitive films. In addition, the SFE of the produced films can be helpful in discussing other interactions that may occur within the packaging surface layer. From the calculated results, it appears that PS films have slightly higher total SFE values compared to MS films and that all film-samples contain higher values of polar (γ^P) than dispersive (γ^D) components. These changes are generally enhanced after the addition of anthocyanins, which is probably due to the polarity of the anthocyanins.



» **Figure 7:** Surface free energy components of PS- and MS-based films, with and without anthocyanins

In order to observe the interaction between polypropylene, the most commonly used substrate for packaging fresh meat, and the films produced, the adhesion parameters were calculated. The SFE of the polypropylene was calculated using the Owens-Wendt-Rabel and Kaelble method by applying probe liquids to the polypropylene surface and using the measured contact angle data. It was calculated that the total SFE of polypropylene is 52.24 mJ/cm², with the dispersive component corresponding to 31.74 mJ/cm² and the polar component corresponding to 19.51 mJ/cm². The results of the adhesion parameters, the interfacial tension (γ_{12}), thermodynamic work of adhesion (W_{12}) and the spreading coefficient (S_{12}) are shown in Table 2. For optimal adhesion, the value of the interfacial tension should be positive or equal to zero, the value of the work of adhesion should be as high as possible and the spreading coefficient should be close to zero.

From the results, the interfacial properties between polypropylene and the starch-based films without and with anthocyanins are similar and show good adhesion

between the films and the substrate. It can be said that starch-based MS films have a slightly poorer adhesion than PS films, as they have a slightly lower work of adhesion value and a slightly lower spreading coefficient value. Although the adhesion results are quite positive, further analyses should be carried out that include additional observations of the interactions between the pH films produced and the substrates used, such as the stability on the surface and sensing properties, the influence of moisture, different storage temperatures, etc.

Table 2

Adhesion parameters between the starch-based films and polypropylene

Sample	γ_{12} (mJ/m ²)	W_{12} (mJ/m ²)	S_{12} (mJ/m ²)
PS-film	2.55	106.75	2.27
PS_RCA	4.92	107.15	2.67
PS_ROA	3.93	102.19	-2.29
MS-film	2.48	97.45	-7.03
MS_RCA	2.08	97.21	-7.27
MS_ROA	1.83	102.26	-2.22

Conclusion

In this research, starch-based films with natural pigments anthocyanins, were used to produce a bio-based pH-responsive indicator. The research results showed that it is possible to produce a pH-responsive indicator based on potato and maize starch with anthocyanins extracted from the peels of red onions and red cabbage leaves.

When measuring the optical properties of the films produced, it was found that the lightness values were slightly higher for the film samples produced from potato starch than for the films produced from maize starch. Immersion of the anthocyanin-containing starch-based films in different buffer solutions (from pH2 to pH10) showed that the prepared films can be used as pH indicators as they changed their color in different pH environments. Different types of starch showed no significant difference in the visual appearance of the films, but the difference was found when different anthocyanins were used. It was proposed to use PS starch with anthocyanins from red cabbage and MS starch with anthocyanins from red onion to produce a pH indicator from PS and MS starch. These polymer composites show expressed color shifts that are easy to detect visually.

The surface free energy of the starch-based films was measured to observe the surface properties of the films and to determine the adhesion of the films to the packaging material. It was found that potato-based films had slightly higher overall surface free energy values compared to maize-based

films and that all samples contained higher values of polar than dispersive components. These results are particularly important for packaging as they can predict the interactions with the substrate that comes into contact with the pH-sensitive films.

The results presented in this study demonstrate the possibility of using starch-based films with anthocyanins as pH indicators in smart packaging. Further research in this area is planned to observe the stability of the produced indicators at different storage temperatures, to further investigate their sensing properties, the influence of moisture, the measurement of mechanical properties and water barrier properties and to define the other interactions with different packaging materials.

Funding

The research did not receive any specific grant from funding agencies in the public, commercial, or not-for-profit sectors.

References

- Benalaya, I., Alves, G., Lopes, J. & Silva, L. R. (2024) A review of natural polysaccharides: sources, characteristics, properties, food, and pharmaceutical applications. *International Journal of Molecular Sciences*. 25 (2), 1–32. Available from: doi: 10.3390/ijms25021322
- Brockgreitens, J. & Abbas, A. (2016) Responsive food packaging: recent progress and technological prospects. *Comprehensive Reviews in Food Science and Food Safety*. 15 (1), 3–15. Available from: doi: 10.1111/1541-4337.12174
- Chayavanich, K., Kaneshige, R., Thiraphibundet, P., Furuike, T., Tamura, H. & Imyim, A. (2023) pH-responsive nanofibrous membrane fabricated from gelatin and red radish anthocyanins for meat spoilage monitoring. *Dyes and Pigments*. 216. Available from: doi: 10.1016/j.dyepig.2023.111331
- Contessa, C. R., Rosa, G. S. d., Moraes, C. C. & Burkert, J. F. d. M. (2023) Agar-agar and chitosan as precursors in the synthesis of functional film for foods: a review. *Macromolecules*. 3, 275–289. Available from: doi: 10.3390/macromol3020017
- Fairchild, M. D. (2013) *Color appearance models*. Hoboken, John Wiley & Sons, Ltd. Available from: doi: 10.1002/9781118653128
- Gregor-Svetec, D. (2018) Intelligent packaging. In: *Nanomaterials for food packaging*. Amsterdam, Elsevier. Available from: doi: 10.1016/B978-0-323-51271-8.00008-5
- Halonen, N., Pálvölgyi, P. S., Bassani, A., Fiorentini, C., Nair, R., Spigno, G. & Kordas, K. (2020) Bio-based smart materials for food packaging and sensors – a review. *Frontiers in Materials*. 7 (82), 1–14. Available from: doi: 10.3389/fmats.2020.00082

- International Organization for Standardization. (2017) *ISO 13655:2017. Graphic technology – spectral measurement and colorimetric computation for graphic arts images*. Geneva, International Organization for Standardization.
- Israelachvili, J. (2011) *Intermolecular and surface forces*. 3rd ed. Waltham, Academic Press. Available from: doi: 10.1016/C2009-0-21560-1
- Liu, D., Zhang, C., Pu, Y., Chen, S., Liu, L., Cui, Z. & Zhong, Y. (2022) Recent advances in pH-responsive freshness indicators using natural food colorants to monitor food freshness. *Foods*. 11 (13), 1–25. Available from: doi: 10.3390/foods11131884
- Luo, Q., Hossen, A., Sameen, D. E., Ahmed, S., Dai, J., Li, S., Qin, W. & Liu, Y. (2021) Recent advances in the fabrication of pH-sensitive indicator films and their application for food quality evaluation. *Critical Reviews in Food Science and Nutrition*. 57, 3373–3383. Available from: doi: 10.1080/10408398.2021.1959296
- Mahović Poljaček, S., Jamnicki Hanzer, S., Strižić Jakovljević, M., Tomašegović, T., Karlovits, I., Kavčič, U. & Lavrič, G. (2024a) Colorimetric properties of starch-based films with anthocyanins from agro waste for smart packaging applications. In: *Proceedings of the 9th Conference on Information and Graphic Arts Technology, 11–12 April 2024, Ljubljana, Slovenia*. Ljubljana, University of Ljubljana, Faculty of Natural Sciences and Engineering. pp. 66–72.
- Mahović Poljaček, S., Tomašegović, T., Strižić Jakovljević, M., Jamnicki Hanzer, S., Murković Steinberg, I., Žuvić, I., Leskovac, M., Lavrič, G., Kavčič, U. & Karlovits, I. (2024b) Starch-based functional films enhanced with bacterial nanocellulose for smart packaging: physicochemical properties, pH sensitivity and colorimetric response. *Polymers*. 16, 1–20. Available from: doi: 10.3390/polym16162259
- Owens, D. K. & Wendt, R. C. (1969) Estimation of the surface free energy of polymers. *Journal of Applied Polymer Science*. 13, 1741–1747. Available from: doi: 10.1002/app.1969.070130815
- Păușescu, I., Dreavă, D. M., Bîțcan, I., Argetoianu, R., Dăescu, D. & Medeleanu, M. (2022) Bio-based pH indicator films for intelligent food packaging applications. *Polymers*. 14. Available from: doi: 10.3390/polym14173622
- Pounds, K., Jairam, S., Bao, X., Meng, S., Zhang, L., Godinez, S. A., Savin, D. A., Pelletier, W., Correll, M. J. & Tong, Z. (2021) Glycerol-based dendrimer nanocomposite film as a tunable pH sensor for food packaging. *ACS Applied Materials & Interfaces*. 13, 23268–23281. Available from: doi: 10.1021/acsami.1c05145
- Schaefer, D. & Cheung, W. M. (2018) Smart packaging: opportunities and challenges. In: *Proceedings of the 51st CIRP Conference on Manufacturing Systems, CIRP CMS 2018, Procedia CIRP 72, 16-18 May 2018, Stockholm, Sweden*. Amsterdam, Elsevier. pp. 1022–1027. Available from: doi: 10.1016/j.procir.2018.03.240
- Sujiwo, J., Kim, D. & Jang, A. (2018) Relation among quality traits of chicken breast meat during cold storage: correlations between freshness traits and torrymeter values. *Poultry Science*. 97 (8), 2887–2894. Available from: doi: 10.3382/ps/pey138
- Tan, J., Han, Y., Han, B., Qi, X., Cai, X., Ge, S. & Xue, H. (2022) Extraction and purification of anthocyanins: a review. *Journal of Agriculture and Food Research*. 8. Available from: doi: 10.1016/j.jafr.2022.100306
- Thirupathi Vasuki, M., Kadirvel, V. & Pejavara Narayana, G. (2023) Smart packaging – an overview of concepts and applications in various food industries. *Food Bioengineering*. 2, 25–41. Available from: doi: 10.1002/fbe2.12038
- Triki, M., Herrero, A. M., Jiménez-Colmenero, F. & Ruiz-Capillas, C. (2018) Quality assessment of fresh meat from several species based on free amino acid and biogenic amine contents during chilled storage. *Foods*. 7 (9). Available from: doi: 10.3390/foods7090132
- Yong, H. & Liu, J. (2020) Recent advances in the preparation, physical and functional properties, and applications of anthocyanin-based active and intelligent packaging films. *Food Packaging and Shelf Life*. 26. Available from: doi: 10.1016/j.fpsl.2020.100550
- Żenkiewicz, M. (2007) Methods for the calculation of surface free energy of solids. *Journal of Achievements in Materials and Manufacturing Engineering*. 24, 137–145.






Geometric synthesis and kinematic analysis of a combined double-wedging mechanism of the pressure plate drive in the die-cutting press

ABSTRACT

The analysis of existing publications highlights a gap in scientific research on mechanisms used in the drive system to move the pressure plate, particularly those that extend the contact duration between the die-cutting mold and cardboard. The authors developed a kinematic scheme of the proposed double-wedging mechanism. The geometric synthesis and kinematic analysis of the mechanism were performed, determining the relative values of key geometric parameters, displacement, velocity, and acceleration of the pressure plate. The geometry and kinematic parameters were calculated using mathematical models based on similarity invariants. To validate the results, a simulation of the work process was conducted in the SolidWorks program for the double-wedging mechanism and the existing mechanism used in Bobst presses. A comparative analysis of the analytically obtained kinematic dependencies and the simulation results demonstrated absolute agreement, confirming the accuracy of the developed mathematical models. The results of the kinematic analysis indicate that using a combined two-wedging mechanism doubles the duration of the die-cutting tool with the cardboard blank. This prolonged contact positively impacts the efficiency of die-cutting operations, particularly for creasing and relief embossing.

KEY WORDS

die-cutting press, cardboard blank, double-wedging mechanism, crank, pressure plate, analysis

Vitalii Vlach 
Ivan Rehei¹ 
Oleh Knysh¹ 

¹ Lviv Polytechnic National University, Lviv, Ukraine

Corresponding author:
Vitalii Vlach
e-mail:
vlakh.v.v@gmail.com

First received: 24.11.2024.
Revised: 3.3.2025.
Accepted: 10.3.2025.

Introduction

Die-cutting of cardboard blanks is the primary method for manufacturing packaging. Using a flat die-cutting mold, operations such as cutting, creasing, and cold embossing of sheet cardboard blanks are carried out (Fig. 1). Flat die-cutting molds allow the production of cardboard packaging in various sizes and shapes (Emblem & Emblem, 2012).

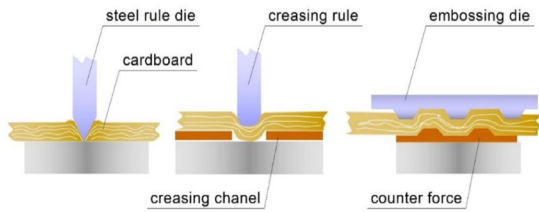
The mold consists of steel cutting and creasing rules embedded in a laser-cut plywood base. The pressure plate contains creasing and embossing matrices for pressing. Ejector elements facilitate the removal of die-cut blanks from the blades.

Paper and cardboard packaging are widely used due to their recyclability, durability, aesthetic appeal, and versatility. Ensuring high quality in production requires precise technological processes (Kirwan, 2013).

The manufacturing process of cardboard containers involves several automated technological operations. The chain of technological operations is carried out automatically during stops of the cardboard blank using transportation in the equipment sections (Rehei, 2011).

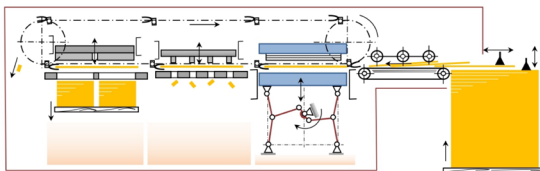
Modern die-cutting equipment is built according to the sectional principle. As an example, the BOBST multi-section die-cutting machine (Fig. 2) consists of the following units:

- cardboard blank feeding and stacking section
- die-cutting press section
- scrap removal section
- separation and stacking section



» **Figure 1:** Tools of the press pair of the die-cutting operation of sweeps for cutting, creasing, and cold embossing

The movement of semi-finished products between sections is performed by carriages attached to chain conveyors. The die-cutting press section is particularly critical as it utilizes wedging mechanisms to drive the pressure plate.



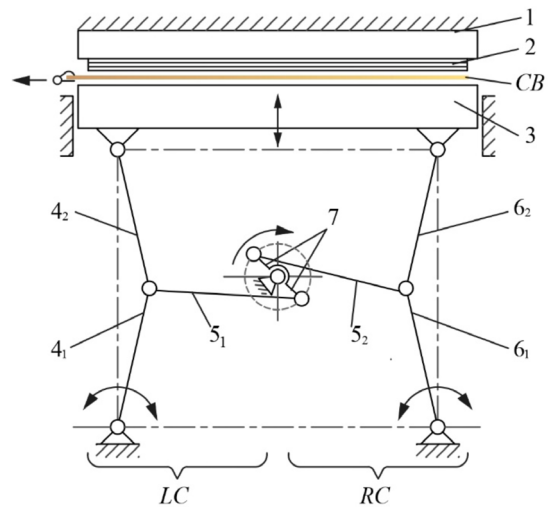
» **Figure 2:** Scheme of a multi-section die-cutting machine

The operation principle of BOBST die-cutting presses has been successfully implemented in such models as AUTOPLATEN, EXPERTCUT, and MASTERCUT. In these machines, a flat die-cutting mold 2 is fixed on the upper stationary plate 1 (Fig. 3). The pressure on the workpiece *CB* is created by the pressure plate 3, which receives reciprocating motion along the guides from the two-circuit lever mechanism of second-class. Hinges connect the two-armed crank 7, to which connecting rods 5_1 and 5_2 transmit motion to driving rods 4, and 6_1 . Connecting rods 4_2 and 6_2 are connected to driving rods, which transmit motion to plate 3.

The mechanism's construction involves the mutual arrangement of lever pairs $4_1, 4_2$, and $6_1, 6_2$ in the uppermost pressure plate position 3, ensuring that the angle between them approaches 180° . This configuration enables the attainment of the "wedging effect"- the significant technological efforts developed by the pressure plate at the moment of contact with the cardboard blank.

Rehei et al. (2022) analyzed four existing drive mechanisms, among which are mechanisms used in the die-cutting equipment of the BOBST and Heidelberg companies. According to the analytical analysis results, the pressure plate's acceleration in the existing wedging mechanism

(BOBST) reaches its maximum value at the moment it contacts the die-cutting mold.



» **Figure 3:** The kinematic scheme of the existing wedging mechanisms of the pressure plate drive

Khvedehyn & Zelenyi (2014) analyzed the existing structures of the pressure plate drive mechanisms in die-cutting equipment. As the authors note, their design causes asymmetry of the right and left parts of the pressure plate during motion. The symmetry of the plate movement is observed only at the final stage of its movement: the working surface of the pressure plate becomes parallel to the support plate surface during the cutting and creasing of cardboard blanks. Such asymmetry causes uneven load distribution and generates pressure plate oscillations in the press, which reduces its operation efficiency. Analytical studies of various pressure plate drive mechanisms allow us to assess their efficiency. In their research work Kuznetsov, Kolomiets & Dimitraschuk (2012) conducted analytical studies of a flat die-cutting press with an existing wedging mechanism in the pressure plate drive. Analytical studies proved the presence of uneven movement during the cycle of movement of the pressure plate.

Lin, Zhou & Huang (2015) also studied a die-cutting press with a wedging mechanism. The analysis carried out by the authors showed high values of the pressure plate's inertia force during its motion. That has a significant impact on the drive mechanism of the die-cutting press and its kinematic accuracy. It is essential that when the maximum acceleration is reached, a shock load will occur. Considering the shortcomings, the authors proposed an optimized pressure plate drive mechanism. The main goal of implementing the proposed mechanism is to improve the characteristics of the pressure plate movement. A cam mechanism is presented in the drive of the pressure plate. However, the design of this mechanism is complicated due to the production of drive cams with two contact profiles.

In addition, such drive cams are dimensional. Shakhbazov et al. (2020) proposed a new design of wedging cam mechanisms to drive the pressure plate in die-cutting presses. The authors conducted theoretical calculations of technological loads that occur during the cutting and creasing of cardboard blanks.

The authors also investigated the driving forces arising in the proposed lever-cam mechanism. Despite some design simplification, the mechanism still needs to be improved to be set up and operated. In addition, the authors did not conduct experimental studies of the proposed mechanism.

Authors Pasika & Vlach (2016) developed a methodology for optimizing the central shaft functioning of the wedging mechanism. It makes it possible to increase the efficiency of die-cutting presses, provided that its energy consumption is reduced. The authors obtained analytical dependencies for the synthesis of the mechanism. The authors suggested using a two-armed crank on the main shaft with a defined swing angle, calculated based on the synthesis results, to avoid uneven pressure plate movement. Vlach & Pasika (2016) also suggested installing an additional four-link or rocker mechanism in the drive to improve the quality of die-cutting cardboard blanks.

However, using additional mechanisms as part of the drive complicates the design and adjustment of die-cutting presses. Kuznetsov, Rehei & Vlach (2017) proposed using a two-slider combined mechanism to eliminate the disadvantages associated with uneven movement of the pressure plate and reduce the press's dimensions. The proposed mechanism consists of two crank-slider circuits: drive and driven. Using this mechanism reduces the overall load and peak kinetic energy consumption.

However, in addition to the significant advantages of the proposed mechanism, it creates much less effort during the die-cutting process than the existing wedging mechanism.

In the research work of Wang, Chen & Li (2023) experimental studies of the existing press with a wedging mechanism of the pressure plate drive were carried out. The press, loaded with the maximum technological die-cutting resistance of 350 tons under the condition of the rotation frequency of the main shaft of 125 rpm, was studied. An engineering decision changed the design of the drive rod, leading to a significant reduction in pressure plate oscillation.

To solve problems related to the shortcomings of the design of the existing mechanism and the task of increasing the duration of contact of the die-cutting tool with the cardboard blank, Rehei et al. (2023) proposed using a gear with an additional driven crank in the driven circuit of the wedging mechanism.

The design of the proposed mechanism, where the driven crank is in the lower initial position, has a positive effect on the creasing and embossing operations of the cardboard. Such a construction of the mechanism should eliminate the operational shortcomings associated with the oscillation of the pressure plate during the mechanism's kinematic cycle. In such a mechanism, the plate approaches more slowly. It is placed parallel to the stationary plate even before the technological operation is performed, and the oscillating movement does not affect the quality of die-cutting cardboard sweeps.

There is no information in the scientific information space on the research of the mechanisms of the movement of the pressure plate with an increased duration of contact of the die-cutting tools with the cardboard. Scientific research in this direction is essential and actual.

The work aims to synthesize and evaluate the quantitative and qualitative characteristics of the kinematic parameters of the double-wedging mechanism in the pressure plate drive of the die-cutting press.

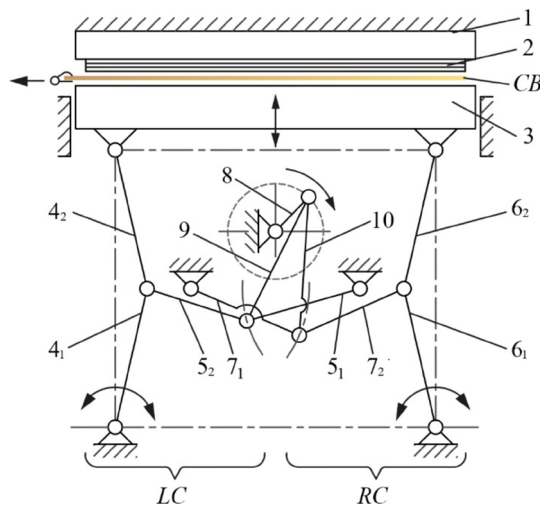
The following tasks must be solved to achieve the goal:

- to conduct a critical analysis of scientific research in the direction of improving die-cutting presses and formulate the goal and objectives of the study
- to develop a kinematic scheme of the double wedging mechanism of the pressure plate drive of the die-cutting press
- to perform a geometric synthesis of the proposed mechanism
- to develop a methodology for calculating the kinematic parameters of the proposed combined double-wedging mechanism
- to calculate the relative kinematic parameters of the proposed combined double-wedging mechanism of the pressure plate drive
- to conduct a virtual experiment of the mechanism and investigate its kinematic parameters in the SolidWorks software (Dassault Systèmes, France)
- to perform a comparative analysis of the analytical studies' results with the results of a virtual experiment of the existing and proposed double-wedging mechanisms in the SolidWorks program

The press of the die-cutting machine proposed by the authors consists of an upper stationary plate 1 (Fig. 4), fixed to the base, with a flat die-cutting mold 2; movable pressure plate 3; a set of wedging mechanisms of the left circuit *LC*: lever 4₁ and connecting rod 4₂ of the vertical wedging circuit, lever 5₁ and connecting rod 5₂ of the horizontal wedging circuit; a set of wedging circuits of the right circuit *RC*: lever 6₁ and connecting rod 6₂ of the vertical wedging mechanism, lever 7₁ and connecting rod 7₂ of the horizontal wedging circuit; crank 8; left 9 and right 10 connecting rods of the driving wedging circuits.

The press of the die-cutting machine works as follows. In the initial position, pressure plate 3 is in the lower position, and the cardboard blank is in the die-cutting zone. When turning the crank 8 clockwise, left 9 and right 10 connecting rods wedge the horizontal circuits by aligning lever 5₁ and connecting rod 5₂ of the left circuit LC and lever 7₁ and connecting rod 7₂ of the right circuit RC.

As a result of this action, the vertical circuits are wedged by aligning lever 4₁ and connecting rod 4₂ of the left circuit LC and lever 6₁ and connecting rod 6₂ of the right circuit RC, which ensures the lifting of the pressure plate 3 and die-cutting the sweeps with tools of mold 2 in its upper position. Further crank rotation clockwise 8 leads to decreased angles between the links of all wedging circuits. This causes pressure plate 3 to be lowered to remove the die-cut cardboard blank CB and feed it into the die-cutting zone.



» **Figure 4:** The kinematic scheme of the double-wedging drive mechanism of the die-cutting press

Methods, CAD/CAE Analysis

Geometric Synthesis of the Mechanism

Two identical combined mechanisms of the left LC and right RC circuits drive the pressure plate. The geometric synthesis and kinematic analysis focus on a single contour, specifically the left circuit.

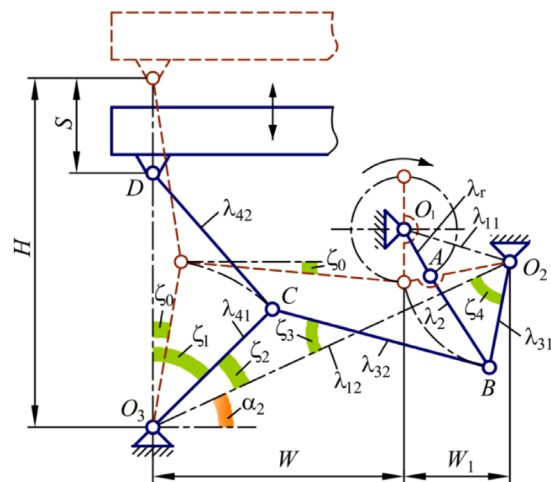
Relative and absolute parameters were defined to calculate the kinematic characteristics of the double-wedging mechanism's left contour.

The values are obtained from the proportion of the actual die-cutting press dimensions:

- $S = 1$ – maximum linear displacement of the pressure plate (Fig. 5)
- $W = 3.125$ – horizontal distance between supports O_1 and O_3 of the wedging mechanism of the left circuit
- $W_1 = 1.5625$ – horizontal distance between supports O_1 and O_2 of the wedging mechanism of the left circuit
- $H = 6.25$ – total height of the mechanism

Designation of absolute parameters:

- ϕ – angle of rotation of the driving crank
- $\gamma_0 = 5^\circ$ restriction angle of wedging contours to avoid "jamming" of the mechanism



» **Figure 5:** Scheme for calculating the left contour of the double-wedging mechanism of the pressure plate drive (determination of links and extreme position angles of the driving and driven contours)

For the kinematic calculation of the mechanism, its main relative geometric parameters are determined based on the conducted synthesis:

- λ_r – the driving crank size (Fig. 5)
- λ_{11} – the interbase distance between axes O_1 and O_2
- λ_{12} – the interbase distance between axes O_3 and O_2
- λ_2 – the connecting rod length of the driving circuit
- λ_{31} – the lever length of the horizontal wedging circuit
- λ_{32} – the power rod length of the horizontal wedging circuit
- λ_{41} – the lever length of the vertical wedging circuit
- λ_{42} – the connecting rod length of the vertical wedging circuit

Mathematical models using similarity invariants were developed to determine the rational design parameters and ensure optimal mechanism operation. Equations were formulated to calculate angles, distances, and link lengths, establishing a foundation for further kinematic analysis. All equations were derived by the authors during the project's work.

The well-known method of calculating initial and combined mechanisms involves using a "single" mechanism (Poliudov, 2005). The driving crank is assumed to be equal to one ($O_1A = 1$, Fig. 5). The synthesis of the double-wedging mechanism of the pressure plate drive developed in this paper involves a "reverse" calculation. Here, the "unit" is the relative linear movement $S = 1$ of the driven link- the pressure plate, corresponding to its movement ($S_{max} = 80$ mm, 3.14961 in) in the BOBST die-cutting presses.

The primary geometric parameters were defined according to the following geometric dependencies to carry out a geometric synthesis of the researched mechanism.

The angle of inclination α_2 of the interbase distance λ_{12} to the vertical axis:

$$\alpha_2 = \arctan\left(\frac{H}{2 \cdot (W + W_1)}\right) \quad (1)$$

The relative length of the drive rod λ_{41} of the driven circuit and the connecting rod length λ_{42} of the driven circuit ($\lambda_{42} = \lambda_{41}$):

$$\lambda_{42} = H \cdot \frac{\sin(\xi_0)}{\sin(\pi - 2 \cdot \xi_0)} \quad (2)$$

The angle of inclination ξ_1 to the vertical of the drive rod λ_{41} in the mechanism's lowermost position:

$$\xi_1 = \arccos\left(\frac{(H - S)^2}{2 \cdot \lambda_{42} \cdot (H - S)}\right) \quad (3)$$

The relative length of the power rod λ_{32} of the driven circuit:

$$\lambda_{32} = \frac{W - \lambda_{42} \cdot \sin(\xi_0)}{\cos(\xi_0)} \quad (4)$$

The relative length of the driven rod λ_{31} of the driving circuit:

$$\lambda_{31} = \sqrt{(\lambda_{32} \cdot \sin(\xi_0))^2 + W_1^2} \quad (5)$$

The inclination angle ξ_2 of the interbase distance λ_{12} to the vertical axis:

$$\xi_2 = \frac{\pi}{2} - \xi_1 - \alpha_2 \quad (6)$$

The relative length of the interbase distance λ_{12} between the O_3 and O_2 axes:

$$\lambda_{12} = \sqrt{(W + W_1)^2 \cdot \left(\frac{H}{2}\right)^2} \quad (7)$$

It is necessary to solve the equations system to determine the angles ξ_3 and ξ_4 and further calculate the mechanism's main parameters:

$$\begin{cases} A \cos \xi_2 + B \cos \xi_3 + C \cos \xi_4 = D \\ A \sin \xi_2 + C \sin \xi_4 = B \sin \xi_3 \end{cases} \quad (8)$$

where $A = \lambda_{41}$, $B = \lambda_{32}$, $C = \lambda_{31}$, $D = \lambda_{12} > 0$; ξ_2, ξ_3, ξ_4 are $(0; \pi/2)$.

Reducing the equations system (8) to the form:

$$\begin{cases} B \cos \xi_3 + C \cos \xi_4 = D - A \cos \xi_2 \\ -B \sin \xi_3 + C \sin \xi_4 = -A \sin \xi_2 \end{cases} \quad (9)$$

Reducing the equations system (9) to a new form:

$$\begin{cases} B \cos \xi_3 + C \cos \xi_4 = K \\ -B \sin \xi_3 + C \sin \xi_4 = L \end{cases} \quad (10)$$

where $K = D - A \cos \xi_2$, $L = -A \sin \xi_2$.

Expressing from the first equations system (10) $\cos \xi_3$:

$$\cos \xi_3 = \frac{K}{B} - \frac{C}{B} \cos \xi_4 \quad (11)$$

Considering the ratio between the trigonometric functions of the same argument:

$$\sin \xi_3 = \sqrt{1 - \left(\frac{K}{B} - \frac{C}{B} \cos \xi_4\right)^2} \quad (12)$$

Substituting the expression (12) into the second equation of system (10):

$$-B \sqrt{1 - \left(\frac{K}{B} - \frac{C}{B} \cos \xi_4\right)^2} + C \sin \xi_4 = L \quad (13)$$

or

$$\sqrt{1 - \left(\frac{K}{B} - \frac{C}{B} \cos \xi_4\right)^2} = \frac{C}{B} \sin \xi_4 - \frac{L}{B} \quad (13)$$

Squaring both parts of equation (13):

$$1 - \left(\frac{K}{B} - \frac{C}{B} \cos \xi_4\right)^2 = \left(\frac{C}{B} \sin \xi_4 - \frac{L}{B}\right)^2 \quad (14)$$

After transformations (14), we got:

$$K \cos \xi_4 + L \sin \xi_4 = \frac{K^2 + C^2 + L^2 - B^2}{2C} \quad (15)$$

Entering the value $\frac{K^2 + C^2 + L^2 - B^2}{2C} = \tilde{L}$, dependence (15) takes the form:

$$K \cos \xi_4 + L \sin \xi_4 = \tilde{L} \quad (16)$$

Using the ratio between trigonometric functions of the same argument, we got:

$$K \sqrt{1 - \sin^2 \xi_4} + L \sin \xi_4 = \tilde{L} \quad (17)$$

or

$$K \sqrt{1 - \sin^2 \xi_4} = \tilde{L} - L \sin \xi_4 \quad (17)$$

Squaring both parts of equation (17):

$$(K^2 + L^2) \sin^2 \xi_4 - 2L \tilde{L} \sin \xi_4 + (\tilde{L}^2 - K^2) = 0 \quad (18)$$

A quadratic equation relative to $\sin \xi_4$ was obtained. The roots of the quadratic equation (18):

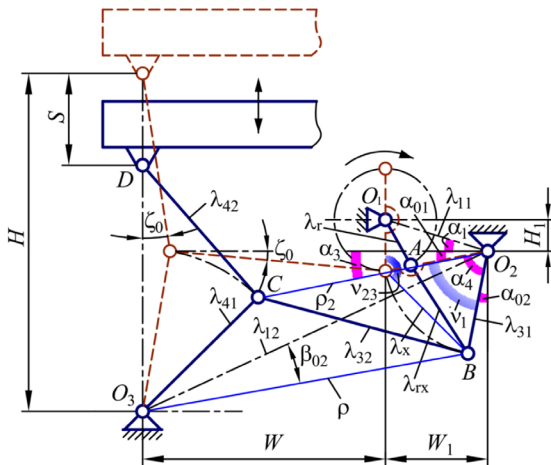
$$\xi_4 = \arcsin \left(\frac{2L \tilde{L} \pm \sqrt{\tilde{D}}}{2(K^2 + L^2)} \right) \quad (19)$$

where $\tilde{D} = (2L \tilde{L})^2 - 4(K^2 + L^2)(\tilde{L}^2 - K^2)$ – discriminant

Substituting (19) into the second equation of system (10), we got:

$$\xi_3 = \arcsin \left(\frac{C(2L \tilde{L} \pm \sqrt{\tilde{D}})}{2B(K^2 + L^2)} - \frac{L}{B} \right) \quad (20)$$

Calculating the following geometric parameters shown in Fig. 6 is necessary to determine the dimensions of crank λ_r and the connecting rod λ_2 .



» **Figure 6:** Scheme for calculating the left contour of the double-wedging mechanism of the pressure plate drive (determining the dimensions of the crank and the driving connecting rod)

The relative length ρ of the straight line from support O_3 to the lowermost position of the kinematic pair B:

$$\rho = \sqrt{\lambda_{12}^2 + \lambda_{31}^2 - 2 \cdot \lambda_{12} \cdot \lambda_{31} \cdot \cos(\xi_4)} \quad (21)$$

The angle β_{02} between the straight line ρ and the interbase distance λ_{12} :

$$\beta_{02} = \arccos \left(\frac{\lambda_{12}^2 + \rho^2 - \lambda_{31}^2}{2 \cdot \lambda_{12} \cdot \rho} \right) \quad (22)$$

The angle α_{01} between the central horizontal axis and the driven rod λ_{31} in the uppermost position of the mechanism:

$$\alpha_{01} = \arccos \left(\frac{\lambda_{31}^2 + W_1^2 - (\lambda_{32} \cdot \sin(\xi_0))^2}{2 \cdot \lambda_{31} \cdot W_1} \right) \quad (23)$$

The inclination angle α_{02} of the driven rod λ_{31} to the vertical axis in the lowest position of the mechanism:

$$\alpha_{02} = \arccos \left(\frac{\lambda_{31}^2 + \frac{H^2}{4} - \rho^2 - (W + W_1)^2 + 2 \cdot \rho \cdot (W + W_1) \cdot \cos(\alpha_2 - \beta_{02})}{2 \cdot \lambda_{31} \cdot \frac{H}{2}} \right) \quad (24)$$

Swing angle v_1 of the driven rod λ_{31} :

$$v_1 = \frac{\pi}{2} - \alpha_{01} - \alpha_{02} \quad (25)$$

The relative length λ_x between the extreme positions of the kinematic pair B:

$$\lambda_x = \sqrt{2 \cdot \lambda_{31}^2 (1 - \cos(v_1))} \quad (26)$$

Angle $O_1 B_1 B_2 v_{23}$:

$$v_{23} = \frac{\pi - v_1}{2} + \arctan \left(\frac{W_1}{\lambda_{32} \cdot \sin(\xi_0)} \right) \quad (27)$$

The relative length of the driving crank λ_r :

$$\lambda_r = \frac{\lambda_x \cdot \sqrt{\cos(v_{23})^2 + 8 - \cos(v_{23})}}{8} \quad (28)$$

The relative vertical distance H_1 between supports O_1 and O_2 :

$$H_1 = \lambda_r - \lambda_{32} \cdot \sin(\xi_0) \quad (29)$$

The relative interbase distance λ_{11} between supports O_1 and O_2 :

$$\lambda_{11} = \sqrt{W_1^2 + H_1^2} \quad (30)$$

The angle α_1 of inclination of the interbase distance to the horizontal axis:

$$\alpha_1 = \arctan\left(\frac{H_1}{W_1}\right) \quad (31)$$

The relative length of the straight line ρ_2 between the uppermost position of the kinematic pair C and the support O_2 :

$$\rho_2 = \sqrt{\lambda_{42}^2 + \lambda_{12}^2 - 2 \cdot \lambda_{42} \cdot \lambda_{12} \cdot \cos(\xi_2)} \quad (32)$$

The angle α_3 between the straight line ρ_2 and the horizontal axis:

$$\alpha_3 = \arccos\left(\frac{(W + W_1 - \lambda_{42} \cdot \sin(\xi_0))^2 + \rho_2^2 - 2 \cdot \lambda_{42}^2 \cdot (1 - \cos(\xi_1 - \xi_0))}{2 \cdot (W + W_1 - \lambda_{42} \cdot \sin(\xi_0)) \cdot \rho_2}\right) \quad (33)$$

The angle α_4 between the straight line ρ_2 and the driven rod λ_{31} , which is in the lowest position:

$$\alpha_4 = \arccos\left(\frac{\rho_2^2 + \lambda_{31}^2 - \lambda_{32}^2}{2 \cdot \rho_2 \cdot \lambda_{31}}\right) \quad (34)$$

The relative length λ_{rx} of the straight line between support O_1 and kinematic pair B in the lowest position:

$$r_x = \sqrt{\lambda_{11}^2 + \lambda_{31}^2 - 2 \cdot \lambda_{31} \cdot \lambda_{11} \cdot \cos(\alpha_1 + \alpha_3 + \alpha_4)} \quad (35)$$

The relative size of the connecting rod λ_2 of the driving circuit:

$$\lambda_2 = r_x - \lambda_r \quad (36)$$

Kinematic Calculation of the Mechanism

The kinematic parameters are initially calculated by determining the end position of the four-link mechanism O_1ABO_2 . Figure 7 shows the mechanism link position angles, and the analytical dependencies for their calculation are given below.

The angle ϕ_0 between the initial position of the driving crank λ_r and the base distance λ_{11} :

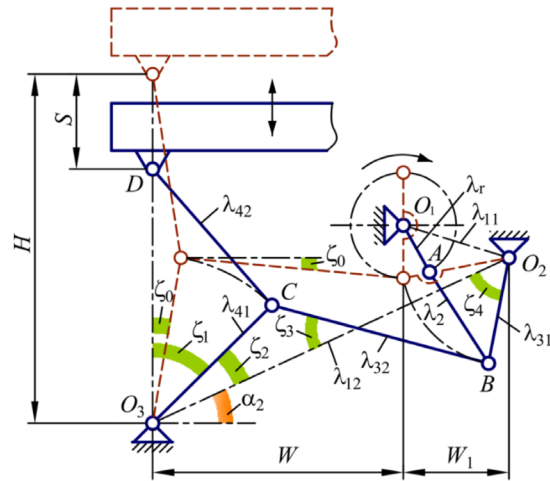
$$\phi_0 = \arccos\left(\frac{(\lambda_r + \lambda_2)^2 + \lambda_{11}^2 - \lambda_{31}^2}{2 \cdot (\lambda_r + \lambda_2) \cdot \lambda_{11}}\right) \quad (37)$$

The angle ϕ_{01} between the initial position of the driving crank λ_r and the vertical axis:

$$\phi_{01} = \arccos\left(\frac{(\lambda_2 - \lambda_r)^2 + \lambda_{11}^2 - \lambda_{31}^2}{2 \cdot (\lambda_2 - \lambda_r) \cdot \lambda_{11}}\right) \quad (38)$$

Angle ϕ_{max} :

$$\phi_{max} = \pi + \phi_0 + \phi_{01} \quad (39)$$



» **Figure 7:** Scheme for calculating the left contour of the double-wedging mechanism of the pressure plate drive (determination of the angles of the extreme position of the four-link mechanism and the driving crank)

Angles γ_{01} and γ_0 between the lowermost position of the driven rod λ_{31} and the interbase distance λ_{11} :

$$\gamma_{01} = \arccos\left(\frac{\lambda_{11}^2 + \lambda_{31}^2 - (\lambda_r + \lambda_2)^2}{2 \cdot \lambda_{11} \cdot \lambda_{31}}\right) \quad (40)$$

$$\gamma_0 = \pi - \gamma_{01} \quad (41)$$

The angle γ_{02} between the uppermost position of the driven rod λ_{31} and the interbase distance λ_{11} :

$$\gamma_{02} = \arccos\left(\frac{\lambda_{31}^2 + \lambda_{11}^2 - (\lambda_2 - \lambda_r)^2}{2 \cdot \lambda_{11} \cdot \lambda_{31}}\right) \quad (42)$$

Swing angle γ_{max} of the driven rod λ_{31} :

$$\gamma_{max} = \pi - \gamma_{02} \quad (43)$$

The following calculation stage determines the mechanism's current position. Figure 8 shows the necessary parameters for this calculation.

The relative diagonal Δ :

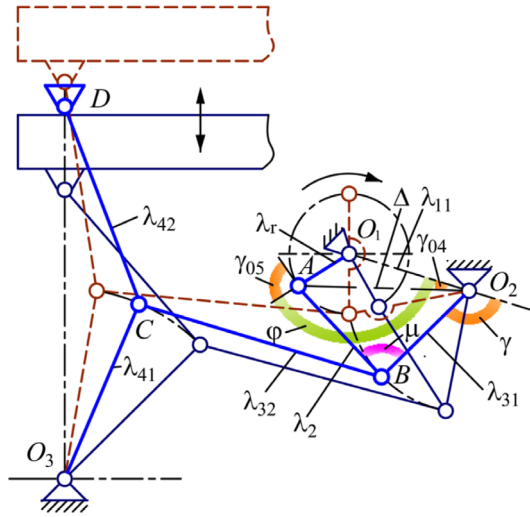
$$\Delta = \sqrt{\lambda_{11}^2 + \lambda_r^2 - 2 \cdot \lambda_r \cdot \lambda_{11} \cdot \cos(\phi)} \quad (44)$$

The angle γ_{04} between the diagonal Δ and the interbase distance λ_{11} :

$$\gamma_{04} = \arccos\left(\frac{\Delta^2 + \lambda_{11}^2 - \lambda_r^2}{2 \cdot \lambda_{11} \cdot \Delta}\right) \quad (45)$$

The angle γ_{05} between the driving crank λ_r and the driving connecting rod λ_2 :

$$\gamma_{05} = \arccos\left(\frac{\Delta^2 + \lambda_2^2 - \lambda_{31}^2}{2 \cdot \lambda_2 \cdot \Delta}\right) \quad (46)$$



» **Figure 8:** Scheme for calculating the left contour of the double-wedging mechanism of the pressure plate drive (determination of the angles of the current position of the mechanism)

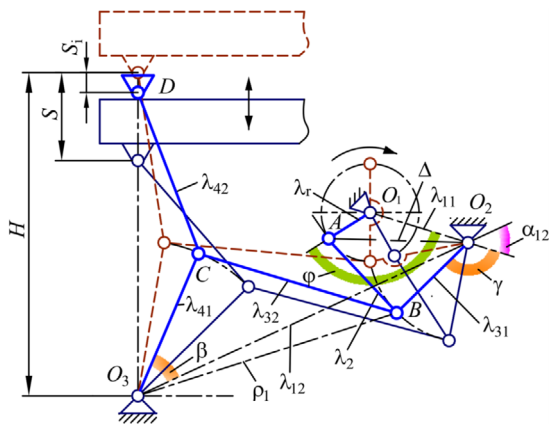
Transmission angle μ between the driven rod λ_{31} and the driving connecting rod λ_2 :

$$\mu = \arccos\left(\frac{\lambda_2^2 + \lambda_{31}^2 - \Delta^2}{2 \cdot \lambda_2 \cdot \lambda_{31}}\right) \quad (47)$$

The inclination angle γ of the driven rod λ_{31} to the interbase distance λ_{11} :

$$\gamma = \mu + \gamma_{04} \pm \gamma_{05} \quad (48)$$

Below is the calculation of kinematic parameters (Fig. 9) for determining the pressure plate's displacement, velocity, and acceleration.



» **Figure 9:** Scheme for calculation of the left contour of the double-wedging mechanism of the pressure plate drive (determination of the current displacement of the pressure plate)

The angle α_{12} between the interbase distances λ_{11} and λ_{12} :

$$\alpha_{12} = \alpha_1 + \alpha_2 \quad (49)$$

Relative diagonal ρ_1 :

$$\rho_1 = \sqrt{\lambda_{12}^2 + \lambda_{31}^2 - 2 \cdot \lambda_{12} \cdot \lambda_{31} \cdot \cos(\pi - \gamma - \alpha_{12})} \quad (50)$$

The inclination angle β of the drive rod λ_{41} to the interbase distance λ_{12} :

$$\beta = \arccos\left(\frac{\lambda_{41}^2 + \rho_1^2 - \lambda_{32}^2}{2 \cdot \lambda_{41} \cdot \rho_1}\right) \pm \arccos\left(\frac{\lambda_{12}^2 + \rho_1^2 - \lambda_{31}^2}{2 \cdot \lambda_{12} \cdot \rho_1}\right) \quad (51)$$

Relative movement of the pressure plate S_i :

$$s_i = 2 \cdot \lambda_{41} \cdot \sin(\alpha_2 + \beta) - H + S \quad (52)$$

The relative velocity of the pressure plate V_i :

$$V_i = \frac{dS_i}{d\varphi} \quad (53)$$

The relative acceleration of the pressure plate a_i :

$$a_i = \frac{dV_i}{d\varphi} \quad (54)$$

To get the absolute values of the kinematic parameters of the mechanism, we use dependencies 55, 56, and 57 (S – linear displacement; V – velocity; a – acceleration):

$$S = s_i \cdot [S_{\max}] \quad (55)$$

$$V = V_i \cdot [S_{\max} \cdot \omega_r] \quad (56)$$

$$a = a_i \cdot [S_{\max} \cdot \omega_r^2] \quad (57)$$

where $S_{\max} = 80$ mm (3.14961 in) is the absolute maximum linear displacement of the pressure plate, $\omega_r = \pi \cdot n / 30$ is the angular velocity of the driving crank, and $n = 60$ rpm is the crankshaft rotation velocity.

Virtual Experiment of the 3D Model of the Mechanism

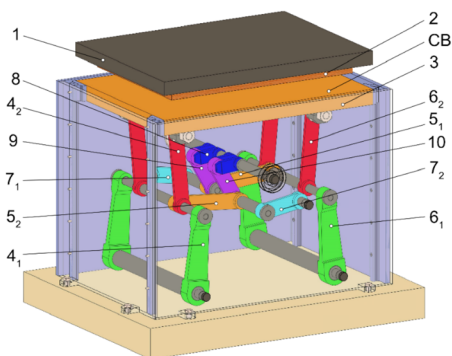
The proposed double-wedging mechanism's virtual kinematic analysis was performed in the SolidWorks program based on a 3D model and mechanism operation simulation (Fig. 10).

In the figure, 1 – fixed plate, 2 – die-cutting form, 3 – pressure plate, 4₁ and 6₁ – drive rods, 4₂ and 6₂ – driven connecting rods, 5₁ and 5₂ – power rods, 7₁ and 7₂ – driven rods, 8 – driven crank, 9 and 10 – driving connecting rods. Analytical dependencies were derived below (Table 1).

Table 1

Geometric parameters for designing a 3D model of the research double-wedging mechanism

Parameters	Dimension (mm)	Dimension (in)
Total width of mechanism, H	500	19.685
Maximum pressure plate linear displacement, S_{max}	80	3.14961
The horizontal distance between the supports O_1 and O_2 , W_1	125	4.92126
The horizontal distance between the supports O_1 and O_3 , W	250	9.84252
The vertical distance between the supports O_1 and O_2 , H_1	45.85	1.80512
Driving crank, pos. 8	62.83	2.4736
Driving connecting rod, pos. 9, 10	182.78	7.196063
Driven rod, pos. 7_1 , 7_2	126.58	4.98346
Power rod, pos. 5_1 , 5_2	229	9.01575
Drive rod, pos. 4_1 , 6_1	250.95	9.8799
Driven connecting rod, pos. 4_2 , 6_2	250.95	9.8799



» **Figure 10:** 3D model of the double-wedging mechanism in the drive of the die-cutting press pressure plate

A kinematic analysis of the researched double-wedging mechanism (Fig. 3) was also performed in the SolidWorks program to compare the results of the kinematic analysis of the existing mechanism. The results are obtained in the form of graphs.

Results

According to the results of the geometric synthesis, considering the initial conditions, the relative geometric parameters of the double-wedging mechanism of the pressure plate drive were determined. They are: $\lambda_1 = 0.823$ – the driving crank size; $\lambda_{11} = 1.664$ – interbase

distance between axes O_1 and O_2 ; $\lambda_{12} = 5.634$ – interbase distance between axes O_3 and O_2 ; $\lambda_2 = 1.645$ – the length of the connecting rod of the driving circuit; $\lambda_{31} = 1.582$ – the lever length of the horizontal wedging circuit; $\lambda_{32} = 2.862$ – the connecting rod length of the horizontal wedging circuit; $\lambda_{41} = 3.137$ – the lever length of the vertical wedging circuit; $\lambda_{42} = 3.137$ – the connecting rod length of the vertical wedging circuit. At the same time, the relative maximum linear displacement of the pressure plate was assumed to be equal to $S=1$, and the main relative basic dimensions were similar to the existing wedging mechanism of the Bobst die-cutting press.

The kinematic parameters calculating results of the wedging and combined double-wedging mechanisms of the pressure plate drive are shown in Fig. 11 and Fig. 12. But Fig. 11a, Fig. 12a, and Fig. 12c show graphical dependences of the double-wedging mechanism kinematic parameters, which were obtained by the analytical method. The solid line (Fig. 11b, c; Fig. 12b, d) shows the graphic results of calculating the kinematic parameters of the double-wedging mechanism obtained by modeling the mechanism's operation using the SolidWorks program. The dashed line (Fig. 11b, c; Fig. 12b, d) shows the graphical dependence of the kinematic parameters for the existing wedging mechanism shown in Fig. 3. Fig. 11c shows graphs of the pressure plate linear displacement during contact with a cardboard blank with a thickness of $h_{CB} = 1$ mm (0.0393701 in) on an enlarged scale.

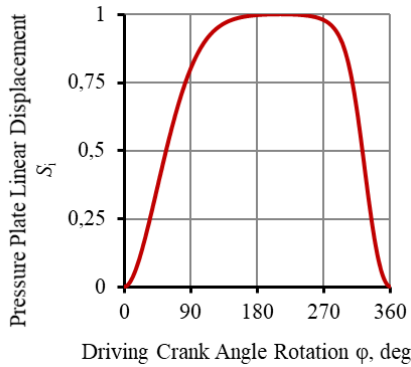
The analysis of linear displacement S_p , velocity V_p , and acceleration α of the double-wedging mechanism according to the derived analytical dependencies was performed in relative values relative to the angle ϕ (degrees) of the driving crank rotation. When simulating the operation of the wedging and double-wedging mechanisms in the SolidWorks program, kinematic parameters were analyzed in absolute values relative to time t (sec). The absolute linear displacement of the pressure plate was assumed to be equal to $S_{max} = 80$ mm (3.14961 in), as in the existing die-cutting presses of the Bobst company. The number of revolutions of the drive crank was $n=60$ rpm, and the duration of one pressure plate movement cycle was $t=1$ sec.

A comparative analysis of graphical dependencies obtained through the analytical method and the double-wedging mechanism simulation in the SolidWorks program demonstrated their complete identity. This confirms the validity of the derived analytical equations for calculating the parameters of the combined double-wedging mechanism of the pressure plate drive.

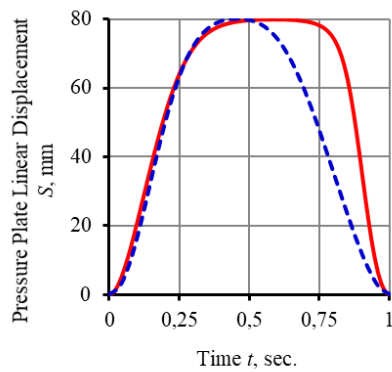
As can be seen from the dependences $S_p=f(\phi)$ (Fig. 11, a) and $S_p=f(t)$ (Fig. 11, b) in sections $\varphi=0^\circ-140^\circ$ ($t=0-0.4$ sec.), there is a rapid increase in the displacement of the pressure plate. When approaching the uppermost position, the movement of the pressure plate slows down.

It increases the contact duration of the pressure plate with the cardboard blank of the short circuit and the mold (die-cutting or relief for embossing), which is an essential positive technological point.

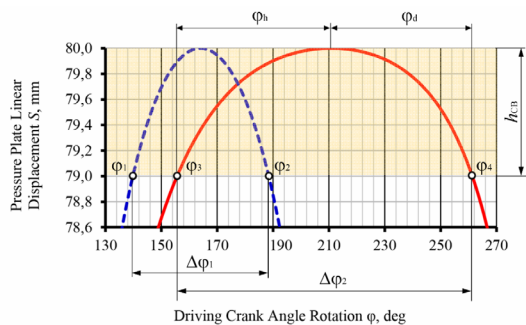
It has a particularly positive effect on the technological operations of relief embossing and creasing, which require long-term contact of the die-cutting mold with the cardboard blank CB.



(a)

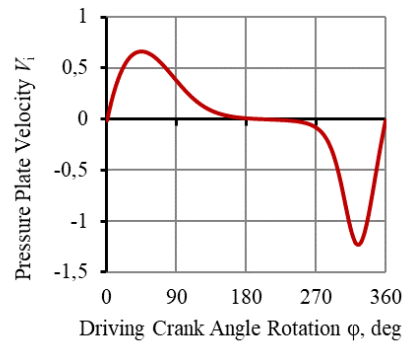


(b)

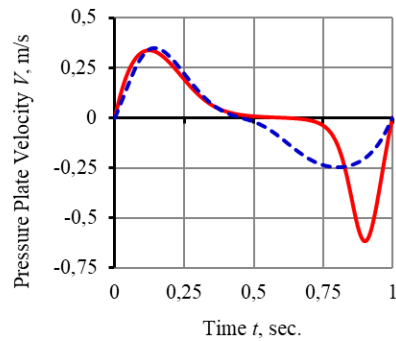


(c)

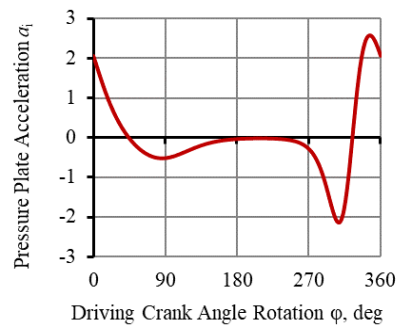
» **Figure 11:** The results of calculating the pressure plate movement of the double-wedging mechanism (solid line) and the existing wedging mechanism (dashed line) obtained by the analytical method (a), modeling in the SolidWorks program (b), the area of the plate movement during contact with the cardboard blank CB (c) of the thickness $h_{CB} = 1 \text{ mm}$ (0.0393701 in)



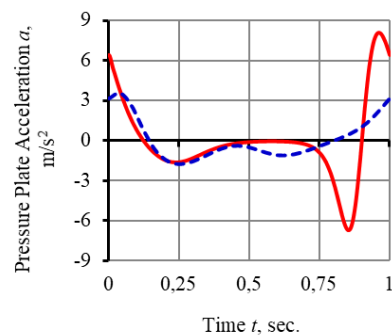
(a)



(b)



(c)



(d)

» **Figure 12:** The results of calculating the velocity and acceleration of the pressure plate of the double-wedging mechanism (solid line) and the existing wedging mechanism (dashed line) obtained by the analytical method (a, c) and modeling in the SolidWorks program (b, d)

For example, for cardboard blank *CB* with a thickness of $h_{cb}=1$ mm (0.0393701 in) (Fig. 11c), the angle of drive crank rotation during the contact of the pressure plate with the cardboard *CB* for the exciting wedging mechanism: $\Delta\varphi_1 = \varphi_2 - \varphi_1 = 188^\circ - 140^\circ = 48^\circ$, for the double-wedging mechanism $\Delta\varphi_2 = \varphi_4 - \varphi_3 = 261^\circ - 156^\circ = 105^\circ$.

As we can see, the proposed double-wedging mechanism ensures that the contact time of the pressure plate with the cardboard blank is 2.18 times longer than the existing wedging mechanism.

An essential point for the proposed double-wedging mechanism is the difference in the pressure plate's working (raising) and idle (lowering) movement during contact with the cardboard *CB*. So, for cardboard with a thickness of $h_{cb}=1$ mm (0.0393701 in), the turning angle of the crank when raising the plate is $\varphi_r = 211^\circ - 156^\circ = 55^\circ$, and when lowering it, $\varphi_d = 261^\circ - 211^\circ = 50^\circ$. It ensures a longer time of compression deformation of the cardboard and, as a result, the formation of the necessary residual deformation during creasing or relief embossing. The difference in the duration of the working (raising) and idle (lowering) movements of the pressure plate is explained by the combined mechanism of its drive.

Analysis of the velocity of pressure plate linear displacement (Fig. 12a, b, solid line) shows that its relative maximum value during the working stroke is observed at the crank's rotation angle $\varphi=44^\circ$ and is $V_{max}=0.67$. At the angle of crank rotation $\varphi=211^\circ$, the velocity of the pressure plate changes its direction to the opposite, and until the end of the cycle, its values are negative. During the reverse stroke, the relative maximum negative value of the velocity is equal to $V_{max}=-1.23$ at the angle of rotation of the crank $\varphi=325^\circ$. The corresponding absolute values of the velocity are $V_{max}=0.33$ m/sec (1.082677 ft/sec) when lifting and $V_{max}=-0.62$ m/sec (-2.034121 ft/sec) when lowering the plate.

The difference between the maximum velocity of the pressure plate during lifting and lowering is explained by the steeper displacement curve (Fig. 11a, solid line) during its lowering.

Analysis of the dependences of velocity (Fig. 12a, b) and acceleration of the pressure plate (Fig. 12c, d) in the double-wedging mechanism (Fig. 12, solid line) shows that at the peak values of the velocity, the acceleration of the plate is equal to $a=0$ m/sec² (0 ft/sec²). It observes values of the angle of crank rotation $\varphi=44^\circ$ and $\varphi=325^\circ$ for the relative values obtained according to analytical dependencies and at $t=0.12$ sec and $t=0.9$ sec for absolute values obtained by modeling in the SolidWorks program. At the same time, the relative maximum acceleration value $a_{imax}=2.57$ is observed at $\varphi=346^\circ$, and the absolute maximum value is $a_{max}=8.09$ m/sec² (26.5419 ft/sec²) at $t=0.96$ sec.

A comparative analysis of the velocity and acceleration of the pressure plate for wedging (Fig. 12b, d, dashed line) and double-wedging mechanisms (Fig. 12b, d, solid line) shows the following. The maximum velocity value for both mechanisms when raising the plate is approximately the same. When lowering it for the wedging mechanism, it is 0.53 times smaller (0.33 m/sec (1.0827 ft/sec) and 0.62 m/sec (2.03412 ft/sec), respectively). The maximum value of the pressure plate acceleration in the wedging mechanism is 3.3 m/sec² (10.8268 ft/sec²), and in the double wedging mechanism, it is 8.09 m/sec² (26.5419 ft/sec²). It is known that inertial forces in a die-cutting press are not decisive, unlike technological ones. Therefore, an increase in acceleration, and accordingly, inertial forces, by 2.4 times will not significantly affect the press drive.

Conclusion

Scientific research on improving die-cutting presses has been critically analyzed. No information exists on the study of the mechanisms of the pressure plate movement with an increased duration of contact of the die-cutting tools with the cardboard. This information is crucial when performing technological operations such as creasing and relief embossing.

A scheme of the double wedging mechanism of its drive is proposed to increase the pressure plate's contact period with the cardboard blank. The proposed mechanism was geometrically synthesized, and its relative geometric parameters were determined. At the same time, the main basic dimensions were assumed to be similar to those of the existing wedging mechanism of the Bobst die-cutting press.

A methodology for calculating the kinematic parameters of the combined double-wedging mechanism of the pressure plate drive has been developed. It involves a "reverse" calculation, in which the "unit" is taken as the relative linear movement $S=1$ of the driven link (the pressure plate), which corresponds to its movement ($S_{max}=80$ mm, 3.14961 in) in Bobst's die-cutting presses.

Mathematical models were created, which made it possible to calculate the relative kinematic parameters of the combined double wedging mechanism of the pressure plate drive. According to the results, it was established that the change in the movement of the pressure plate ensures its long-term contact with the cardboard blank. For example, for cardboard with a thickness of 1 mm, the plate's contact period with the cardboard corresponds to the rotation angle of the drive crank of 105° . It is 29% of the total movement period of the pressure plate. The change in the direction of the velocity from positive to negative at the angle of rotation of the crank $\varphi=211^\circ$ proves that the period of raising the plate is greater than the period of its lowering.

A comparative analysis of the results of analytical studies with the results of a virtual experiment of the existing wedging and the proposed double-wedging mechanisms in the SolidWorks program was performed. According to his results, it was established that for the existing mechanism, the contact of the pressure plate with the cardboard blank occurs during the angle of rotation of the crank, which is equal to $\phi=48^\circ$. It accounts for 13.3% of the total period of plate movement, which is 0.46 times less than for the case of the double-wedging mechanism.

Thus, a combined double-wedging mechanism provides twice as prolonged contact between the pressure plate and the cardboard blank. It creates better prerequisites for obtaining the technologically necessary residual deformation during the creasing and relief embossing of cardboard blanks.

Funding

This research did not receive any specific grant from funding agencies in the public, commercial, or not-for-profit sectors.

References

- Emblem, A. & Emblem H. (2012) *Packaging technology Fundamentals, Materials and Processes*. Oxford, Woodhead Publishing.
- Khvedchyn, Y. Y. & Zelenyi, V. V. (2014) Analysis of The Mechanisms of Press in Die-cutting Automat. *Scientific Papers*. 4 (49), 21-30.
- Kirwan, M. J. (2013) *Handbook of Paper and Paperboard Packaging Technology*. Oxford, John Wiley & Sons. Available from: doi: 10.1002/9781118470930
- Kuznetsov, V. O. Rehei, I. I. & Vlach, V. V. (2017) Modification of a drive mechanism of a press plate in a die-cutting press. *Printing and Publishing*. 1 (73), 56-62.
- Kuznetsov, V. O., Kolomiets, A. B. & Dmitraschuk, V. S. (2012) Parametric Researches of the Press Plate Drive in Die-cutting Automat. *Packaging*. 6, 31-34.
- Lin, W., Zhou, C. & Huang, W. (2015) Optimum design for mechanical Structures and Material Properties of the dual-elbow-bar mechanism. *Advances in Materials Science and Engineering*. 2015. Available from: doi: 10.1155/2015/724171
- Pasika, V. R. & Vlach, V. V. (2016) Kinematic synthesis of die-cutting press mechanism with equality of forward and reverse moves. *Printing and Publishing*. 1 (71), 129-139.
- Poliudov, O. M. (2005) *Mechanics of printing and packaging machines*. Lviv, Ukrainian Academy of Printing.
- Rehei, I. I., Vlach, V. V., Knysh, O. M. & Mlynko, O. I. (2022) Complex analysis of the pressure plate drive mechanisms functioning in die-cutting presses. *Printing and Publishing*. 2 (84), 88–98. Available from: doi: 10.32403/0554-4866-2022-2-84-88-98
- Rehei, I., Vlach, V., Knysh, O., Knysh, R. & Mlynko, O. (2023) Combined double crank wedging drive mechanisms of the press plate used in die-cutting press: synthesis, kinematic and functional. *Academic journal of manufacturing engineering*. 3 (21), 53-60.
- Rehei, I. I. (2011) *Consumer Cardboard Packaging: Materials, Design Manufacturing Equipment*. Lviv, Ukrainian Academy of Printing.
- Shakhbazov, Y. O., Cheterbuh, O. Y., Shyrokov, V. V. & Palamar, O. O. (2020) The drive mechanism of a pressure plate of a flat die-cutting press. *Printing and Publishing*. 1 (79), 112-120. Available from: doi: 10.32403/0554-4866-2020-1-79-112-120
- Vlach, V. & Pasika, V. (2016) Automated synthesis of mechanism of press of diecutting machine. *Technological Complexes*. 1 (13), 57-63.
- Wang, J., Chen, X. & Li, Y. (2023) Structure Design and Optimization Algorithm of a Lightweight Drive Rod for Precision Die-Cutting Machine. *Applied Sciences*. 13 (7). Available from: doi: 10.3390/app13074211




A framework of project-based learning (PBL) pedagogy for graphic design education

ABSTRACT

Design programmes commonly employ project-based learning (PBL) in studio settings, emphasising hands-on learning through real-world projects. However, there are multiple practices in the name of PBL. There is confusion about what is and what is not PBL. Furthermore, real-world or authentic projects are integral to PBL but have no clear interpretations. Many studies inform about the advantages of real-world or authentic projects; however, very few about its integration into teaching and even fewer in graphic design education. This action research proposes a framework for the clarity and application of PBL in a graphic design studio class using a real-world design project. The proposed framework in the study derived from the work by Blumenfeld et al., 1991; Krajcik & Blumenfeld, 2005, shows the implementation of a real-world project for graphic design students—an area where the PBL research is scarce. Applied in a communication design course at an Indian university, the framework imparts structure, clarity, and alignment with curricular requirements. This approach ensures successful course completion with tangible outcomes, enriching students' portfolios. The study serves as a model for employing a comprehensive framework based on PBL, demystifies real-world or authentic projects and demonstrates how they can be tailored for holistic learning in graphic design education.

KEY WORDS

project-based learning (PBL), graphic design, real-world projects, authentic projects, design pedagogy, design education, learning by doing

Kanupriya Taneja 

Nirma University, Institute of Design, Ahmedabad, India

Corresponding author:

Kanupriya Taneja

e-mail:

taneja.kanupriya@gmail.com

First received: 16.5.2024.

Revised: 20.3.2025.

Accepted: 14.4.2025.

Introduction

In India, there is a presence of undergraduate, post-graduate, diploma, and certificate programmes in design education (British Council & India Design Council, 2016). These programmes have manifested in diverse forms, including departments within universities, standalone design schools, and small independent design education ventures (Bothra, 2024). The graphic design and related degree programmes are known by different names, such as the four-year programme in “communication design, visual communication, graphic and communication design, graphic design, visual arts, etc.” (Taneja, 2021a). Communication design has become an umbrella term under which graphic design, publication design, UI/UX, moving

Images—animation and live-action films, branding, and advertising related inputs are given (Taneja, 2021b).

Graphic design is a practice-based profession; thus, educators and policymakers are always concerned about students' industry readiness upon graduation. 'Learning by doing' is commonplace in design education. Students undergo numerous praxis-based projects to address some existing gaps or problems that need solutions. This helps acquire new knowledge and build on intellectual and skill-based capacities.

The PBL pedagogical model within a studio environment is common in learning design. PBL is an approach that engages students in real-world or authentic projects to foster learning (Jones, 2019).

This project method, initially popularized by William Heard Kilpatrick, has experienced a revival in modern education, particularly under the framework of PBL (Pecore, 2015). Although high-quality resources are readily available, misconceptions about PBL continue to prevail. Therefore, it is essential to take a step back and clearly distinguish what PBL truly entails and what it does not (Wolk, 2022). PBL instruction demands teachers to thoroughly understand its pedagogical approach for effective teaching (Han et al., 2015).

Providing effective materials and models to teachers and decision-makers would support the adoption of PBL effectively (Hasni et al., 2016). Clarity is also required about what truly constitutes a PBL project or a real-world project (Thomas, 2000). The PBL method emphasises employing real-world projects. Learning through real-world projects is critical in design education. However, there is a lot of confusion around what can or cannot be considered a real-world project. The term real-world projects is interpreted in many ways, and working on industry projects¹ is just one of those interpretations. Post-liberalisation, there has been a phenomenal rise in the number of design institutes in India (Bothra, 2019). However, access to industry projects for most of the new institutes is far and few between.

Mathur (2014) points out that education at a premier institute, the National Institute of Design (NID) in India has declined due to this reason. It has been observed that due to the inaccessibility of industry projects, there is a lot of dependence on hypothetical projects² in graphic design education. Such projects rarely have actual users, clients, and context; thus, they lack applicability in the real-world. In most cases, the instructors are the only source of feedback and critique. Many times the decisions are based on presumptions and assumptions due to the absence of an actual user or the client. These projects may not go through the complete production cycle, in which case the learning related to project implementation in the real-world is compromised. These projects look pretty in students' portfolios but rarely see the light of day.

¹ Industry projects are intended to give real-world experiences to students as a result of collaboration between academic institutions and businesses/organisations. These industry-academic partnerships give opportunities to the students to apply the learned skills and theory into practice before they embark on a professional journey.

² According to Collins dictionary, if something is hypothetical, it is based on conjectures rather than an actual situation. In design education, students learn through an assortment of assignments and projects. Oftentimes, the assignments or projects are simulated, contoured with conjectures in the absence of a real client, a real need, and lack the actual implementation of the end product.

This study explores and gives clarity about real-world or authentic projects within PBL to reduce reliance on hypothetical projects in the realm of graphic design education. It offers examples of authentic opportunities, a structured PBL framework for educators, and guidance amid varied PBL practices. Given the limited research on design pedagogy in India and globally, this study seeks to bridge the gap and contribute to theoretical advancements in graphic design.

Scope of the Study

The third-year students enrolled in the Bachelor of Design (BDes), a four-year degree programme, were selected for the study. The cohort of thirty-five students was studying in the Communication Design programme at an Indian university. A PBL framework focused on a real-world learning environment was derived primarily from the work of Blumenfeld et al., 1991 and Krajcik & Blumenfeld, 2005. The framework was applied for five weeks during the Publication Design course offered in the third year. This action research examines the functionality of the proposed framework, demystifying PBL and real-world projects in the context of graphic design education. It aims to help academics engage learners in authentic tasks that simulate workplace experiences.

The idea of the study was based on observations in multiple prior courses with different cohorts that demonstrated the usefulness of generating real-world projects for the learners. The lack of research and examples of PBL in design education, especially graphic design education, and the confusion around real-world or authentic projects under PBL became important catalysts for this research.

What is Project-based Learning?

The literature highlights that PBL is a student-centric approach where learning occurs through projects (Farrow, Kavanagh & Samudra, 2022; Rensburg, 2020; Thomas, 2000). It engages students in real-world, authentic projects (Jones, 2019). The students take charge of their learning, with teachers as facilitators. They engage in inquiry, collaborate with peers, utilise technology to tackle real-world challenges, and thereby cultivate various skills essential for the 21st century (Bell, 2010). The final outcome is a well-designed product/artefact (Krajcik & Blumenfeld, 2014; Sumarni, 2015; Thomas, 2000). Project-based learning places the learner at its centre, providing ample opportunity for deep exploration of relevant subjects.

This method fosters learner autonomy; the learners have a choice in both what knowledge they acquire and how they acquire it. The motivation is high as they develop personally meaningful representations of their acquired knowledge (Grant, 2002; Kwietniewski, 2017).

Blumenfeld et al. (1991) support the notion that PBL is a holistic instructional approach that immerses students in authentic, real-world tasks. Within this framework, students navigate complex challenges by actively engaging in various activities such as formulating and refining questions, debating concepts, predicting outcomes, devising plans or experiments, gathering and evaluating data, formulating conclusions, sharing insights, asking further questions, and developing meaningful artefacts. 'Projects' require two critical factors—a central query/driving question or problems leading to actions. Based on the central question, the actions taken lead to an array of artefacts or products that come together to form the final product. They further explained that artefacts or end-products serve as tangible representations of the solutions put forth by students, showcasing the evolution of their knowledge. These tangible and explicit outcomes can take the form of models, reports, videotapes, or computer programmes.

This hands-on, research-focused approach involves learners in extended engagement, where they collaboratively create, develop, and test their creations, both within and beyond the classroom setting. It emphasises student-centredness where learners actively engage in planning, designing, and implementing projects in real-world contexts. Collaboration among peers is an important feature while the teacher supports the learning process through scaffolding. The process engages students in a range of activities. The real-world projects help cultivate diverse skills, including communication, presentation, critical thinking, problem-solving creativity, teamwork, research, technical proficiency, and project management (Giri, 2016).

Rooted in constructivist theory, PBL views learning as the construction of new ideas based on prior knowledge (Thu, 2018). Thomas (2000), in his research review on PBL, attempts to understand the identifying markers of PBL and exclude what does not represent this method. Through his study, he investigates, "What must a project have in order to be considered an instance of PBL?" He established five criteria to describe a 'project'. "The five criteria are 'centrality, driving question, constructive investigations, autonomy, and realism". Bell (2010) articulates, "PBL is not a supplementary activity to support learning. It is the basis of the curriculum".

Thomas (2000) stressed, "PBL projects are central, not peripheral to the curriculum", and it must involve constructive investigation by the students. He further stressed that "straightforward service projects such as planting a garden or cleaning a stream bed are projects, but may not be PBL projects".

Projects are not predetermined or controlled by teachers, instead are student-driven and conducted in collaboration where the solutions have the potential to be put into practice. The projects involve real-life challenges with an emphasis on authentic problems or questions.

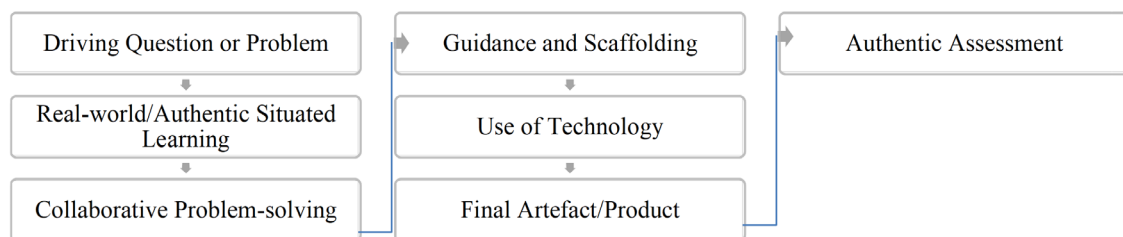
Framework Design

Professor Joseph Krajcik and P.C. Blumenfeld have been doing some noteworthy work in the area of PBL. Some of their well-cited works include, *Motivating Project-based Learning: Sustaining the Doing, Supporting the Learning*; *Enacting Project-based Science*; *A Collaborative Model for Helping Middle Grade Science Teachers Learn Project-based Instruction*; *Enquiry in Project-based Science Classrooms: Initial Attempts by Middle School Students*. Their book chapter called "Project-based Learning", published in the *Cambridge Handbook of the Learning Sciences* in 2006, gives a systematic and comprehensive framework.

The framework draws upon some of their previous works and the work of some other authors and propounders of PBL theory, like John Dewey, a well-known educator and philosopher. Krajcik & Blumenfeld (2005) underscore Dewey's belief that students cultivate a genuine interest in the content when engaged in authentic tasks and problems that mirror the practice of professionals in real-world scenarios.

Project-based environments have five essential characteristics (Blumenfeld et al., 1991; Krajcik et al., 1994; S. J. Krajcik & Blumenfeld, 2005; Krajcik & Shin, 2014).

- a. A driving question or a problem
- b. The driving question leads learners on the path of authentic, situated learning enquiry. In the process of problem-solving, they acquire and apply the core disciplinary knowledge and skills and become proficient performers



» **Figure 1:** PBL Model Adapted from Blumenfeld et al. (1991); Krajcik & Blumenfeld (2005)

- c. Collaborative problem-solving initiatives and engagement between students, instructors, and community members towards the driving question, emulate complex social situations of expert problem-solving
- d. Scaffolding with technology, and learning support facilitates learners to transcend beyond their ability
- e. The tangible end-product/products or the artefacts are the manifestations of the process of answering the driving question available publicly as an external representation of the class learning

The seven-point framework of PBL explained in Figure 1 has been further refined by reviewing the related literature.

Understanding the Realm of Real-world/Authentic

Educators in design emphasise learning by engaging the students in authentic tasks to reflect the experience of real-world practitioners. PBL provides real-world experience to learners, thereby helping prepare them optimally for the workplace (Giri, 2016). Theorists too support the idea of exposing learners to authentic experiences—the experience of real-world ways of knowing and doing. Such experiences lead to relevant learning, bringing them closer to praxis (Krajcik & Shin, 2014; Qin, 2022). Boss & Krauss (2014) argue, “at the end of the day, would you rather see your students dumping their ‘work’ into the recycling bin, or talking about an authentic project in which they are driving their own learning?”. They corroborate that the best learning method is via real-world activities, considered most relatable for learners to capture their interest.

The terms "real-world" and "authentic" are often used interchangeably in the literature in the context of PBL. Real-world is described as "the realm of practical or actual experience, as opposed to the abstract, theoretical, or idealised sphere of the classroom, laboratory, etc. (Dictionary.com, 2024). It is also referred to as "the set of situations most humans have to deal with in their lives, rather than what happens in stories and films, etc." (Cambridge Dictionary, 2025). Real-world learning refers to tasks that closely resemble those encountered in the professional spheres involving learning by doing and problem-solving (Krajcik & Shin, 2014).

‘Authentic’ is described as something real, true, accurate and not a copy (Oxford Learner’s Dictionaries, 2025). An authentic learning environment captivates students because the content and context are seen as relevant to their personal needs, while the teacher views them as reflecting real-life situations beyond the classroom (Calli-

son & Lamb, 2015). Larmer (2012) in his article PBL: What does it take for a project to be "authentic"? points out, that *fully authentic* projects are authentic to the lives of learners having a direct impact or use in the real-world. Herrington, Reeves & Oliver (2014) describe authentic learning as a pedagogical approach focusing on practical significance and applicability to real-world contexts. The learning experience is deep and transferable, which is situated in the context of its future applications.

The concept of authenticity is tied to factors such as motivation, participation, and enhanced learning. The authentic problems may reflect challenges faced by professionals, involve real-world processes and tools, create tangible impacts, and address students' interests or concerns (Jones, 2019). Reeves, Herrington & Oliver (2002) conducted a detailed literature review and identified ten key features of authentic activities:

Authentic activities have real-world relevance; are ill-defined, requiring students to define the tasks and sub-tasks needed to complete the activity; comprise complex tasks to be investigated by students over a sustained period; provide the opportunity for students to examine the task from different perspectives, using a variety of resources; provide the opportunity to collaborate; provide the opportunity to reflect; can be integrated and applied across different subject areas and lead beyond domain-specific outcomes; are seamlessly integrated with the assessment; create polished products valuable in their own right rather than as preparation for something else; allow competing solutions and diversity of outcome.

Petraglia (1998) emphasises the significance of understanding what may appear real and meaningful to students rather than aiming for absolute realism. The tasks perceived as real and meaningful by students lead to increased engagement and learning.

In this study, the words authentic and real-world are used to communicate what is real or authentic to the lives of the learners; situated in their immediate context and have a potential for real-world application.

Real-world Project Case

The study is based on the application of a real-world project under the PBL framework. This section gives a brief account of how the project was designed and implemented in the studio setting.

Background Information

Institute of Design, Nirma University offers Communication Design—a four-year degree programme. The thirty-five students who participated in the study had completed two years, of which the first year was the

foundation year³ that introduced them to various design skills, design concepts, design thinking, and design theory. In year two they had a focused Communication Design engagement. The Publication Design I (course code—DSK 311) course was selected for the study, offered in year three of the programme. The framework began with identifying an authentic design project that aligns with the specifications outlined in the prescribed course syllabus. The literature review suggests that PBL doesn't serve as an ancillary exercise for aiding learning; rather, it forms the foundation of the curriculum. (Bell, 2010; Thomas, 2000; Boss & Krauss, 2014; Jones, 2019). The course syllabus addressed the core fundamentals of graphic design for print publications.

The previous two years of education in the Communication Design programme had equipped students with the prerequisite skills in typography, layout, print production, and design software. The literature review places much emphasis on the long duration of the class for the effective implementation of PBL. This gives learners an opportunity for sustained efforts towards addressing the driving question or problem. The course was assigned 132 hours in the academic calendar with twenty-two teaching days. The course lasted for about a month, including the non-working days. Students did not have any parallel academic engagement during this period.

The course was divided into three phases; the first three weeks were dedicated to Phase 1, and weeks 4 and 5 were dedicated to Phase 2 and Phase 3. The groups decided on multiple intermediate task completion targets with the help of the instructors in view of the end goal. Bell (2010) suggests that PBL is divided into multiple phases for which the timeline must be sacrosanct. Thus, for the smooth flow of various tasks and to conclude the project successfully, it is imperative to chalk out a well-thought-out plan. A detailed course plan, approved university syllabus, an outline of objectives, expected outcomes, and suggested readings were shared with the concerned students before the course commencement.

Application of the Framework

The PBL model was adopted from Blumenfeld et al., 1991 and Krajcik & Blumenfeld, 2005. It consisted of seven major components mentioned in Figure 1 and discussed below.

³ A foundation year in design education is a preparatory programme to teach the fundamental skills and knowledge related to design principles, techniques, and tools. In India, the first year of the four-year degree programme in design is the foundation year, which is common for all the students interested in studying any specific design specialisation. After the completion of the foundation year, students advance to their chosen specialisations.

Driving Question

Jones (2019) suggests that "teachers select the real-world challenge and should write the overarching problem in the form of a question"; the project was guided by the driving question, "How may we design books that these become a future library resource for students and the academic community?" The driving question was designed keeping to the views of Krajcik, suggesting that a good driving question is "*feasible, worthwhile, contextualised, meaningful and ethical*" (Krajcik & Shin, 2014).

Books for print medium were to be designed; however, the exact nature of the books was decided by the students. Blumenfeld et al. (1991) pointed out that students, teachers or curriculum developers can be responsible for creating a driving question or the activities; however, the driving question must not be trivial or the outcomes predefined, leaving no scope for learners to answer the question independently. The instructors ensured that the pre-defined curriculum needs were addressed and students would not feel overwhelmed by the daunting tasks of project work.

The choice of projects, design decisions, project planning & management, goal setting, work distribution, etc. were at the discretion of the students. Scholars over the years have suggested—for students' motivation, they must be given autonomy over the choice of the project, how to carry it forward and the end-products (Blumenfeld et al., 1991; Jones, 2019; Lepper, 1988). Furthermore, teachers take on the role of facilitators or mentors, guiding and overseeing the entire process of learners as they carry out their projects (Thu, 2018).

Project Authenticity and Situated Learning

Blumenfeld et al. (1991) stressed that a learning environment when authentic with real-world context, allowing learners to see the value and meaning of the performed tasks, has a positive impact on the learners. As learners investigate and answer the driving question personally meaningful in their lives and immediate communities, they stand testimony to the application of their work that solved problems of significance.

Furthermore, according to the concept of situated learning, learning occurs in the situation of its intended application and "authentic contexts are the cornerstone of the theory" (Onda, 2012). The research on "situated cognition," suggests that the learning is maximised in situations where the learning context resembles real-life context, allowing the application and utility of the learning outcome. Conversely, learning is minimised in unfamiliar contexts where there is a discord between the learning context and the application of the end-product (Brown, Collins & Duguid, 1995).

The students who wanted to work on a hypothetical design brief⁴ were discouraged, as that would have contradicted the framework of a real-world project laid out for the study. The class unanimously decided to collaborate on designing four books in a group setting. The authenticity and utility of the end-products were ensured. The originality of the content was addressed—three books were based on the process and the outcome of the courses completed by the students in previous years and one coffee table book for their university.

Students were encouraged to clearly articulate the design brief, the driving question, and define the purpose of the project and users before moving to the stage of design activity. This stage encompasses learners' involvement in *learning by doing* by following the design process (Ellmers, 2014). This *learning by doing approach* is at the heart of PBL and design education (Taneja, 2022).

Collaboration

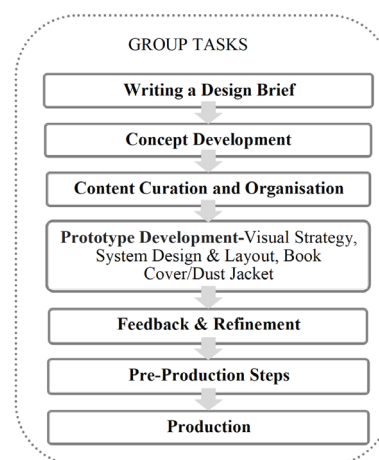
Collaboration is essential for the successful implementation of PBL. Collaborative learning encompasses diverse educational strategies wherein students, or both students and educators, collaboratively engage in intellectual activities (Smith & MacGregor, 1992). When students work in collaboration, they are faced with unavoidable differences, which they learn to acknowledge and tackle. Central components of community life involve developing the ability to accept and resolve differences, create environments to respect different voices and care for others (Smith & MacGregor, 1992). The instructors divided the class into four groups. The group size was determined by the workload associated with the projects. Paredes, Ortigosa & Rodríguez (2010) stressed that “heterogeneous groups tend to perform better than groups formed by students with similar characteristics”. Bell (2010) emphasises, “In the real world, people use their individual strengths and talents in their jobs”. Thus, individuals were chosen based on their varying skills to guarantee diversity within the groups. The identified skills for the project were “content writing, illustration, photography, layout, typography, software, and knowledge of print production” (Taneja, 2022). There was some resistance from some students who wanted to work with friends, but the instructors thought it would be counterproductive. When students work with friends, they may be hesitant to provide honest criticism or challenge each other's ideas, fearing that it could damage the interpersonal dynamics of the group (Le, Janssen & Wubbles, 2018).

⁴ A design brief is a document prepared to guide designers throughout the project. It outlines the background, purpose, scope, deliverables, end-users, stakeholders, project timeline, budget, etc. to facilitate decision-making at different project stages right from the project conception to its completion.

To increase groups' productivity, instructors did not allow the self-selection of group members. Each group had at least one member with each of the identified skills. Students collaborated at three levels: Collaboration with group members was the project's central collaboration point, with team members working together at different stages and addressing design challenges. They also connected beyond regular class hours employing various digital collaboration tools for feedback and project monitoring. Besides the group members, the class collaborated to contribute their previous semester's coursework for the books. They shared their learning notes and sought feedback from classmates for content and design clarity. Further, the instructors helped refine and edit the content for the books (Taneja, 2022).

The Design Process

The design process encompasses a range of activities—analysing the situation from different perspectives, defining the problem, exploring ideas, creating prototypes, conducting tests, receiving feedback, making improvements, and ultimately delivering the final solution or end-product. The stages of a design process are iterative and may not follow a strict linear progression (Taneja, 2022). According to Dorst, the design activity stage is often described as the 'learning by doing' approach and is a key aspect of creating authentic learning environments in PBL (Dorst 2006 as cited in Ellmers, 2014). Groups A to D independently chose themes for their books, detailed in Table 3. Students actively participated in all design stages, from synthesising design briefs to prototypes that facilitated feedback and refinement. They were intensely involved in pre-production, production and post-production decisions. The project offered learning opportunities through multiple intermediate activities supporting research, collaboration, visual design, and systemic thinking. Students were engaged in problem-solving and critical thinking through extensive group discussions at all project stages. Figure 2 outlines the project's key stages.



» **Figure 2:** Main Stages of the Design Process (Taneja, 2022)

Guidance and Scaffolding

In education, scaffolding refers to instructional techniques used for a progressive movement of learners towards stronger understanding and independence in the process of learning. Educators offer different stages of temporary assistance to students, allowing them to attain higher levels of understanding and skills that they would not have been able to achieve without guidance and support (Great Schools Partnership, 2015).

The group projects were divided into three main stages. Each stage was broken down into smaller tasks to give an overview and provide a structural framework for the design project as indicated in Table 1 and 2. Blumenfeld et al. (1991) contend that teachers should employ scaffolding techniques akin to those utilized by experts, breaking down tasks and employing methods such as modelling, prompting, and coaching to teach problem-solving strategies, progressively transferring autonomy to students. Grant (2002) expands on this idea, stating that these scaffolding techniques may involve interactions between students and teachers, practice resources, peer guidance, guiding questions, support tools, project frameworks, and similar aids.

Table 1

Task break-up for scaffolding (Taneja, 2022)

Project Stages	Scaffolding Plan
Stage 1	Anatomic structure of publications Study and analysis of well-designed publications Design brief articulation—objective, users, tone of voice, timeline User study Concept development Content development, curation and organization · Content system and hierarchy Pre-production planning—substrate, printed size, binding techniques, production technology. Visual strategy · Visual design—grids, margins, columns, gutter-space, header, footer, negative space · Typography—type pairing, point size, leading, kerning, line length, drop letters, indents, page numbers, text hierarchy · Colour—primary, secondary and tertiary colour palettes · Image making—illustrations, photographs, icons, infographics etc. · Image management—scan, image size, resolution, edit, colour mode · Visual system design · Book cover/Dust jacket
Stage 2	Prototype Feedback and Refinement
Stage 3	Pre-production—print run, artwork, proofs Production Post-production—UV, embossing, creasing, folding, cropping, lamination, binding, etc.

Note:

Production requirements were considered across all course stages. Certain intermediate tasks were characterised by iterative approaches rather than adhering strictly to a sequential progression.

Table 2

Guidance and Scaffolding Provided During the Three Stages

Project Stages	Guidances
Stage 1	Recurring discussions & formative feedback for clarity of steps in Stage 1: · Case studies of professional work · Developing, curating & organising visual & written content · Visual strategy feedback & refinement loop · Key decisions at the pre-production stage · Collaboration tools to connect after-hours
Stage 2	Discussion & formative feedback for clarity of steps in Stage 2: · Understanding paper sizes, GSM, and coated/uncoated stock, UV printing, etc. · Visual strategy, prototype, feedback & refinement · Case studies for the design of book covers & dust jackets · Staying connected outside of teaching hours
Stage 3	Discussion & formative feedback clarity of steps in Stage 3: · Prototype, feedback, proof-reading, editing · Artwork for the production stage · Specification sheet · Post-production steps · Staying connected outside of teaching hours

Use of Technology

Technology can play a significant role in motivating students and teachers by facilitating the availability of information, implementation, and production of artefacts. Participants of this study worked on a professional publication design software prevalent in the industry and used by professionals. This allowed them to emulate tools used by experts to produce artefacts. The students were trained in using this software through earlier exposure. Comfort in using the software facilitated explorations of ideas, altering representations, and developing the artefact with ease and comfort. Blumenfeld et al. (1991) emphasize that students' familiarity and proficiency with software enhance motivation. Mastery of software applications encourages students to explore alternative approaches and take risks. The use of internet technology for secondary research, real-time collaboration tools such as concept boards, Google Docs, video conferencing for presentations and discussions, mind mapping tools, and social media groups to stay connected throughout the course allowed the project work to be continued beyond the university studio hours.

Integrating modern technology into PBL enhances student engagement, fosters real-world connections, and adds authenticity to projects. Students can present their outcomes to a larger community through social media campaigns, blog posts, films, or podcasts, amplifying visibility and impact. Modern technological tools support real-time collaboration, streamline the design process, facilitate data collection for research, and improve outreach, ensuring that project outcomes effectively reach

the intended audience, users, and stakeholders, thereby maximising their impact. Some technological tools for utilisation during PBL are mentioned in Table 3. Further, artificial intelligence tools (AI) can be integrated into research, data-analysis, problem-solving and presentation development. The tools mentioned in Table 3 have integrated AI to facilitate the users with predictive text, grammar and spell-check, automated meeting summaries, chatbots, transcriptions, content recommendations, etc.

Table 3

List of some technology tools that may be utilized by the design students during PBL

Category	Technology Tools
Real-time Collaboration	Google Docs, Google Jamboard, Miro Board, Concept Board, Google Meet, Zoom, Microsoft Teams, Webex Meetings, Skype, Slack, Microsoft Whiteboard, Nuclino
Design Process	Jamboard, Miro Board, Concept Board, Figma, Canva, Trello, Asana
Data Collection for Research	Zoom, Microsoft Teams, Typeform, Google Forms, SurveyMonkey, Otter.ai
Outreach	Google Meet, Zoom, Microsoft Teams, Webex Meetings, Skype, BlueJeans, GoToMeeting, Twitter, Facebook, LinkedIn, Instagram, Threads
Sharing Project Outcomes	Behance, Dribbble, Vimeo, YouTube, Medium, Weebly, Wix
Documentation Tools	Wedocs, Clickup, Betterdocs, Scribe
Artificial Intelligence (AI) Tools for Image Generation and Visual Enhancement	Midjourney, DALL-E, Let's Enhance, Leonardo.AI, Adobe Firefly, Vizcom, Jasper.ai, Khroma, Autodraw

Artefacts

Study participants went through various stages in the design process before they designed the final artefact. The four groups, from Group A to Group D, successfully designed four books, as mentioned in Table 4.

Table 4

Details of Final Artefacts Made in Four Different Groups (Taneja, 2020)

Group	Book Title	No. of Pages
Group A	Type Under Construction	256
Group B	Identity Please	368
Group C	Bidi and Bori – Packaging Graphics	188
Group D	Nirma University	204

The books designed by the students were printed as final finished products and presented to university officials for feedback. Annexure 1-2 shows the photographs of the four books designed by the students.

In PBL, students collaboratively tackle real-world challenges, producing tangible outcomes presented in a public setting (Jones, 2019). The artefacts represent students' proposed solutions, reflecting the evolution of their knowledge. These tangible outcomes, such as models, reports, videotapes, or computer programmes, facilitate feedback through presentation and critique. This process offers opportunities for reflection and refining the artefact to enhance their emerging knowledge (Blumenfeld et al., 1991).

Authentic Assessment

One of the key aspects of PBL is the emphasis on authentic assessment. PBL is a process-driven approach, thus, the assessment must also focus on the learning journey rather than just the final outcome for a holistic view of students' performance. "Authentic assessments are formative, not summative", thus, must take place during the learning process. The information about the strengths and weaknesses collected in transit to give feedback improves the quality of learning and eventually the learning outcome (Parwati et al., 2019).

Authentic assessment in PBL may take various forms where the students may create working models or prototypes and present their findings to an expert panel or stakeholders for evaluation or feedback.

Krajcik & Blumenfeld (2005) insist that the feedback must be extensive and preference must be given to individual feedback over group feedback. Blumenfeld et al. (1991) stressed that for assessing the learning of the students, knowing what they already know before the project commences is important. Unconventional assessment based on observing the journal or notebook entries, portfolio reviews, and examining students' discourse works better for PBL as opposed to conventional methods such as standardised tests or workbook questions. Furthermore, the integration of self-assessment and peer assessment can make PBL very effective. Mansur & Alves (2018) have stressed that the formative method of peer assessment and self-assessment helps provide feedback during the project process phase, leading to more adaptive and effective learning.

Self-assessment encourages reflection about the learning experience, key decisions and actions, and develops critical thinking and problem-solving skills. The course instructors may design a rubric to address the key areas—core domain knowledge and skills, collaboration, technical skills, critical thinking, problem-solving, communication, presentation skills and artefact or the final outcome.

The formative and summative assessments which are comprised of self-assessment, peer assessment, the instructor's evaluation, and feedback from the community can be fruitful and holistic in the case of PBL.

Conclusion

The study helps enhance understanding of PBL. It also gives clarity about how the real-world project may be interpreted in the context of graphic design education. The PBL framework proposed in the study was successfully applied in the studio classroom of the year III communication design programme.

The popularity of design education is on the rise in India. While there is an emphasis on real-world projects in teaching design, there is a paucity of industry projects in the academic setting, which increases the dependence on hypothetical projects. The popular phenomenon of working on industry projects to which institutes have limited access may be substantiated by projects generated within the university or the institute to meet their graphic design requirements; this outlook can help bridge the gap of academic-industry partnerships and enhance transferability to the professional world. Generating real-world opportunities with an authentic context to fulfil an actual graphic design requirement in an academic space can be a win-win situation for both the institutes/universities and the students. Thus, such opportunities must be identified or generated for an enriched learning experience and fulfil the need to prepare students for the real-world. Be it designing the promotional material for an event or the annual calendar or planner—the real-project can lead to real-learning.

However, it may be noted that different learning pedagogies may be appropriate for different learning stages. At some stages, an application-based approach to developing disciplinary foundational skills is apt. At a different learning stage, a hypothetical approach may be necessary to achieve a curricular milestone. Furthermore, for the successful implementation of PBL in which students deliver implementable solutions, learners must acquire some core disciplinary knowledge and skills before they embark on this journey. It was observed that group formation based on individual skills may compromise the overall learning experience by limiting students to perform only in the area of their proficiency. Instructors must ensure that the overarching course learning objectives are met by all the participating students by encouraging their active participation at different project stages for a holistic learning experience. The course duration must be long enough to give students enough time for optimal results in PBL. Thus, it would be ideal to have the course continuously, at one go, rather than having more than one parallel course input, as that might hinder the flow of the PBL project.

The proposed framework covers all the essential ingredients to realise a successful project in the area of graphic design. The framework may also benefit allied disciplines in design and serve a larger community of design educators. While there is literature on PBL, it is unrelated to the graphic design context. This study not only addresses the problem of identifying projects that fall under PBL for graphic design education but also serves as an example for educators to implement the framework for the best results of PBL pedagogy.

In the era of revolutionary technological advancement and available AI tools, future research could study how, within the existing framework these tools may be integrated to improve the learning journey.

Funding

The research did not receive any specific grant from funding agencies in the public, commercial, or not-for-profit sectors.

References

- Bell, S. (2010) Project-based learning for the 21st century: skills for the future. *The Clearing House: A Journal of Educational Strategies, Issues and Ideas*. 83 (2), 39–43. Available from: doi: 10.1080/00098650903505415
- Blumenfeld, P. C., Soloway, E., Marx, R. W., Krajcik, J. S., Guzdial, M. & Palincsar, A. (1991) Motivating project-based learning: sustaining the doing, supporting the learning. *Educational Psychologist*. 26 (3–4), 369–398. Available from: doi: 10.1080/00461520.1991.9653139
- Boss, S. & Krauss, J. (2014) *Reinventing project-based learning: your field guide to real-world projects in the digital age*. 2nd ed. Eugene, OR: International Society for Technology in Education.
- Bothra, S. (2019) *Design education in India: Its role in imparting values of socially responsible design*. Rajasthan, Banasthali Vidyapith.
- Bothra, S. (2024) Contemporary design education and concern for social responsibility. In: *Design Education in India – Values of Socially Responsible Design*. London, Routledge, p. 125.
- British Council & India Design Council. (2016) *The future of design education in India*. Delhi, British Council.
- Brown, J. S., Collins, A. & Duguid, P. (1995) Situated cognition and the culture of learning. In: Murphy, P., Selinger, M. & Briggs, M. (eds.) *Subject Learning in the Primary Curriculum: Issues in English, Science and Mathematics*. London, Routledge, Taylor & Francis Group, pp. 301–319.
- Callison, D. & Lamb, A. (2015) *The Evolution of Inquiry: Controlled, Guided, Modeled, and Free*. Bloomsbury Publishing USA, p. 272.

- Cambridge Dictionary. (2025) *the real world*. Cambridge Dictionary Online. Available from: <https://dictionary.cambridge.org/dictionary/english/real-world> [Accessed: 5th October 2025].
- Dictionary.com. (2024) *Meanings & Definitions of English Words*. Dictionary.com.
- Ellmers, G. (2014) *Graphic design education: fostering the conditions for transfer in a project-based and studio-based learning environment, through a structured and critical approach to reflective practice*. PhD thesis. University of Wollongong.
- Farrow, J., Kavanagh, S. S. & Samudra, P. (2022) Exploring relationships between professional development and teachers' enactments of project-based learning. *Education Sciences*. 12 (4), 282. Available from: doi: 10.3390/educsci12040282
- Giri, D. R. (2016) Project-based learning as 21st century teaching approach: a study in Nepalese private schools. *US-China Education Review A*. 6 (8), 487–497. Available from: doi: 10.17265/2161-623X/2016.08.004
- Grant, M. M. (2002) Getting a grip on project-based learning: theory, cases and recommendations. *Meridian: A Middle School Computer Technologies Journal*. 5 (1), 1-17.
- Great Schools Partnership. (2015) *Scaffolding*. The Glossary of Education Reform. Available from: <https://www.edglossary.org/scaffolding/> [Accessed: 5th May 2020].
- Han, S., Yalvac, B., Capraro, M. M. & Capraro, R. M. (2015) In-service teachers' implementation and understanding of STEM project-based learning. *EURASIA Journal of Mathematics, Science and Technology Education*. 11 (1), 63–76. Available from: doi: 10.12973/eurasia.2015.1306a
- Hasni, A., Bousadra, F., Belletête, V., Benabdallah, A., Nicole, M.-C. & Dumais, N. (2016) Trends in research on project-based science and technology teaching and learning at K–12 levels: a systematic review. *Studies in Science Education*. 52 (2), 199–231. Available from: doi: 10.1080/03057267.2016.1226573
- Herrington, J., Reeves, T. C. & Oliver, R. (2014) Authentic learning environments. In: Spector, J. M., Merrill, M. D., Elen, J. & Bishop, M. J. (eds.) *Handbook of Research on Educational Communications and Technology*. 4th ed. New York, Springer, pp. 401–412. Available from: doi: 10.1007/978-1-4614-3185-5_32
- Jones, B. (2019) Good practice: scaffolded, collaborative project-based learning. *Journal of Education, Humanities and Communication*. 3 (2), 1–16. Available from: doi: 10.31378/jehc.85
- Krajcik, J. S. & Shin, N. (2014) Project-based learning. In: Sawyer, R. K. (ed.) *The Cambridge Handbook of the Learning Sciences*. 2nd ed. Cambridge, Cambridge University Press, pp. 275–297. Available from: doi: 10.1017/CBO9781139519526.018
- Krajcik, J. S., Blumenfeld, P. C., Marx, R. W. & Soloway, E. (1994) A collaborative model for helping middle grade science teachers learn project-based instruction. *The Elementary School Journal*. 94 (5), 483–497. Available from: doi: 10.1086/461779
- Krajcik, S. J. & Blumenfeld, P. C. (2005) Project-based learning. In: Sawyer, R. K. (ed.) *The Cambridge Handbook of the Learning Sciences*. New York, Cambridge University Press. Available from: doi: 10.1017/CBO9780511816833
- Krajcik, S. J. & Blumenfeld, P. C. (2014) Project-based learning. In: Sawyer, R. K. (ed.) *The Cambridge Handbook of the Learning Sciences*. New York, Cambridge University Press, pp. 317–333.
- Kwietniewski, K. (2017) *Literature review of project-based learning*. State University of New York, College at Buffalo. Available from: https://digitalcommons.buffalostate.edu/careereducation_theses/1/ [Accessed: 5th October 2025].
- Larmer, J. (2012) *PBL: What Does It Take for a Project to Be 'Authentic'?*. Available from: <https://www.edutopia.org/blog/authentic-project-based-learning-john-larmer> [Accessed: 4th June 2020].
- Le, H., Janssen, J. & Wubbels, T. (2018) Collaborative learning practices: teacher and student perceived obstacles to effective student collaboration. *Cambridge Journal of Education*. 48 (1), 103–122. Available from: doi: 10.1080/0305764X.2016.1259389
- Lepper, M. R. (1988) Motivational considerations in the study of instruction. *Cognition and Instruction*. 5 (4), 289–309. Available from: doi: 10.1207/s1532690xci0504_3
- Mansur, A. F. U. & Alves, A. C. (2018) The importance of peer assessment and self-assessment in PBL applied to an administration course. *Revista Ibero-Americana de Estudos em Educação*. 13 (special issue), 451–467. Available from: doi: 10.21723/riaee.nesp1.v13.2018.10347
- Mathur, I. S. (ed.) (2014) *Design education in India: retrospect, introspection, and perspective*. Ahmedabad, National Institute of Design.
- Onda, E. L. (2012) Situated Cognition: Its Relationship to Simulation in Nursing Education. *Clinical Simulation in Nursing*. 8 (6), e273–e280. Available from: doi: 10.1016/j.ecns.2010.11.004
- Oxford Learner's Dictionaries. (2025) *authentic adjective – definition, pictures, pronunciation and usage notes*. Oxford Advanced Learner's Dictionary. Available from: <https://www.oxfordlearnersdictionaries.com/definition/english/authentic> [Accessed: 5th October 2025].
- Paredes, P., Ortigosa, A. & Rodríguez, P. (2010) A method for supporting heterogeneous-group formation through heuristics and visualization. *Journal of Universal Computer Science*. 16 (19), 2882–2901.
- Parwati, N. W., Suarni, N. K., Suastra, I. W. & Adnyana, P. B. (2019) The effect of project-based learning and authentic assessment on students' natural science learning outcomes by controlling critical thinking skill. *Journal of Physics: Conference Series*. 1318 (1), 012096. Available from: doi: 10.1088/1742-6596/1318/1/012096

- Pecore, J. L. (2015) From Kilpatrick's project method to project-based learning. In: *International Handbook of Progressive Education*. New York, Peter Lang, pp. 155-171.
- Petraglia, J. (1998) *Reality by design: the rhetoric and technology of authenticity in education*. Abingdon, Routledge.
- Qin, J. (2022) On the reform of education methods that adapt to STEM development demand. *International Journal of Education and Humanities*. 6 (2), 141-143. Available from: doi: 10.54097/ijeh.v6i2.3660
- Reeves, T. C., Herrington, J. & Oliver, R. (2002) Authentic activities and online learning. In: *Proceedings of the HERDSA 2002 Quality Conversations, 7-10 July 2002, Perth, Australia*. Perth, HERDSA. pp. 562-567.
- Rensburg, J. R. J. T. (2020) *Developing guidelines for bridging the gap between IT theory and IT practice*. PhD thesis. North-West University.
- Smith, L. B. & MacGregor, T. J. (1992) What is collaborative learning? In: *Collaborative Learning: A Sourcebook for Higher Education*. Pennsylvania, National Center on Postsecondary Teaching, Learning, and Assessment at Pennsylvania State University.
- Sumarni, W. (2015) The strengths and weaknesses of the implementation of project-based learning: a review. *International Journal of Science and Research*. 4 (3), 478-484.
- Taneja, K. (2020) Project-based Learning: Real-world Project for Encouraging Students' Motivation in Graphic Design Education. In: *Proceedings of Online National Conference on "Innovations in Visual Arts", NCIVA 2020, Education 4.0: Perspectives on Visual Arts Practice, Pedagogy and Representation, 7 October 2020, Noida, India*. New Delhi, Excellent Publishing House. p. 164.
- Taneja, K. (2021a) Bridging the gap between graphic design education and profession in India. *International Design and Art Journal*. 3 (2), 198-209.
- Taneja, K. (2021b) Graphic design in search of its identity. *Acta Graphica*. 30 (2), 17-28. Available from: doi: 10.25027/agj2017.28.v30i2.202
- Taneja, K. (2022) Employing project-based learning to foster essential professional skills in students of graphic design. *International Journal of Art and Design Education*. 4 (2), 45-52.
- Thomas, J. W. (2000) *A review of research on project-based learning*. The Autodesk Foundation. Available from: http://www.bobpearlman.org/BestPractices/PBL_Research.pdf [Accessed: 5th October 2025].
- Thu, L. T. K. (2018) Project-based learning in the 21st century: a review of dimensions for implementation in university-level teaching and learning. In: *Proceedings of the 4th International Conference on English Across Cultures, ICEAC, 19-20 October 2018, Singaraja, Indonesia*. Singaraja, Undiksha Press. pp. 229-240.
- Wolk, S. (2022) Clearing up misconceptions about project-based learning. *Kappan*. Available from: <https://kappanonline.org/misconceptions-project-based-learning-wolk/> [Accessed: 5th October 2025].

[org/misconceptions-project-based-learning-wolk/](https://kappanonline.org/misconceptions-project-based-learning-wolk/) [Accessed: 5th October 2025].

Annex 01 - Group A Book Title: Type under Construction



Annex 02 - Group B Book Title: Identity Please



**Annex 03 - Group C Book Title:
Bidi; Bori, Packaging Graphics**



**Annex 04 - Group D Book Title:
Nirma University**







Prediction of dot gain in flexographic color printing using machine learning

ABSTRACT

This work focuses on using machine learning algorithms in the prediction of dot gain related to flexographic process color printing. The way these advanced aspects of machine learning techniques are applied can revolutionize the various uses of printing technology. The machine learning techniques can be used to a wide range of applications since they adhere to dynamic programming methodology and computational learning theory. The machine learning algorithms can generate a trained input dataset framework, allowing them to make logical and dynamic predictions and judgments based on input data. Two grades of paper substrates with varying surface textures, two levels of anilox screen rulings, and a total of 100 steps of halftone square dot percentages with 4% intervals for each process colors are selected as the experimental process variables. An algorithm for evaluating a flexographic print output response, known as Dot Gain was generated using the Python machine learning technique. For data analysis and performance evaluation, machine learning techniques such as linear regression, decision tree, random forest regression, XG (Extreme Gradient) boost regression, SVM (Support Vector Machine) regression and neural network algorithms were used. The findings of this research work demonstrate that, out of all the machine learning algorithms used in this investigation, neural network methods had the highest accuracy. The accuracy of the neural network algorithm is 96.43, 98.32, 97.01 & 95.30 respectively in the prediction of dot gain for cyan, magenta, yellow and black.

KEY WORDS

flexography, dot gain, machine learning, regression, neural network

Soumen Basak¹ 
Saritha P.C² 
Alenrex Maity³ 
Kanai Chandra Paul¹ 

¹ Jadavpur University,
Department of Printing
Engineering, Kolkata, India

² Institute of Printing Technology
and Government Polytechnic
College, Department of Printing
Technology, Kerala, India

³ Jadavpur University,
Department of Information
Technology, Kolkata, India

Corresponding author:

Soumen Basak

e-mail:

soumen.basak@jadavpuruniversity.in

First received: 2.1.2025.

Revised: 7.4.2025.

Accepted: 5.5.2025.

Introduction

The printing background

A rotary relief image carrier that is appropriately flexible is used in the direct printing process known as flexographic printing to transfer printing ink to a range of substrates, including paper, paperboards, plastic films, foils and more (Abusaq et al., 2023).

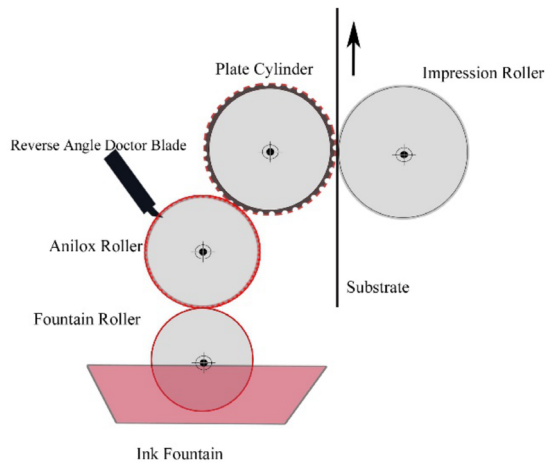
While using the flexible relief printing plates, a very small amount of printing pressure at the printing nip is sufficient to transfer the ink from the plate onto

the substrates which have a variety of surface textures (Joshi, 2022). The anilox roller cell engraving requirements played a significant role in flexographic printing by dictating the amount of ink that is needed to be applied to the substrate. Consequently, this has an impact on the finished print's optical density and halftone reproduction (Bould et al., 2010). Furthermore, the optimum outcome-oriented printing practices in flexographic presses are ensured by the anilox roller cell characteristics (Dendge, 2023).

Smoother paper can increase print density, but an increase in substrate surface roughness can also result in a sudden decrease in print density (Theohari et al., 2014).

The dispersion and absorption of ink, which is influenced by the paper's inherent tone, roughness, and porous surface, affects print quality. The smoothness or roughness of the paper directly affects how much the ink diffuses across the print (Tomasegovic et al., 2021).

The dot gain or Tonal Value Increase (TVI) indicates the increase of dot size in the final print than that of the original dot size given at the input. The Print Contrast indicates the accuracy of halftone reproduction at the shadow areas of a print (Dharavath, Bensen & Gaddam, 2005).



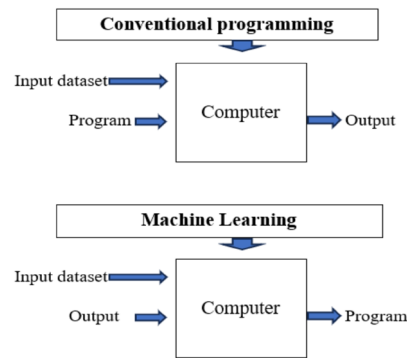
» **Figure 1:** Schematic diagram of flexographic printing unit

The Machine Learning

A branch of artificial intelligence and computer science known as "machine learning" is concerned with simulating human learning processes and gradually improving their accuracy via the use of data and algorithms (Chandel et al., 2022). Alan Turing originally put out the ideas of machine learning in the 1950s.

Machine learning helps computers to draw lessons from their prior experiences and, when needed, form their own opinions. The main objective of machine learning is to create computer programs in advance without requiring human intervention. Any computer can learn by using patterns, predictions, input and prior experience. This allows the machine to make decisions on its own without human intervention and get the right outcomes (Sisodia & Seth, 2022).

Through the use of machine learning techniques, computers are trained to carry out ordinary chores with ease and naturalness. As seen in Figure 2, raw data is fed into a machine learning model, which analyzes it and forecasts the result based on its comprehension of the incoming data (Sodhi, Awasthi & Sharma, 2019).



» **Figure 2:** Conventional Programming vs Machine Learning

As illustrated in Figure 3, there are four common methods for training machine learning algorithms. Machine learning is a collection of algorithms that are learned from data and/or experiences rather than being purposefully coded. Each task necessitates a unique set of algorithms and these algorithms find patterns to complete specific tasks (Çelik & Altunaydin, 2018). They are: Supervised learning, Unsupervised Learning, Reinforcement learning and Semi-supervised Learning.

Some Machine Learning Algorithms

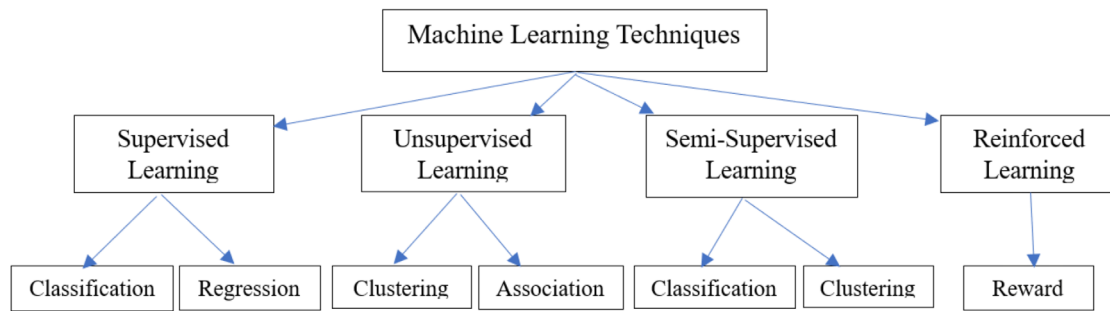
Algorithms are used in the development and instruction of machine learning models. These are the kind of actions that a machine learning model learns via observation and then applies the same technique. Machine learning algorithms have the ability to improve themselves through training (Jin, 2020). Linear regression, decision tree regression, random forest regression, extreme gradient boosting or XG Boost, support vector machine or SVM regression, neural network learning techniques are some of the frequently used algorithms.

Linear regression

A relationship between the dependent variable and one or more independent variables—known as the regression line—is established by linear regression using the best-fitting straight line. The value of the target variable can be predicted using the regression equation and the given predictor variable or variables. Multiple linear regression models are an extension of simple linear regression, where a response variable functions as a linear function of two or more predictor variables.

Decision tree regression

The decision tree sorts the tree from the root to a few leaf nodes in order to classify the instances. By analysing the attribute defined by that node, instances are categorized, beginning at the root node of the tree and proceeding along the branch that corresponds to the attribute value.



» **Figure 3:** *The machine learning techniques*

Random forest regression

It is a technique that fits many decision tree classifiers simultaneously on different subsamples of the dataset. The final outcome is decided by averages or majority vote. The outcome is an improvement in control and forecast accuracy while lowering the problem of over-fitting. It creates a series of decision trees with controlled variance by combining random feature selection with bootstrap aggregation or bagging.

Extreme gradient boosting regression

Extreme Gradient Boosting (XG Boost), a kind of gradient boosting, takes into account more accurate approximations. It calculates the loss function's second-order gradients to minimize loss and accomplish advanced regularization. This reduces over-fitting and improves the model's performance and generalization. XG Boost can swiftly evaluate results and process massive datasets effectively.

Support vector machine regression

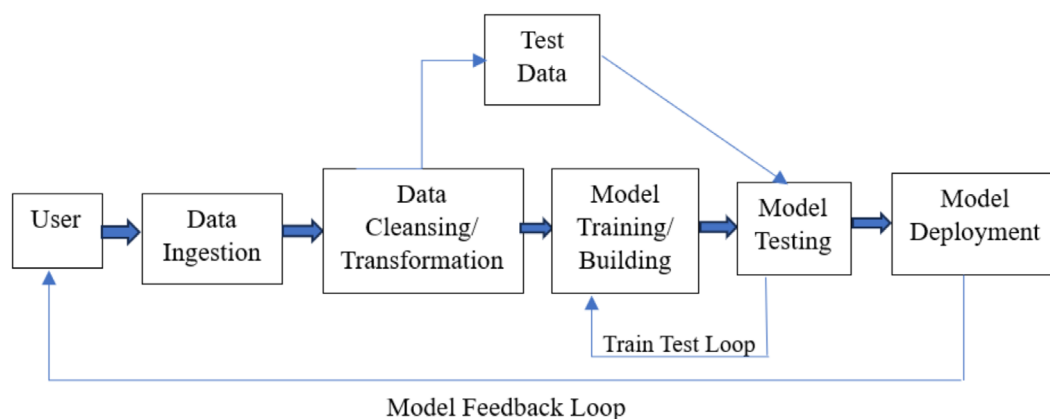
The Support Vector Machine (SVM) algorithm will simultaneously analyze the data to be processed in order to improve the data information. It collects many sets of analysis samples during the

analysis process and determines the sample data of the boundary value in order to improve the scientific quality of the final data analysis results.

Neural network algorithms

The phrase "artificial neural network" refers to a system that simulates human information transmission by classifying different facts into a single neuron and connecting those neurons online to carry out complex memory tasks. However, this dynamic data analysis process forms the basis of the artificial neural network algorithm. A layered structure consisting of multiple interconnected nodes makes up the algorithm. These nodes represent the real neurons in the human brain. Each unique neuron has a high degree of authenticity and the data can complete the process of external output. The human body moves forward, stops and then takes off in a manner similar to this. After the weighting coefficient has been selected, setting the output threshold will facilitate computation and data processing. This makes the process of numerical analysis more systematic overall. This adaptive strategy allows the machines to keep improving by learning from their mistakes.

The machine learning system



» **Figure 4:** *The machine learning workflow: The input dataset is processed and converts into valid format that best fits the needs of the machine learning model being employed*

The fundamental workflow related to machine learning techniques is depicted in Figure 4. The machine learning method that creates a trained model is used in the training phase. The accuracy of the trained model is then repeatedly assessed using the test data. The model is then deployed so that the application can use it after it has reached the required level of accuracy. Establishing a machine learning system to forecast dot gain in the flexographic color printing is the aim study.

Methods

Experiment

Different paper samples having varying paper roughness were printed by flexographic printing varying different input parameters such as anilox screen rulings. Effects of varying dot percentages on different colored dot gain were also considered. Prints were taken in four process colors separately on two sets of different paper samples. Table 1 displays the three input variables that were selected for the research. In the present research, Dot gain was used as the response variable.

Table 1

Parameters in the study

Factors	Unit	Sym- bol	Levels	Response
Anilox Ruling	Lines per inch (lpi)	A	900, 1200	Dot Gain
Paper Roughness	Millilitre per minute (ml/min)	B	76, 109	
Dot Percentage	Percentage (%)	C	4% to 100 % with 4% increments	
Halftone dot shape	-	D	Square Shaped AM dot	

The anilox roller screen rulings used in the work had lines per inch (lpi) of 900 and 1200 respectively. The chosen roughness levels for the paper were 76 and 109 milliliters per minute. The roughness was measured using Roughness tester (Bendtsen type) following IS 1060 (Part 5/ Sec 20) RA2018. The engraved anilox roller cells were 60° hexagonal in form. The OMET LAB230 Iflex flexographic printing machine, which uses process color inks of Cyan (C), Magenta (M), Yellow (Y) and Black (K), was utilized for the printing. The inks used were solvent based liquid inks and have viscosity of 300 cp. A photopolymer plate (Manufacturer – Dupont, Type of the plate – Digital solid photopolymer, Plate production process – Laser engraving process) with a

magnetic backing and of 1.14 mm thickness was used as the printing image carrier. All of the parameters, including the ink characteristics (UV ink), room temperature (23° C), printing speed (35 m/min) and nip pressure (3 mm), were kept constant during the printing process.

Measurements and data collection

The print quality score was determined using the output response. As a result, the output parameters were quantitatively measured using the X-Rite Spectro Eye Spectro-densitometer. Visual examination of the printed area was done using a digital microscope, the LEICA-S8APO. The machine learning algorithms employed the readings of 100 print trials of input data sets for every color. It is expected that the split ratio of the training to test dataset is 7:3. The collected data is fed into the Python program, which processes it using machine learning techniques.

Results

The Tables 2 and 3 display the results of machine learning techniques for each of the C, M, Y, and K process colors. The evaluation instrument for comparison is the performance accuracy of different algorithms for every color. The capacity of the developed model to forecast the result based on the given input variables is referred to as performance accuracy.

Table 2

Splitting of dataset

Shape of data	(100, 4)
Shape of split data	The shape of X_train : (75, 3)
	The shape of X_test : (25, 3)
	The shape of Y_train : (75, 3)
	The shape of Y_test : (25, 3)

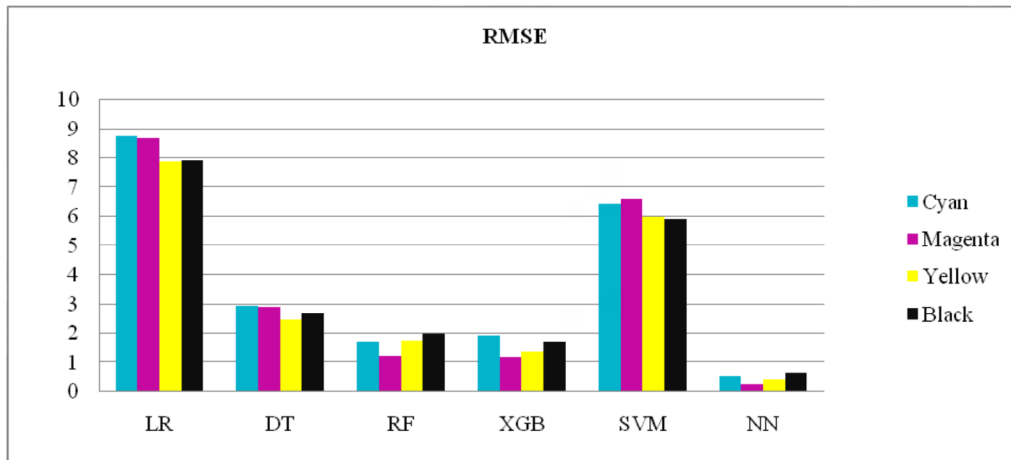
Figure 5 shows the Root Mean Square Error (RMSE) for the different machine learning algorithms. RMSE quantifies the differences between the predicted values and actual values. It has been observed that RMSE is least for Neural Network which implies it is best for this prediction.

Figure 6 represents bar chart of Mean Absolute Error (MAE) for the different machine learning algorithms adopted for prediction MAE measures the average absolute differences between the actual and the predicted values. It has been found that MAE value is the lowest for the Neural Network. This means that Neural Network is the best of all the machine learning algorithms considered for the prediction of dot gain in the present work

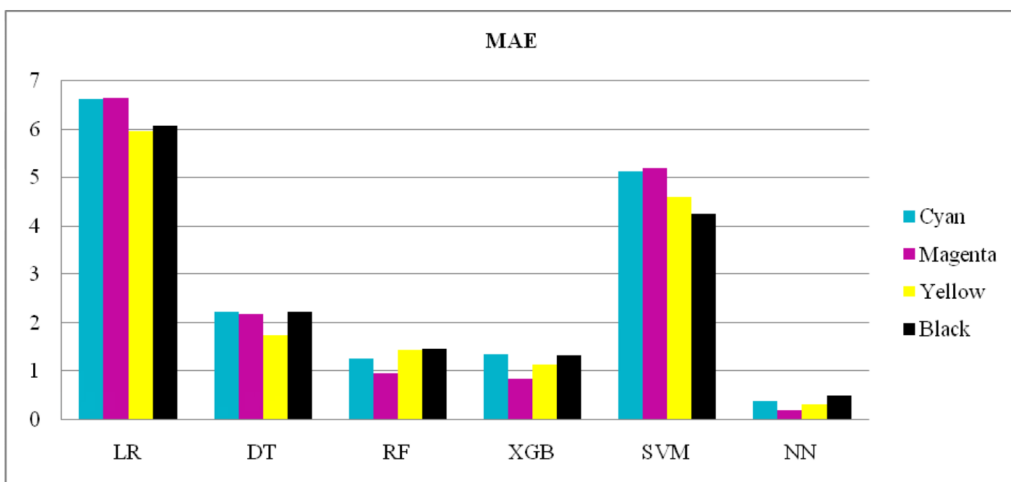
Figure 7 shows the bar chart of R² values for the different machine learning algorithms adopted for the prediction of dot gain.

It indicates the percentage of variation in the target variables that can be obtained by the independent variables. The maximum value of R^2 is 1. The higher the R^2 value, the better is the prediction. It has been found that R^2 value for the Neural Network method

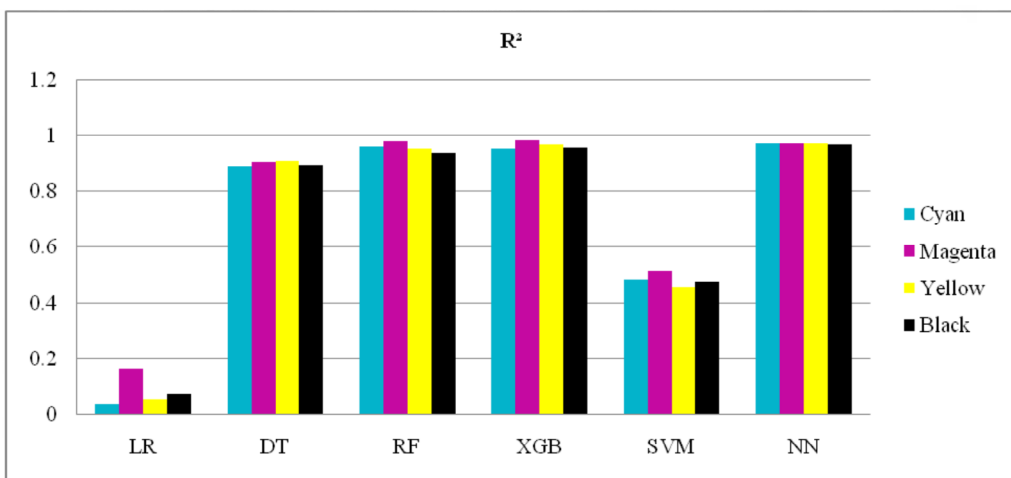
is maximum and near about 1 which implies that this method is the best for the prediction of dot gain in the current investigation. The values of accuracy of different machine learning algorithms given in Table 3 were decided by considering the values given in Figures 5-7.



» **Figure 5:** Bar chart of RMSE values for different machine learning algorithms



» **Figure 6:** Bar chart of MAE values for different machine learning algorithms



» **Figure 7:** Bar chart of R^2 score for different machine learning algorithms

Table 3

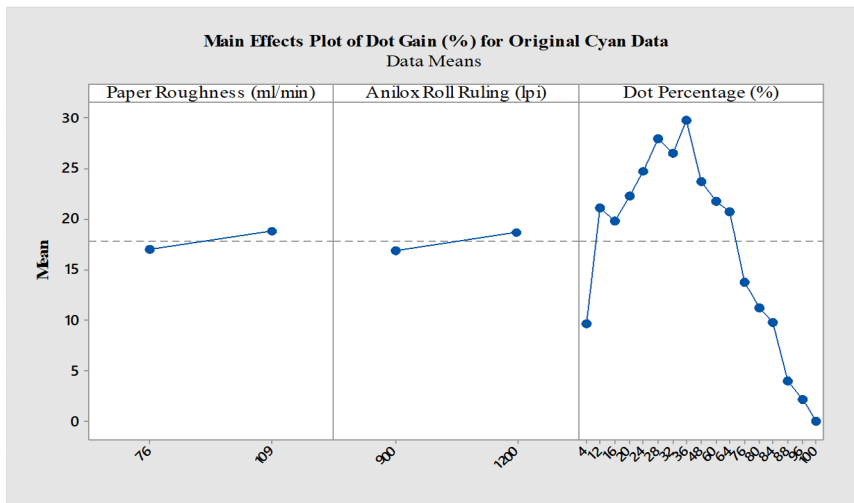
The prediction of Dot Gain with different algorithms

Sl. No.	Process Colors	Machine Learning Algorithms					
		Linear Regression (LR)	Decision Tree (DT)	Random Forest Regression (RF)	XG Boost Regression (XGB)	Support Vector Machine (SVM)	Neural Network (NN)
1.	Cyan	66.43	78.29	87.76	84.78	71.47	96.43
2.	Magenta	66.07	79.76	88.84	89.10	71.35	98.32
3.	Yellow	67.54	88.09	85.05	88.24	73.10	97.01
4.	Black	67.72	85.18	85.22	86.38	75.67	95.30

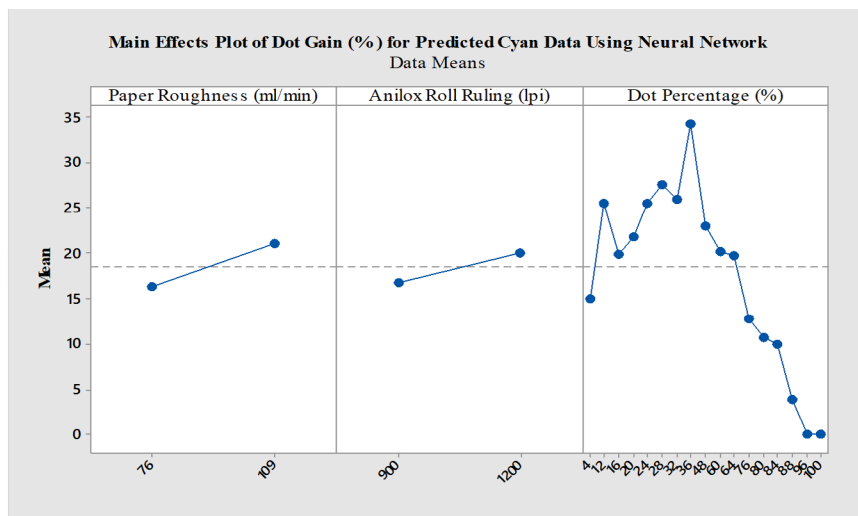
Graphical analysis

The graphical depictions that display the interplay between the various experimental factors that was identified during the analysis stage. The Figures 8-15 display the main effects plot of each experimental factors over

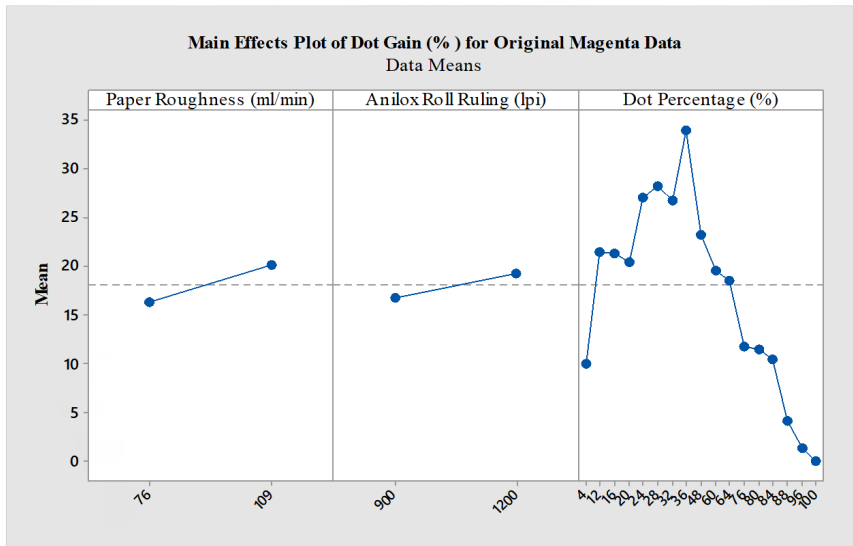
dot gain of original data and predicted data obtained by neural network and the Figures 16-23 displays the interaction effects of original experimental data as well as predicted data. The Figures 8-23 have been plotted using Minitab 17.



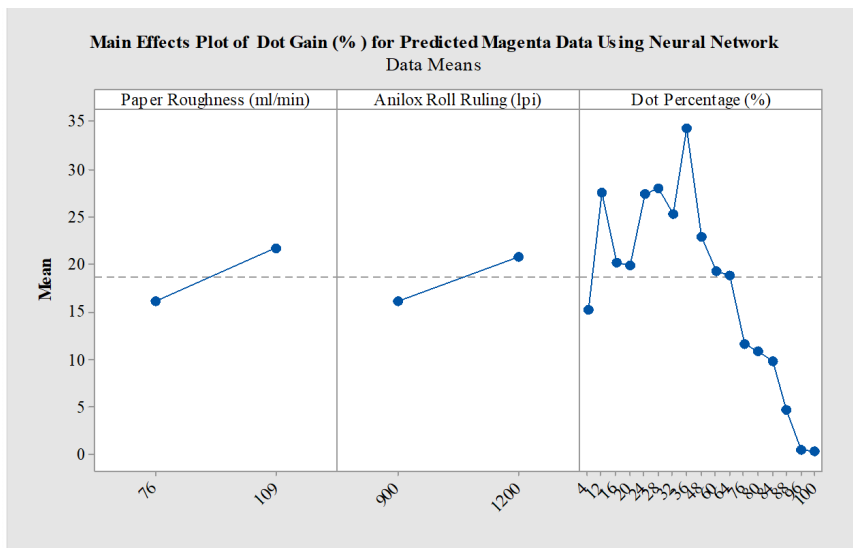
» **Figure 8:** Main effects plot of dot gain for original cyan data



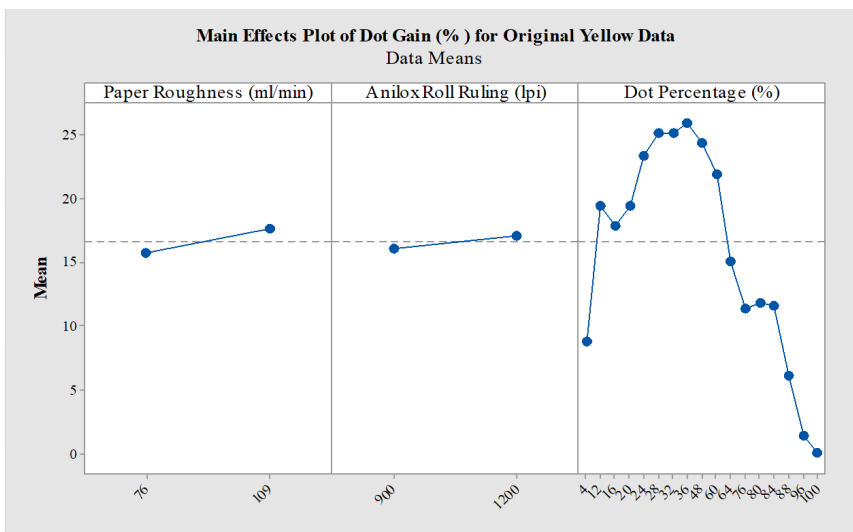
» **Figure 9:** Main effects plot of dot gain for predicted cyan data using neural network



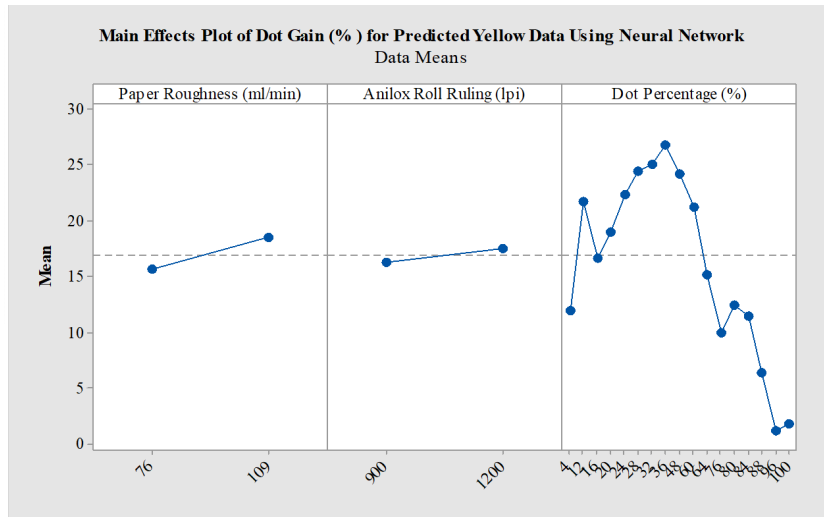
» **Figure 10:** Main effects plot of dot gain for original magenta data



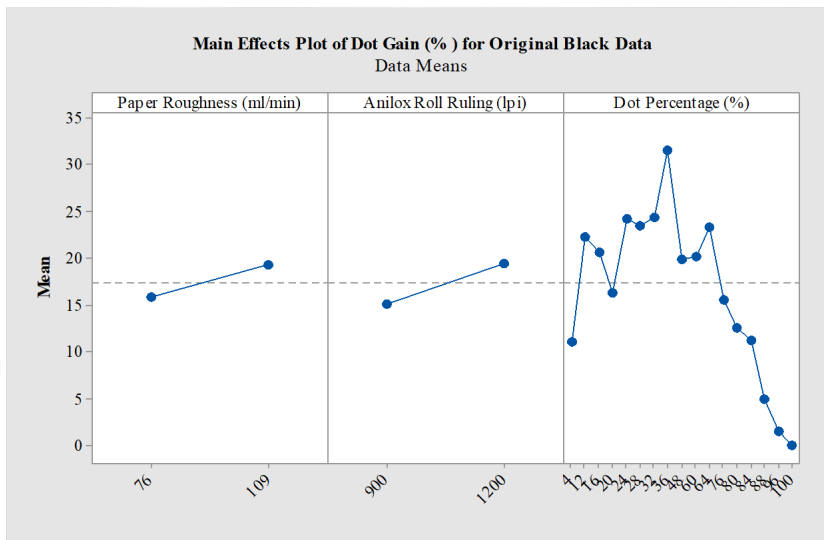
» **Figure 11:** Main effects plot of dot gain for predicted magenta data using neural network



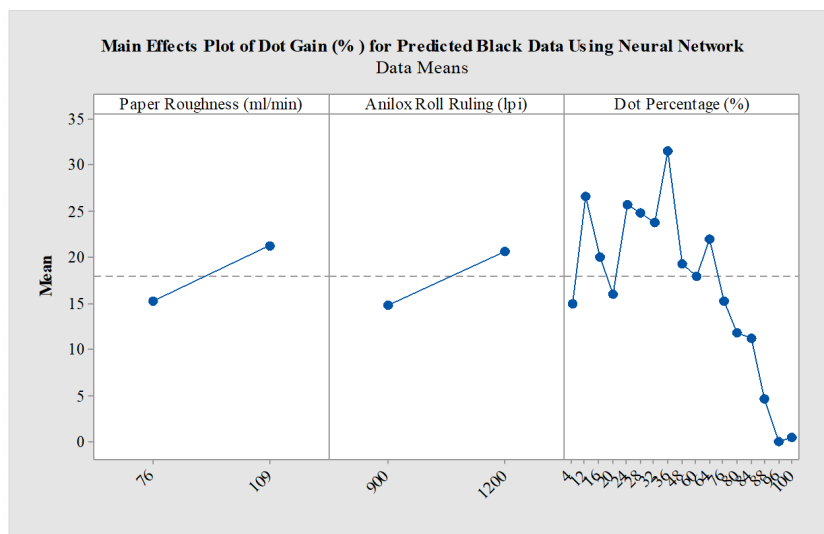
» **Figure 12:** Main effects plot of dot gain for original yellow data



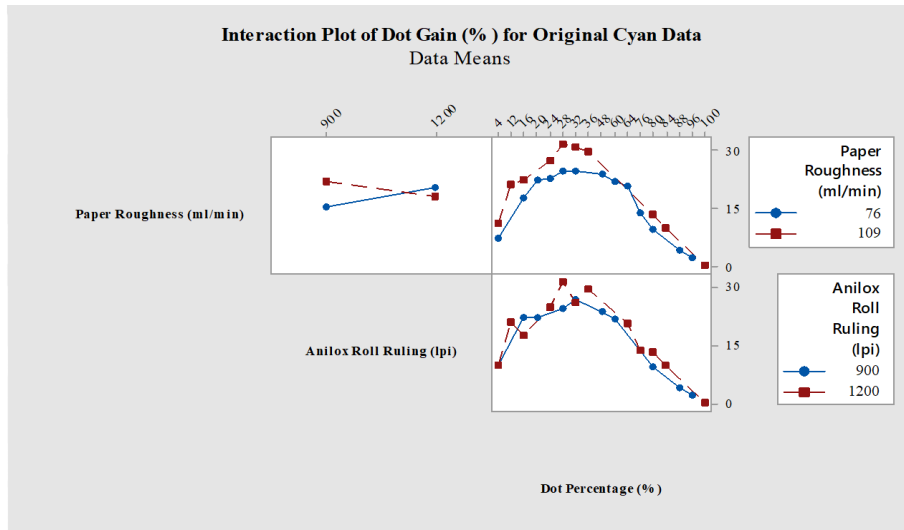
» **Figure 13:** Main effects plot of dot gain for predicted yellow data using neural network



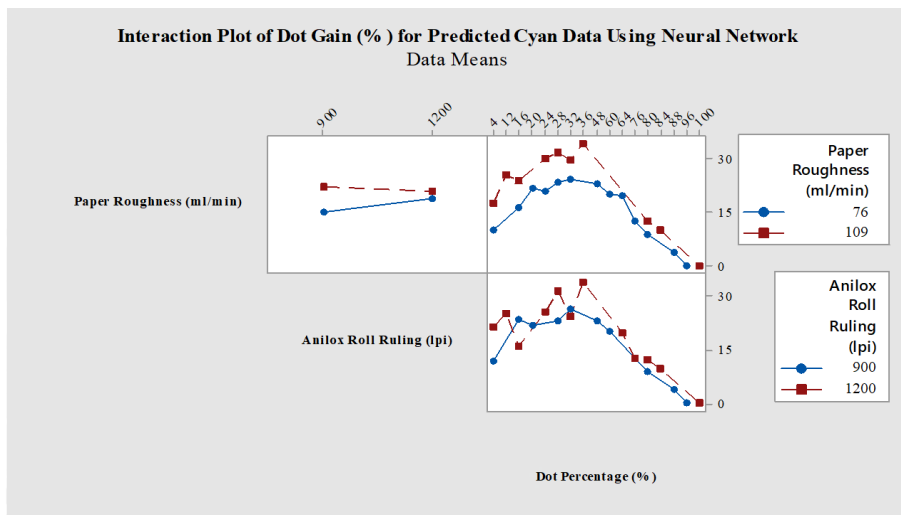
» **Figure 14:** Main effects plot of dot gain for original black data



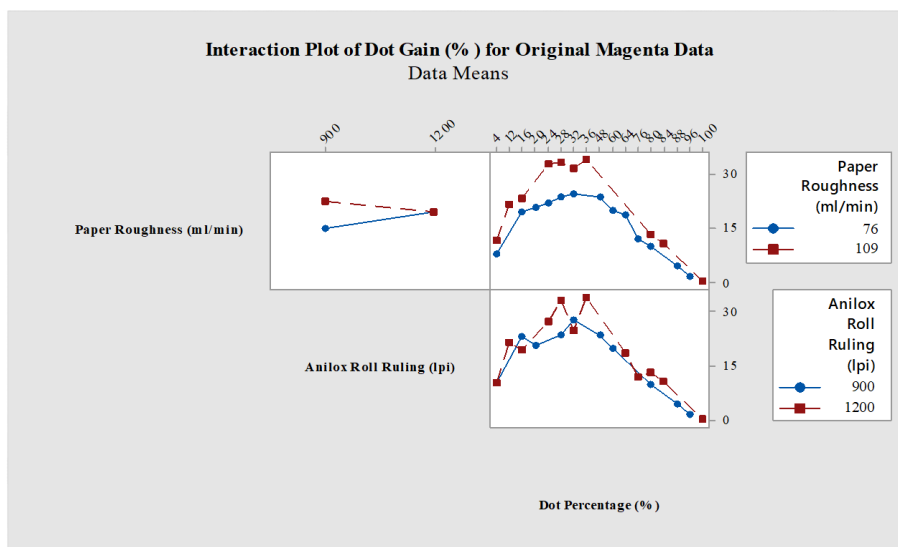
» **Figure 15:** Main effects plot of dot gain for predicted black data using neural network



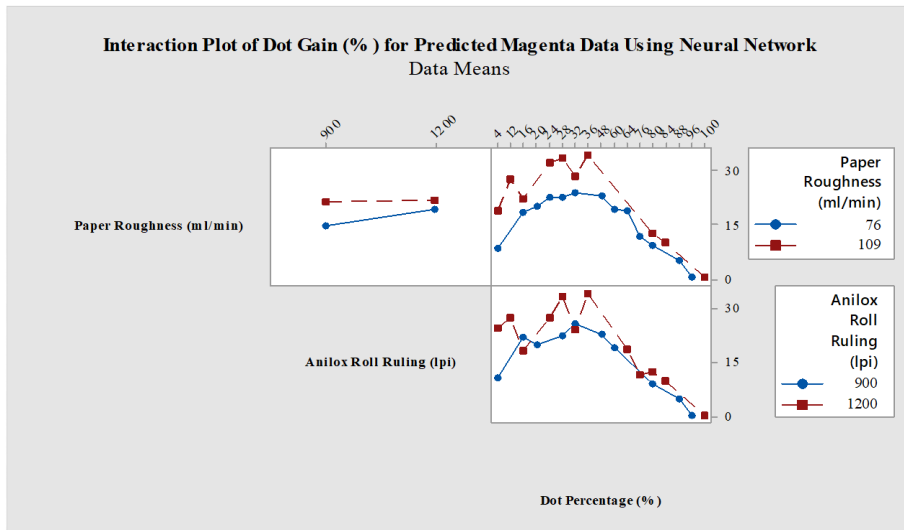
» **Figure 16:** Interaction plot of dot gain for original cyan data



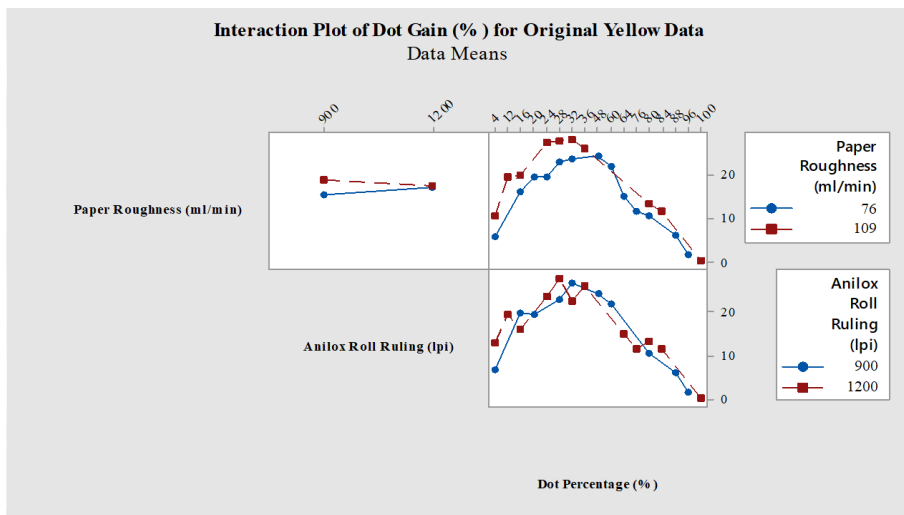
» **Figure 17:** Interaction plot of dot gain for predicted cyan data using neural network



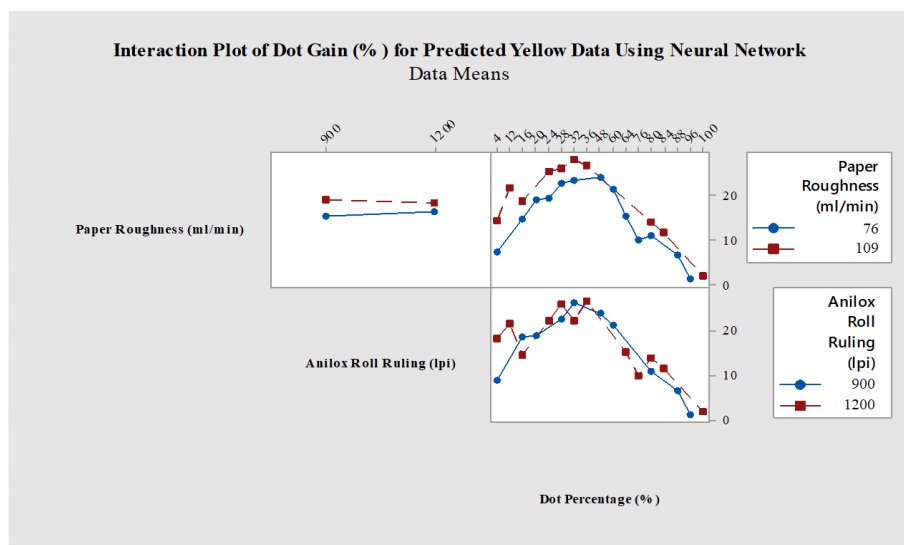
» **Figure 18:** Interaction plot of dot gain for original magenta data



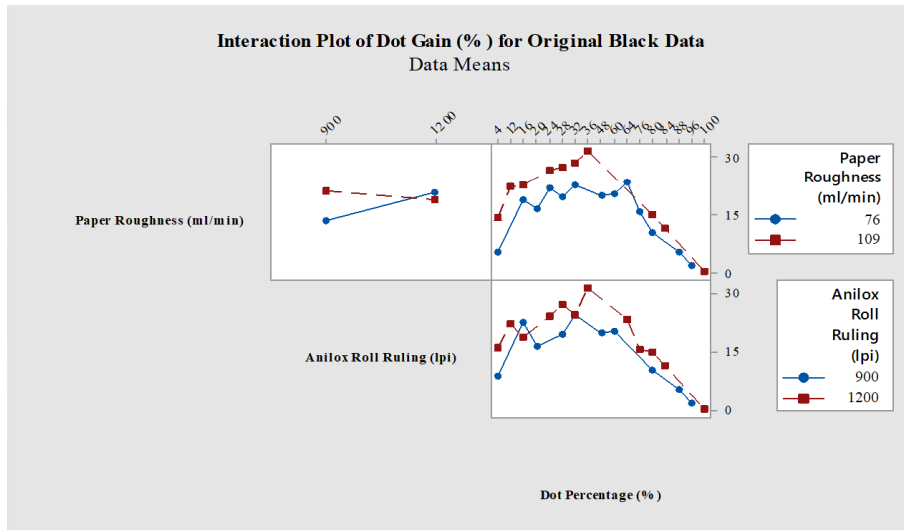
» **Figure 19:** Interaction plot of dot gain for predicted magenta data using neural network



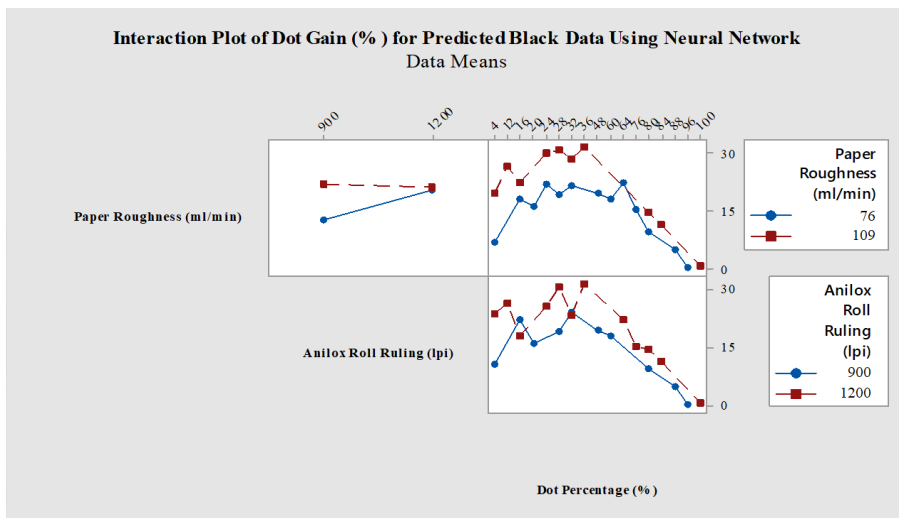
» **Figure 20:** Interaction plot of dot gain for original yellow data



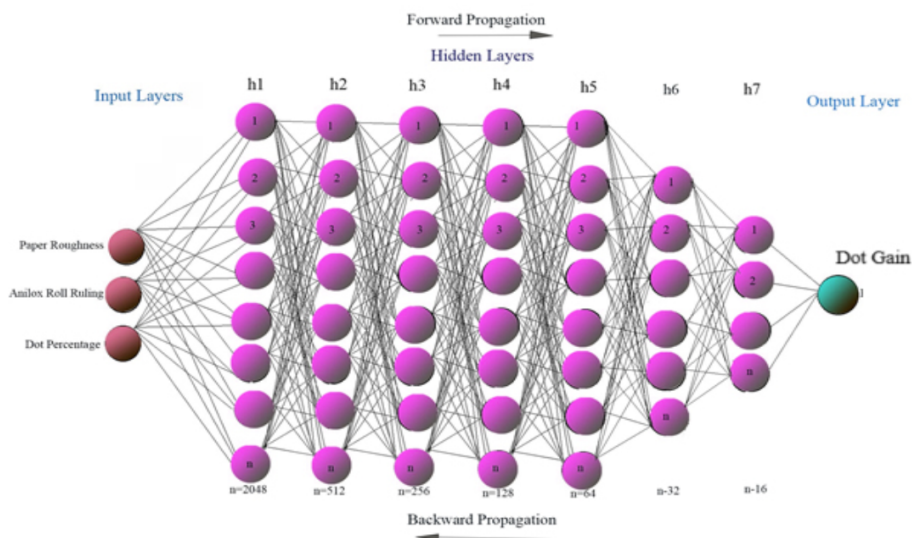
» **Figure 21:** Interaction plot of dot gain for predicted yellow data using neural network



» **Figure 22:** Interaction plot of dot gain for original black data



» **Figure 23:** Interaction plot of dot gain for predicted black data using neural network



» **Figure 24:** The Neural Network Architecture in the study

Discussions

In recent years, machine learning has rapidly grown inside the computing and data analysis framework, which typically allows programs to function intelligently. A few machine learning techniques have been applied in this work to evaluate the dot gain of four-color flexographic printing.

The summary of performance accuracy attained for several machine learning models in dot gain prediction is shown in Table 3. It is discovered through the execution of a Python program that the Neural Network algorithm provides a very notable method for estimating optical dot gain for cyan, magenta, yellow, and black colors. This demonstrates that neural networks outperform tested algorithms like SVM, XG boost regression, random forest, decision tree, and linear regression in the prediction process. With its unique properties, such as a somewhat higher number of hyperparameters, epochs, layers, etc., than other algorithms, the neural network performs exceptionally well.

The main effects plot of original data as well as predicted data for Cyan, Magenta, Yellow and Black reproductions with Dot Gain are shown from Figures 8-15 and the interaction plots of original data and predicted data are illustrated by the Figures 16-23. The results of these plots indicate that the dot gain is comparatively less with coated paper than uncoated paper. As the anilox line frequency increases the dot gain tends to decrease. The lower anilox screen frequency together with the uneven texture of uncoated paper accelerates the dot gain effects considerably.

Figures 8-15 shows the nature of the output response (dot gain) of main effects plot with respect to paper roughness and anilox roll ruling (lpi) is more or less similar in both the original data and predicted data. Interaction plots represented by Figures 16-23 of original data and predicted data obtained by neural networking machine learning shows the nature of the curve is almost similar. Figure 24 shows that the suggested design of the Neural Network algorithm in this study has three input layers, one output layer, seven hidden layers, and 5000 epochs. This method of operation enhanced its level of automation and general effectiveness.

Conclusion

The goal of this research is to develop a machine learning model for predicting dot gain effect associated with flexographic four-process color printing. This paper's primary sections are as follows: a theoretical review of the history of printing and machine learning, Python programming using some key machine learning algorithms, performance assessment and outcome analysis.

The different machine learning techniques are implemented and assessed using neural networks, XG boost regressors, SVM regressors, random forest regressors, decision trees and linear regression. The result shows that when compared to all other evaluated algorithms, Neural Network algorithm performs noticeably better due to the superior properties of neural networks.

This research may be extended by varying the different parameters such as dot shapes, anilox roller cell shapes, varying ink viscosity and also the printing speed.

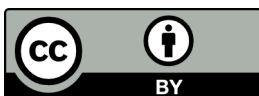
Funding

The research did not receive any specific grant from funding agencies in the public, commercial, or not-for-profit sectors.

References

- Abusaq, Z., Zahoor, S., Habib, S. M., Rehman, M., Mahmood, J., Kanan, M. & Mustaq, T. R. (2023) Improving energy performance in flexographic printing process through lean and AI techniques: A Case Study. *Energies*. 16 (4), 1972. Available from: doi: 10.3390/en16041972
- Bould, C. D., Hamblyn, S. M., Gethin, T. D. & Claypole, C.T. (2010) Effect of impression pressure and anilox specification on solid and halftone density. *Journal of Engineering Manufacture*. 225 (5). Available from: doi: 10.1177/2041297510394072
- Çelik, Ö. & Altunaydin, S. S. (2018) A research on machine learning methods and its applications. *Journal of Educational Technology and Online Learning*. 1 (3), 25-40. Available from: doi: 10.31681/jetol.457046
- Chandel, M., Silakari, S., Pandey, R. & Sharma, S. (2022) A study on machine learning and Python's framework. *International Journal of Computer Sciences and Engineering*. 10 (5). Available from: doi: 10.26438/ijcse/v10i5.5864
- Dendge, R. R. (2023) Analysis of dot gain produced by interactions of flexographic plate and anilox roll screen frequencies. *Acta Graphica*. 31 (1), 35-44
- Dharavath, N. H., Bensen, M. T. & Gaddam, B. (2005) Analysis of print attributes of Amplitude Modulated (AM) vs. Frequency Modulated (FM) screening of multicolour offset printing. *Journal of Industrial Technology*. 21 (3).
- Jin, W. (2020) Research on machine learning and its algorithms and development. In: *5th International Conference on Intelligent Computing and Signal Processing: Journal of Physics Conference Series, ICSP, 20-22 March 2020, Suzhou, China*. Purpose-LED Publishing. Available from: doi: 10.1088/1742-6596/1544/1/012003
- Joshi, V. A. (2022) Optimization of flexo process parameters to reduce the overall manufactur-

- ing cost. *An International Journal of Optimization and Control: Theories & Applications*. 12 (1). Available from: doi: 10.11121/ijocta.2022.1137
- Sisodia, P. & Seth, B. (2022) An implementation on Python for data science and machine learning. *International Journal of Creative Research Thoughts*. 10 (3).
- Sodhi, P., Awasthi, N. & Sharma, V. (2019) Introduction to machine learning and its basic application in Python. In: *Proceedings of 10th International Conference on Digital Strategies for Organizational Success, 5-7 January 2019*. pp. 1354-1375. Available from: doi: 10.2139/ssrn.3323796
- Theohari, S., Fraggadakis, E., Tsimis, D., Tsigonias, M. & Mandis, D. (2014) Effect of paper properties on print quality by flexographic method. In: *46th Annual International Conference on Graphic Arts and Media Technology, Management and Education, 25-29 May 2014, Athens, Greece*. Athens, Hellenic Union of Graphic Arts and Media Technology Engineers.
- Tomašegović, T., Pibernik, J., Mahović Poljaček, S. & Madžar, A. (2021) Optimization of flexographic print properties on ecologically favorable paper substrates. *Journal of Graphic Engineering and Design*. 12 (1), 37-44. Available from: doi: 10.24867/JGED-2021-1-037



© 2025 Authors. Published by the University of Novi Sad, Faculty of Technical Sciences, Department of Graphic Engineering and Design. This article is an open access article distributed under the terms and conditions of the Creative Commons Attribution license 4.0 Serbia (<https://creativecommons.org/licenses/by/4.0/deed.en>).



Sustainable active packaging for the EU green transition: HEC/vitamin C antioxidant films enhancing food safety and reducing waste

ABSTRACT

The growing demand for sustainable food packaging is driven not only by consumer awareness of food safety but also by international strategies such as national development plans and European Union regulations, which emphasize the replacement of conventional plastics with bio-based and functional alternatives. In this context, active antioxidant packaging plays a critical role in extending food shelf life, reducing waste, and ensuring safer products. Hydroxyethyl cellulose (HEC) was selected as the matrix material due to its good film-forming properties, biodegradability, biocompatibility, odorlessness, and non-toxicity or low toxicity, while vitamin C (ascorbic acid), a natural antioxidant, was incorporated as the active agent. HEC solution was prepared by dissolving HEC powder in distilled water, and vitamin C was incorporated. The resulting mixtures were homogenized and cast onto glass plates, followed by drying to produce uniform films. The obtained films were systematically characterized in terms of contact angle (wettability), and antioxidant capacity. In addition, their surface performance was evaluated through IGT F1 flexographic test printing trials to assess practical applicability. The results demonstrated that the incorporation of vitamin C enhanced the antioxidant functionality of HEC films, while altering their barrier and surface properties depending on the concentration used. These findings suggest that HEC-based films containing vitamin C have significant potential as active packaging materials that meet both sustainability goals and food safety requirements.

KEY WORDS

active packaging, antioxidant films, food safety, vitamin C, HEC

Emine Arman
Kandirmaz¹ 
Arif Ozcan¹ 

¹ Marmara University, Faculty of Applied Sciences, Department of Printing Technologies, Kartal, Istanbul, Turkey

Corresponding author:
Emine Arman Kandirmaz
e-mail:
earman@marmara.edu.tr

First received: 3.10.2025.
Revised: 27.10.2025.
Accepted: 10.11.2025.

Introduction

Plastic packaging is widely preferred in the food industry due to its low cost, ease of production, good barrier properties, and ability to protect products against both chemical degradation and physical impacts encountered during the distribution process (Chen et al., 2024; Haghighi-Manesh & Azizi, 2017). However, the widespread use of these materials and their slow biodegradation pose various risks to both environmental pollution and health. The rise of single-use plastic packaging is seen as one of the primary causes of this problem (Rojas et al., 2021; Velásquez et al., 2021).

In recent years, the environmental problems caused by plastic waste have attracted public attention and led to increased consumer demand for unprocessed and additive-free products (Gao et al., 2023). Consequently, the need for packaging materials is both diversifying and increasing. In this regard, the European Union's new Packaging and Packaging Waste Regulation (PPWR) mandates critical steps in the food packaging sector within the framework of circular economy and sustainability goals. The regulation aims to ensure that all packaging is recyclable by 2030, that plastic packaging contains a certain percentage of recycled materials, and that reusable systems are expanded.

This regulation aims to minimize the environmental impact of packaging and encourage the development of environmentally friendly materials produced from sustainable sources (Mohammadi et al., 2019; Shankar, Wang & Rhim, 2019).

Furthermore, in recent years, there has been a notable increase in the use of films made from natural polymers due to their non-toxicity and biocompatibility (Si et al., 2022; Kanatt & Makwana, 2020).

The primary function of food packaging is to protect products against air, moisture, dust, light, and chemical and microbiological contamination. Another important function of packaging materials is to extend the shelf life of products. However, most traditional packaging is made from non-biodegradable plastics. The inability to eliminate these plastics has led to increasing calls from consumers and environmentalists to reduce unnecessary plastic use in packaging (Velásquez et al., 2021; Arrieta et al., 2019).

Biodegradable polymers are naturally degraded by bacteria, fungi, and other microorganisms, converting biomass into water and carbon dioxide. They are typically produced using plant resources or other renewable materials. In recent years, these polymers have been intensively researched in various fields due to their potential to reduce environmental pollution and alleviate waste management problems (Brockgreitens & Abbas, 2016).

Antioxidant and antimicrobial active packaging refer to methods that aim to limit oxidation and microbial activity to preserve the freshness and quality of foods. These types of packaging materials are prepared using either natural or synthetic ingredients, thereby delaying the oxidation of oils and inhibiting the growth of microorganisms, thus extending the product's shelf life. In antimicrobial packaging, active ingredients are released into the food environment to inhibit the growth of bacteria, yeast, and mold. In contrast, in antioxidant systems, antioxidants are incorporated directly into the packaging material and neutralize free radicals, slowing the oxidative deterioration of oils in food. Examples include vitamin E, ascorbic acid, and plant polyphenols (Zende, Ghase & Jamdar, 2025; Choe & Min, 2006). Active packaging ensures longer shelf life while ensuring fewer additives and preservatives in food formulations, greater flavor retention, and higher food quality. Antioxidant controlled release generally provides long-term food protection against lipid oxidation through the continuous or gradual release of antioxidants, particularly at the food surface (Yam, Schaich & Obinata, 2008; Jamshidian, Tehrani & Desobry, 2013).

HEC is used as a thickener, preservative or binder, suspension, and colloid stabilizer in cosmetics, biomedical, pharmaceuticals and coatings and food applications

and many more due to its biodegradable, odorless and non-toxic properties and is approved by the U.S. Food and Drug Administration (FDA) (Noreen et al., 2020; El Fawal et al., 2020; Yang & Li, 2018). HEC has poor toughness and load-carrying properties, so combining it with other materials makes it more useful (Cen et al., 2023). Studies in the literature have investigated the use of nanoparticulate HEC as a body scaffold material in biomedical engineering (Zulkifli et al., 2017), its use in combination with hyaluronic acid for wound dressing (Luo et al., 2018), the enhancement of UV resistance and mechanical properties through nanofiber reinforcement (Huang et al., 2021), and the enhancement of solvent resistance and load-carrying capacity, as well as UV protection properties, of HEC films through the addition of zinc oxide and carboxymethyl chitosan (Cen et al., 2023).

HEC is expected to provide high UV protection in outdoor conditions, but it lacks both mechanical and UV protection. Experiments are underway with CNF, CNC, and inorganic materials to address these weaknesses (Lu et al., 2020). Vitamin C, also known as ascorbic acid, is a naturally occurring plant-based compound with high polarity and high antioxidant and antimicrobial activity. It is a water-based compound found in fruits such as mangoes, oranges, lemons, and blackberries, as well as various vegetables (Zou et al., 2016). Vitamin C has been incorporated into whey protein (Min & Krochta, 2007) and alginate (De'Nobili et al., 2016) based films, along with aloe vera coating gel (Sogvar, Saba & Emamifar, 2016), to provide food protection.

In this study, an active antioxidant packaging film will be produced using hydroxyethyl cellulose (HEC). Vitamin C (ascorbic acid), a natural antioxidant, will be added as the active ingredient. The films will be subjected to the necessary characterization and antioxidant tests. Additionally, to evaluate printability parameters, prints will be made using an IGT F1 flexo printability test press, and relevant parameters will be evaluated.

Experimental

Materials

Hydroxyethyl cellulose (HEC) powder was purchased from Sigma-Aldrich (USA), while glycerol used as a plasticizer and L-ascorbic acid as an antioxidant were obtained from Merck (Germany). Polystyrene petri dishes were sourced from Greiner Bio-One (Germany).

Process blue ink was (Siegwerk, Germany) employed for printability assessments. The antioxidant reagent 2,2-diphenyl-1-picrylhydrazyl (DPPH) and analytical-grade methanol were both procured from Sigma-Aldrich (USA). Adhesion tests utilized Tesa tape (Tesa SE, Germany).

All reagents and materials were of analytical grade or higher to ensure experimental reliability and reproducibility.

Methods

Active packaging films were prepared following the method described by Chen et al. (2024) with modifications. A 2% (w/v) HEC solution was prepared by dissolving 2.0 g of HEC powder in 100 mL of distilled water under continuous magnetic stirring at 50°C until complete homogenization was achieved. Glycerol was added as a plasticizer at 30% (w/w) relative to the weight of HEC (i.e., 0.6 g glycerol per 2.0 g HEC). Subsequently, ascorbic acid was incorporated into the formulation at 5% (w/w) of the total solid content (HEC + glycerol + ascorbic acid).

The resulting film-forming solution was cast onto polystyrene petri dishes and dried at 40°C for 24 h in a ventilated oven. Dried films were then carefully peeled off and conditioned at 25 ± 2°C and 50 ± 5% relative humidity for 48 h prior to characterization.

Color characteristics of the films were evaluated using an X-Rite eXact portable spectrophotometer, following the ISO 13655:2017 standard. The device operated with a 0/45° geometry and polarization filter, using a 2° standard observer angle and D50 illumination. Measurements were performed across the visible spectrum (400–700 nm). A white background with $L^* = 95.98$, $a^* = -1.36$, and $b^* = 1.63$ was used as the reference. Each sample was measured four times, and the total color difference (ΔE_{00}) and whiteness index (WI) were calculated to evaluate optical quality.

$$\Delta E_{00} = \sqrt{\left(\frac{\Delta L'}{k_L S_L}\right)^2 + \left(\frac{\Delta C'}{k_C S_C}\right)^2 + \left(\frac{\Delta H'}{k_H S_H}\right)^2} + R_T \frac{\Delta C'}{k_C S_C} \frac{\Delta H'}{k_H S_H} \quad (1)$$

$$WI = 100 - \sqrt{(100 - L)^2 + a^2 + b^2} \quad (2)$$

Color differences between the films and the reference background were determined using the CIEDE2000 formula (ΔE_{00}), in accordance with the ISO 11664-6:2014 standard. Calculations were based on the mean values from five independent measurements per sample. In this method, ΔL^* , Δa^* , and Δb^* represent the differences in lightness, red–green, and yellow–blue coordinates, respectively, between the sample and the reference. The L^* axis denotes lightness (ranging from black to white), the a^* axis spans from green (negative values) to red (positive values), and the b^* axis ranges from blue (negative) to yellow (positive).

The ΔE_{00} formula accounts for perceptual non-uniformities by incorporating ΔL^* (lightness difference), ΔC^* (chroma difference), and ΔH^* (hue difference), along with an interactive rotation term (RT) that

addresses the interplay between chroma and hue in the blue region. Weighting functions SL , SC , and SH are applied to adjust the influence of lightness, chroma, and hue components based on the color's position in CIE $L^*a^*b^*$ space. Parametric factors k_L , k_C , and k_H , typically set to 1 under standard conditions, account for variations due to observation conditions such as texture, background, and sample geometry.

Gloss properties of the films were measured using a BYK-Gardner micro-gloss meter at a fixed incident angle of 75°, following the ISO 8254-1:2009 standard. All measurements were conducted under consistent environmental conditions to ensure accuracy and reproducibility.

Surface wettability was evaluated via static contact angle analysis using a Pocket Goniometer (Model PG-X+, Version 3.4, FIBRO Systems AB, Sweden). Deionized water droplets were carefully dispensed onto the film surfaces, and the contact angles were recorded using a CCD video camera system. Surface free energy (SFE) was subsequently calculated in accordance with ASTM D5946, based on the measured water contact angles. Surface morphology was examined using a Troika SurfaceCAM HD 3D microscope (Troika Systems, UK).

The printability of the films was assessed using an IGT F1 flexographic test printing system (IGT Testing Systems, Netherlands), print settings are printing force of 250 N/M and printing speed of 0.30 m/s. The anilox cell frequency is 150 lpi. Siegwerk process blue ink as the printing ink. Printed surfaces were evaluated for color uniformity using an X-Rite eXact spectrophotometer (X-Rite, USA), and print adhesion was examined by applying and removing Tesa tape (Tesa SE, Germany) in accordance with standard tape test procedures.

The integrity of the printed layer after tape removal was used to qualitatively assess ink adhesion performance.

The antioxidant activity of the active films was determined by measuring their DPPH (2,2-diphenyl-1-picrylhydrazyl) radical scavenging capacity, following the method described by Doh, Dunno & Whiteside (2020). The antioxidant potential of the active films was assessed using the 2,2-diphenyl-1-picrylhydrazyl (DPPH) radical scavenging assay.

Film samples (20 mg) were immersed in 5 mL of methanol and incubated at 25°C for 12 h to extract antioxidant compounds. Following incubation, 0.2 mL of the film extract was mixed with 2.0 mL of freshly prepared DPPH solution (0.025 g/L in methanol). The mixture was then incubated in the dark at 25°C for 30 minutes to allow for the reaction between antioxidants and DPPH radicals. The absorbance of the reaction mixture was subsequently measured at 517 nm using a UV–visible spectrophotometer (Shimadzu, Japan).

The DPPH radical scavenging activity (RSA) was calculated using the following equation:

$$DPPH \text{ scavenging effect (\%)} = \frac{A_{DPPH} - A_{extract}}{A_{DPPH}} \times 100 \quad (3)$$

where, and are the absorbance values of the solution of DPPH and the sample extracts, respectively. The experiment was carried out in triplicate for each film sample, and the results were expressed as mean values \pm standard deviation.

Results and Discussion

Hydroxyethyl cellulose (HEC)-based films, both with and without vitamin C, were successfully fabricated, exhibiting uniform, continuous, and defect-free surfaces. The films were subsequently characterized for a comprehensive set of properties, including optical attributes (color, gloss, whiteness index), transparency, water contact angle, antioxidant activity, and surface morphology.

These analyses confirmed that the incorporation of vitamin C did not compromise the structural integrity of the films, while allowing evaluation of the functional effects of the bioactive compound on both physicochemical and optical properties. The successful production and systematic characterization of these films provide a solid foundation for investigating their potential applications in active packaging and other functional biomaterial fields.

The incorporation of vitamin C into the hydroxyethyl cellulose–glycerol film formulation led to a noticeable modification in the optical properties, as evidenced by the CIE color parameters (Table 1). While the control film (without vitamin C) exhibited minimal changes in color, the vitamin C-loaded film displayed a yellowish hue when measured against a white background.

This phenomenon can be attributed to the intrinsic optical characteristics of vitamin C and its distribution within the polymeric matrix. Similar observations have been reported in the literature, where the addition of bioactive compounds, particularly vitamins and phenolic antioxidants, induced slight yellowing or enhanced color intensity in biopolymer-based films (Periyasamy, Asrafali & Lee, 2025).

In contrast, the hydroxyethyl cellulose–glycerol film without vitamin C maintained high color stability, which is consistent with previous findings indicating that polysaccharide–plasticizer matrices generally provide high transparency and minimal coloration unless bioactive additives are incorporated (Sothornvit & Krochta, 2000; Rhim, Park & Ha, 2013).

Therefore, the yellowish tone observed in the vitamin C-loaded film can be considered consistent with the literature and is mainly attributed to the inherent color properties of vitamin C and its influence on the optical behavior of the polymeric matrix.

Color differences (ΔE_{00}) were calculated using the CIE ΔE_{00} formula with the white paper as the reference. The HEC film placed on white paper exhibited a minimal color difference of 1.77, indicating negligible visual alteration relative to the substrate. In contrast, the HEC film containing vitamin C showed a markedly higher color difference of 28.01, reflecting a pronounced yellowish shift. This substantial ΔE_{00} value indicates that vitamin C significantly affects the visual appearance of the film when applied to a white background.

These results are consistent with previous studies reporting that the incorporation of bioactive compounds, such as vitamins or phenolic antioxidants, into polysaccharide-based films can induce notable color changes, often leading to yellowing or other perceptible chromatic shifts (Pan et al., 2024). The contrast between the minimal ΔE_{00} of the HEC film without vitamin C and the pronounced ΔE_{00} of the vitamin C-loaded film underscores the strong influence of functional additives on the optical and colorimetric properties of biodegradable films.

Although the vitamin C-loaded HEC film exhibited a noticeable yellowish hue when placed on a white substrate, the whiteness index (*WI*) calculated according to the ASTM E313 standard increased (Table 1). This phenomenon can be attributed to the contribution of the *b** (yellow-blue) component in the ASTM E313 formula, which positively influences the *WI* value.

Consequently, even though the film appears yellow to the naked eye, the enhanced *b** value results in a higher calculated whiteness index, reflecting a measurable change in optical properties.

Table 1

Colorimetric and optical parameters of unprinted hydroxyethyl cellulose–glycerol films with and without vitamin C

	L*	a*	b*	ΔE_{00}	Gloss	WI
Base white paper	90.45	3.05	-11.96	Ref.	5.2	15.61
Unprinted HEC film	87.67	3.12	-11.71	1.77	11.2	17.29
Unprinted vitamin C-loaded HEC film	84.27	2.14	27.18	28.01	9.6	31.48

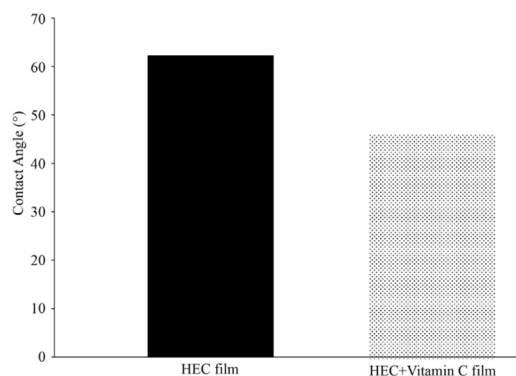
Similar observations have been reported in the literature, where the addition of vitamins or phenolic compounds to biopolymer-based films caused a slight yellowing yet led to an increase in the whiteness index (Rhim, Park & Ha, 2013). These findings indicate that vitamin C affects not only the visible color of HEC films but also the whiteness index as quantified by standard colorimetric methods.

The gloss values of the films were also evaluated to assess their surface optical properties. The white paper exhibited a gloss of 5.2, whereas the HEC film on a white substrate demonstrated a higher gloss of 11.2, indicating an increase in surface reflectivity due to the polymer matrix. Interestingly, the incorporation of vitamin C slightly reduced the gloss to 9.6 compared to the HEC film without vitamin C, suggesting that the presence of the bioactive compound modifies the surface characteristics of the film.

These findings are consistent with literature reports indicating that the addition of functional additives, such as vitamins, phenolics, or other bioactive compounds, can influence the surface gloss of biopolymer films by altering the film's microstructure and light scattering properties (Sothornvit & Krochta, 2000). The comparison among the samples demonstrates that while the HEC matrix inherently increases surface reflectivity relative to the base paper, the incorporation of vitamin C slightly decreases gloss, likely due to changes in surface morphology or light absorption characteristics.

The water contact angles (WCA) of the films were measured to assess their surface wettability (Figure 1). The HEC film exhibited a WCA of 62.3°, indicating a moderately hydrophilic surface.

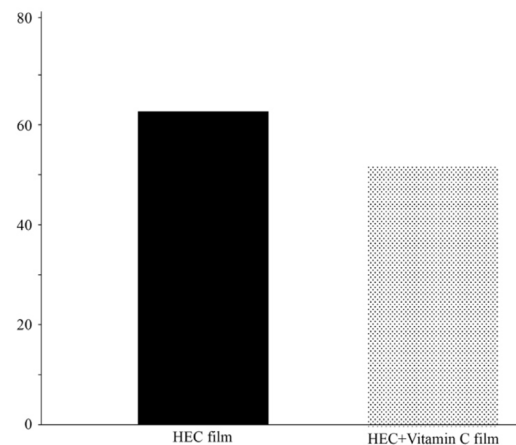
Upon incorporation of vitamin C, the WCA decreased to 46.3°, demonstrating an increase in surface hydrophilicity. This decrease can be attributed to the introduction of polar hydroxyl groups from vitamin C, which enhance hydrogen bonding interactions with water molecules, thereby improving the film's wettability.



» **Figure 1:** Contact angle of HEC film and vitamin C loaded HEC film

These findings agree with previous studies reporting that the addition of hydrophilic bioactive compounds, such as vitamins or phenolic antioxidants, can significantly reduce the contact angle of polysaccharide-based films, enhancing their hydrophilic character (Cui et al., 2023). The comparison between the two films highlights the pronounced effect of vitamin C on the surface properties of HEC films, suggesting potential implications for applications requiring improved water interaction or controlled wettability.

The antioxidant activity of the films was evaluated using the DPPH radical scavenging assay to determine the functional contribution of the incorporated bioactive compound (Figure 2). The pristine HEC film exhibited a negligible scavenging activity of 2%, consistent with the inherent lack of antioxidant groups in polysaccharide matrices. In contrast, the HEC film containing vitamin C demonstrated a markedly enhanced radical scavenging activity of 58%, confirming the effective integration and functionality of the bioactive molecule within the polymer network. The substantial increase in DPPH inhibition highlights the ability of vitamin C to provide potent antioxidant properties while maintaining the structural integrity of the film. These findings align with previous studies reporting that the addition of hydrophilic antioxidants such as vitamins or phenolic compounds can significantly elevate the radical scavenging capacity of polysaccharide-based films, transforming chemically inert matrices into functional materials suitable for active packaging and food preservation applications (Pereira, Lonni & Mali, 2022).

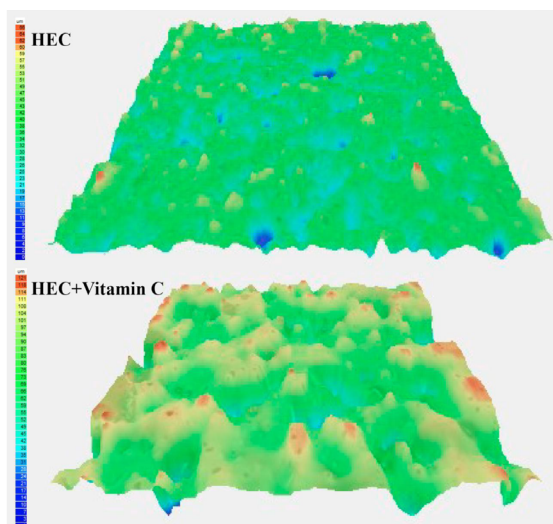


» **Figure 2:** The antioxidant activity of the HEC film and vitamin C loaded film

Surface morphology of the films was evaluated using a Troika AniCAM HD+ 3D scan microscope. The microscope images given in Figure 3.

The neat HEC film exhibited a smooth and uniform surface with a low roughness value of approximately 0.2 μm , indicating a homogeneous polymeric matrix. In contrast, the incorporation of vitamin C clearly modified the surface microstructure.

The vitamin C-loaded HEC film displayed discernible crystalline particulates that were homogeneously distributed across the surface, with localized roughness values reaching up to $\sim 1 \mu\text{m}$. This morphological alteration indicates that vitamin C acted not only as a functional additive but also as a structuring agent within the film matrix.



» **Figure 3:** Surface topography of HEC film and vitamin C-loaded HEC film

These findings are in close agreement with the contact angle and gloss measurements. The vitamin C-loaded film exhibited a lower water contact angle (46.3°) compared to the neat HEC film (62.3°), which can be attributed to the increased hydrophilicity and enhanced surface heterogeneity introduced by vitamin C. Likewise, the reduction in surface gloss of the vitamin C-containing film is consistent with the higher micro-scale roughness observed in the topographical analysis.

Together, these complementary results confirm that the incorporation of vitamin C significantly influences both the physical and surface-related properties of HEC films.

The observed trends are consistent with previous reports in the literature, which have demonstrated that the addition of bioactive compounds or antioxidants into biopolymer matrices increases surface roughness, alters wettability, and reduces optical gloss due to microstructural heterogeneity (Mikus & Galus, 2025).

Table 2

Colorimetric and optical parameters of flexographic printed hydroxyethyl cellulose–glycerol films with and without vitamin C

	L^*	a^*	b^*	ΔE_{00}	Gloss
Printed base white paper	85.30	-7.97	-18.46	Ref.	8.9
Printed HEC film	82.81	-8.40	-18.94	1.70	14.7
Printed vitamin C-loaded HEC film	71.62	-6.98	-7.63	11.72	11.1

Overall, the combination of microscopy, wettability, and optical analyses indicates that vitamin C not only enhanced the antioxidant functionality of HEC films but also induced pronounced changes in surface topography in a manner fully consistent with earlier findings on active packaging materials.

Flexographic printability of the prepared films was evaluated using an IGT F1 printability tester. Both the neat HEC film and the vitamin C-loaded HEC film provided defect-free surfaces for solid area printing, indicating that the substrate morphology did not hinder ink transfer or coverage. The colorimetric parameters (CIE $L^*a^*b^*$), gloss, and ΔE_{00} values of the obtained prints are summarized in Table 2.

A clear shift toward the yellow region of the color space was observed for the vitamin C-containing film, which can be ascribed to the intrinsic coloration and distribution of vitamin C within the polymeric matrix.

This finding implies that when such films are intended for use as printable packaging substrates, appropriate color management and ink formulation adjustments are necessary to achieve target shades and minimize deviations in brand color consistency. The adhesion of the printed flexographic ink was evaluated using the standardized tape (cross-hatch) test, which is a widely accepted and ISO/ASTM-standardized qualitative method for assessing print and coating adhesion on flexible polymeric substrates.

According to ASTM D3359 and ISO 2409, the absence of any visible ink residue transferred onto the tape is classified as the highest adhesion rating (5B) and is considered evidence of excellent anchorage between the ink layer and the substrate.

This outcome was indeed observed in our study, indicating that no delamination or cohesive failure occurred and confirming that the incorporation of vitamin C did not adversely affect the printability or adhesion performance. The tape test was selected because it is routinely employed in both industrial practice and academic research as a fast, reproducible, and directly comparable screening method for printed or coated packaging films, particularly in flexographic applications.

Conclusions

In this study, HEC-based films incorporating vitamin C were successfully fabricated and comprehensively characterized, revealing a unique combination of functional and processable properties. The incorporation of vitamin C not only enhanced the antioxidant activity of the films but also conferred notable oxygen-scavenging capacity, a feature of relevance for active packaging applications aimed at extending shelf life and preserving product quality. Optical, surface, and wettability analyses demonstrated that the films maintained structural integrity and uniformity, while subtle modifications in color, gloss, and surface roughness reflected the controlled incorporation of the bioactive compound.

Importantly, flexographic printability tests confirmed defect-free ink transfer and excellent adhesion, highlighting the compatibility of these functional films with conventional packaging processes.

The synergy between bioactivity, oxygen scavenging, and industrially relevant printability underscores the originality of this work, providing a rare example of a biopolymer-based material that combines active functionality with practical application potential.

Overall, this study highlights the promise of vitamin C-loaded HEC films as sustainable, functional, and printable substrates for active packaging, bridging the gap between laboratory-scale material innovation and industrial implementation. The demonstrated oxygen scavenging, and antioxidant functionalities position these films as compelling candidates for next-generation packaging solutions that actively contribute to food preservation and quality maintenance.

Acknowledgment

We thank Troika Systems, UK for the surface morphology measurements of the films used in the study.

Funding

This research did not receive any specific grant from funding agencies in the public, commercial, or not-for-profit sectors.

References

Arrieta, M. P., Diez Garcia, A., López, D., Fiori, S. & Peponi, L. (2019) Antioxidant bilayers based on PHBV and plasticized electrospun PLA-PHB fibers encapsulating catechin. *Nanomaterials*. 9 (3), 346. Available from: doi: 10.3390/nano9030346

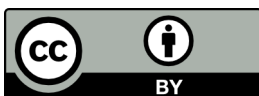
- Brockgreitens, J. & Abbas, A. (2016) Responsive food packaging: recent progress and technological prospects. *Comprehensive Reviews in Food Science and Food Safety*. 15 (1), 3–15. Available from: doi: 10.1111/1541-4337.12174
- Cen, C., Wang, F., Wang, Y., Li, H., Fu, L., Li, Y., Chen, J. & Wang, Y. (2023) Design and characterization of an antibacterial film composited by hydroxyethyl cellulose, carboxymethyl chitosan, and nano-ZnO for food packaging. *International Journal of Biological Macromolecules*. 231, 123203. Available from: doi: 10.1016/j.ijbiomac.2023.123203
- Chen, B. J., Liu, G. G., Wang, X., Liu, H. R., Zhang, Y., Wang, C. F., Liu, C. X. & Qiao, Y. J. (2024) Development and characterization of an antioxidant and antimicrobial film composited by hydroxyethyl cellulose and sulfated rice bran polysaccharides for food packaging. *Foods*. 13 (6), 819. Available from: doi: 10.3390/foods13060819
- Choe, E. & Min, D. B. (2006) Mechanisms and factors for edible oil oxidation. *Comprehensive Reviews in Food Science and Food Safety*. 5 (4), 169–186. Available from: doi: 10.1111/j.1541-4337.2006.00009.x
- Cui, C., Gao, L., Dai, L., Ji, N., Qin, Y., Shi, R., Qiao, Y., Xiong, L. & Sun, Q. (2023) Hydrophobic biopolymer-based films: strategies, properties, and food applications. *Food Engineering Reviews*. 15 (2), 360–379. Available from: doi: 10.1007/s12393-023-09342-6
- De'Nobili, M. D., Soria, M., Martinefski, M. R., Tripodi, V. P., Fissore, E. N. & Rojas, A. M. (2016) Stability of L-(+)-ascorbic acid in alginate edible films loaded with citric acid for antioxidant food preservation. *Journal of Food Engineering*. 175, 1–7. Available from: doi: 10.1016/j.jfoodeng.2015.11.015
- Doh, H., Dunno, K. D. & Whiteside, W. S. (2020) Preparation of novel seaweed nanocomposite film from brown seaweeds *Laminaria japonica* and *Sargassum natans*. *Food Hydrocolloids*. 105, 105744. Available from: doi: 10.1016/j.foodhyd.2020.105744
- El Fawal, G., Hong, H., Song, X., Wu, J., Sun, M., He, C., Mo, X., Jiang, Y. & Wang, H. (2020) Fabrication of antimicrobial films based on hydroxyethylcellulose and ZnO for food packaging application. *Food Packaging and Shelf Life*. 23, 100462. Available from: doi: 10.1016/j.fpsl.2020.100462
- Gao, C., Chen, P., Ma, Y., Sun, L., Yan, Y., Ding, Y. & Sun, L. (2023) Multifunctional polylactic acid biocomposite film for active food packaging with UV resistance, antioxidant and antibacterial properties. *International Journal of Biological Macromolecules*. 253, 126494. Available from: doi: 10.1016/j.ijbiomac.2023.126494
- Haghighi-Manesh, S. & Azizi, M. H. (2017) Active packaging systems with emphasis on its applications in dairy products. *Journal of Food Process Engineering*. 40 (5), e12542. Available from: doi: 10.1111/jfpe.12542
- Huang, J., Lu, Z., Li, J., Ning, D., Jin, Z., Ma, Q., Hua, L., E, S. & Zhang, M. (2021) Improved mechanical and ultraviolet shielding performances of hydroxyethyl

- cellulose film by using aramid nanofibers as additives. *Carbohydrate Polymers*. 255, 117330. Available from: doi: 10.1016/j.carbpol.2020.117330
- Jamshidian, M., Tehrani, E. A. & Desobry, S. (2013) Antioxidants release from solvent-cast PLA film: investigation of PLA antioxidant-active packaging. *Food and Bioprocess Technology*. 6 (6), 1450–1463. Available from: doi: 10.1007/s11947-012-0830-9
- Kanatt, S. R. & Makwana, S. H. (2020) Development of active, water-resistant carboxymethyl cellulose–polyvinyl alcohol–Aloe vera packaging film. *Carbohydrate Polymers*. 227, 115303. Available from: doi: 10.1016/j.carbpol.2019.115303
- Lu, Z., Huang, J., Li, J., Si, L., Yao, C., Jia, F. & Zhang, M. (2020) All-cellulose composites prepared by hydroxyethyl cellulose and cellulose nanocrystals through the crosslink of polyisocyanate. *Carbohydrate Polymers*. 250, 116919. Available from: doi: 10.1016/j.carbpol.2020.116919
- Luo, P., Liu, L., Xu, W., Fan, L. & Nie, M. (2018) Preparation and characterization of aminated hyaluronic acid/oxidized hydroxyethyl cellulose hydrogel. *Carbohydrate Polymers*. 199, 170–177. Available from: doi: 10.1016/j.carbpol.2018.06.065
- Mikus, M. & Galus, S. (2025) The effect of phenolic acids on the sorption and wetting properties of apple pectin-based packaging films. *Molecules*. 30 (9), 1960. Available from: doi: 10.3390/molecules30091960
- Min, S. & Krochta, J. M. (2007) Ascorbic acid-containing whey protein film coatings for control of oxidation. *Journal of Agricultural and Food Chemistry*. 55 (8), 2964–2969. Available from: doi: 10.1021/jf062698r
- Mohammadi, H., Kamkar, A., Misaghi, A., Zunabovic-Pichler, M. & Fatehi, S. (2019) Nanocomposite films with CMC, okra mucilage, and ZnO nanoparticles: extending the shelf-life of chicken breast meat. *Food Packaging and Shelf Life*. 21, 100330. Available from: doi: 10.1016/j.fpsl.2019.100330
- Noreen, A., Zia, K. M., Tabasum, S., Aftab, W., Shahid, M. & Zuber, M. (2020) Hydroxyethylcellulose-g-poly(l-lactic acid) blended polyurethanes: preparation, characterization and biological studies. *International Journal of Biological Macromolecules*. 151, 993–1003. Available from: doi: 10.1016/j.ijbiomac.2019.10.254
- Pan, J., Li, C., Liu, J., Jiao, Z., Zhang, Q., Lv, Z., Yang, W., Chen, D. & Liu, H. (2024) Polysaccharide-based packaging coatings and films with phenolic compounds in preservation of fruits and vegetables – a review. *Foods*. 13 (23), 3896. Available from: doi: 10.3390/foods13233896
- Pereira, J. F., Lonni, A. A. G. & Mali, S. (2022) Development of biopolymeric films with addition of vitamin C and catuaba extract as natural antioxidants. *Preparative Biochemistry & Biotechnology*. 52 (1), 1–10. Available from: doi: 10.1080/10826068.2021.1916755
- Periyasamy, T., Asrafali, S. P. & Lee, J. (2025) Recent advances in functional biopolymer films with antimicrobial and antioxidant properties for enhanced food packaging. *Polymers*. 17 (9), 1257. Available from: doi: 10.3390/polym17091257
- Rhim, J. W., Park, H. M. & Ha, C. S. (2013) Bio-nanocomposites for food packaging applications. *Progress in Polymer Science*. 38 (10–11), 1629–1652. Available from: doi: 10.1016/j.progpolymsci.2013.05.008
- Rojas, A., Velásquez, E., Patiño Vidal, C., Guarda, A., Galotto, M. J. & López de Dicastillo, C. (2021) Active PLA packaging films: effect of processing and the addition of natural antimicrobials and antioxidants on physical properties, release kinetics, and compostability. *Antioxidants*. 10 (12), 1976. Available from: doi: 10.3390/antiox10121976
- Schaich, K. M., Obinata, N. & Yam, K. (2008) Delivering natural antioxidants via controlled release packaging. In: Havkin-Frenkel, D., Dudai, N. and van der Mheen, H. J. C. J. (eds.) *Proceedings of the 2nd International Symposium on Natural Preservatives in Food, Feed, and Cosmetics, 7-8 June 2006, Amsterdam, Netherlands*. Leuven, International Society for Horticultural Science. pp. 53–64. Available from: doi: 10.17660/ActaHortic.2008.778.5
- Shankar, S., Wang, L. F. & Rhim, J. W. (2019) Effect of melanin nanoparticles on the mechanical, water vapor barrier, and antioxidant properties of gelatin-based films for food packaging application. *Food Packaging and Shelf Life*. 21, 100363. Available from: doi: 10.1016/j.fpsl.2019.100363
- Si, Y., Lin, Q., Zhou, F., Qing, J., Luo, H., Zhang, C., Zhang, J. & Cha, R. (2022) The interaction between nanocellulose and microorganisms for new degradable packaging: a review. *Carbohydrate Polymers*. 295, 119899. Available from: doi: 10.1016/j.carbpol.2022.119899
- Sogvar, O. B., Saba, M. K. & Emamifar, A. (2016) Aloe vera and ascorbic acid coatings maintain postharvest quality and reduce microbial load of strawberry fruit. *Postharvest Biology and Technology*. 114, 29–35. Available from: doi: 10.1016/j.postharvbio.2015.11.019
- Sothornvit, R. & Krochta, J. M. (2000) Plasticizer effect on oxygen permeability of β -lactoglobulin films. *Journal of Agricultural and Food Chemistry*. 48 (12), 6298–6302. Available from: doi: 10.1021/jf000836f
- Velásquez, E., Patiño Vidal, C., Rojas, A., Guarda, A., Galotto, M. J. & López de Dicastillo, C. (2021) Natural antimicrobials and antioxidants added to polylactic acid packaging films. Part I: polymer processing techniques. *Comprehensive Reviews in Food Science and Food Safety*. 20 (4), 3388–3403. Available from: doi: 10.1111/1541-4337.12777
- Yang, J. & Li, J. (2018) Self-assembled cellulose materials for biomedicine: a review. *Carbohydrate Polymers*. 181, 264–274. Available from: doi: 10.1016/j.carbpol.2017.10.067
- Zende, R., Ghase, V. & Jamdar, V. (2025) Recent advances in the antimicrobial and antioxidant capabilities of PLA-based active food packaging. *Polymer-Plastics Technology and Materials*. 64 (4), 439–464. Available from: doi: 10.1080/25740881.2024.2409311

Zou, Z., Xi, W., Hu, Y., Nie, C. & Zhou, Z. (2016) Antioxidant activity of citrus fruits. *Food Chemistry*. 196, 885–896. Available from: doi: 10.1016/j.foodchem.2015.09.072

Zulkifli, F. H., Hussain, F. S. J., Zeyohannes, S. S., Rasad, M. S. B. A. & Yusuff, M. M. (2017) A facile synthesis

method of hydroxyethyl cellulose–silver nanoparticle scaffolds for skin tissue engineering applications. *Materials Science and Engineering: C*. 79, 151–160. Available from: doi: 10.1016/j.msec.2017.05.028



© 2025 Authors. Published by the University of Novi Sad, Faculty of Technical Sciences, Department of Graphic Engineering and Design. This article is an open access article distributed under the terms and conditions of the Creative Commons Attribution license 4.0 Serbia (<https://creativecommons.org/licenses/by/4.0/deed.en>).

